


ADVANCED MASTERS IN STRUCTURAL ANALYSIS
OF MONUMENTS AND HISTORICAL CONSTRUCTIONS

Master's Thesis

Chandan Chinnagiri Gowda

Numerical Modelling of Experimental Tests on Cylindrical Masonry Specimens

UNIVERSITAT POLITÈCNICA
DE CATALUNYA

University of Minho

Erasmus Mundus

ADVANCED MASTERS IN STRUCTURAL ANALYSIS
OF MONUMENTS AND HISTORICAL CONSTRUCTIONS

Master's Thesis

Chandan Chinnagiri Gowda

Numerical Modelling of Experimental Tests on Cylindrical Masonry Specimens

This Masters Course has been funded with support from the European Commission. This publication reflects the views only of the author, and the Commission cannot be held responsible for any use which may be made of the information contained therein.

Spain | 2014

DECLARATION

Name: Chandan Chinnagiri Gowda

Email: chandu627@gmail.com

Title of the Msc Dissertation: Numerical Modelling of Experimental Tests on Cylindrical Masonry Specimens

Supervisor(s): Prof. Luca Pelà

Prof. Pere Roca

Year: 2013/2014

I hereby declare that all information in this document has been obtained and presented in accordance with academic rules and ethical conduct. I also declare that, as required by these rules and conduct, I have fully cited and referenced all material and results that are not original to this work.

I hereby declare that the MSc Consortium responsible for the Advanced Masters in Structural Analysis of Monuments and Historical Constructions is allowed to store and make available electronically the present MSc Dissertation.

University: Technical University of Catalonia, Spain

Date: 15/07/2014

Signature: _____

ACKNOWLEDGEMENTS

First and foremost I offer my sincerest gratitude to my supervisors, Prof. Luca Pelà and Prof. Pere Roca, who have supported me throughout my thesis with their patience and knowledge. I attribute the level of my Master's degree to their encouragement and effort, and without them the thesis would not have been completed. I could not wish for better or friendlier supervisors.

I thank all the laboratory technicians who have helped me with my experimental campaign carried for a short period of time.

I gratefully acknowledge the support of Savvas Saloustros throughout my thesis. Also Elisa Canella, Lucia Garijo and Tasos Drougkas for their valuable feedback at times.

I am also thankful to all the professors from University of Minho, Portugal and Technical University of Catalonia, Spain for sharing their knowledge during the course.

My heartfelt thanks to my fellow classmates and friends who made this degree a lot more memorable and fun filled.

Finally I thank my parents, sister and brother for their support and encouragement throughout in all possible ways.

ABSTRACT

The main objective of this study is to carry out numerical modelling of laboratory destructive tests on small cylindrical masonry specimens. The extraction of cores is a useful technique for the mechanical characterization of existing masonry, since it moderately damages the structure. It is possible to extract cores including four brick pieces, with two horizontal joints and a vertical joint, or cores with three brick pieces and two horizontal joints. The extracted cylinders can be subjected to or compression test. The correct interpretation of the results of the test is not easy due to the limited availability of experimental results. Numerical modelling can complement the experimental activity and help to understand the complex interaction among the masonry components.

An effort on this is carried out using a Continuum Damage Mechanics constitutive model with split in tensors, in tension and compression. The failure criterion in tension is defined according to Mohr-Coulomb and in compression according to Rui Faria (similar to Drucker-Prager).

The results of linear, non-linear analysis and experimental testing, along with their comparison confirms that the failure is mainly due to tension in brick. An explanation regarding the damage evolution and the contribution of area below the loaded cap of the specimen is discussed. The results of sensitivity analysis reveal that compressive strength of mortar and the tensile strength of brick have more influence on compressive strength of masonry with respect to other mechanical parameters. Finally, an attempt to relate the compressive strength of the cylindrical specimens to that of standard stack prism is proposed.

RESUMEN

Título: “Modelización numérica de ensayos experimentales en testigos cilíndricos de obra de fábrica”

El principal objetivo de este estudio es llevar a cabo el modelo numérico de los resultados obtenidos en laboratorio de ensayos destructivos en pequeñas muestras cilíndricas de muros de fábrica. La extracción de testigos es una técnica muy útil para la caracterización mecánica de los muros de fábrica existentes, ya que no provoca daños importantes en ésta. De hecho, es posible extraer muestras compuestas por dos ladrillos y una junta de mortero entre ellos o, incluso de mayor dimensión incluyendo cuatro ladrillos con dos juntas horizontales y una junta vertical, o con sólo dos juntas horizontales. Los cilindros extraídos pueden ser sometidos a ensayos de compresión o ensayos de tracción. La correcta interpretación de los resultados de estos ensayos no resulta sencilla, debido a la escasa disponibilidad de datos. Así pues, el modelo numérico puede ser un complemento a la actividad empírica para ayudar a entender la compleja interacción entre los distintos componentes de la fábrica estudiada.

En este sentido, la labor realizada es un esfuerzo enfocado a crear un modelo constitutivo con tensores de separación, ambos en tensión y compresión. El criterio de plasticidad en tensión es definido de acuerdo con Mohr-Coulomb y con Rui Faria en compresión (similar al de Drucker-Prager), donde la resistencia a compresión biaxial es tomada como 1.25 veces el esfuerzo axial.

Los resultados de análisis lineal, no-lineal y ensayos experimentales, incluyendo comparaciones entre ellos, confirman que la rotura es debida a la tensión en el ladrillo. Una explicación teniendo en cuenta la evolución del daño y la contribución del área resistente es discutida. Los resultados de un detallado análisis revelan que la resistencia a compresión del mortero y la resistencia a tracción del ladrillo tienen más influencia en la resistencia a compresión de la fábrica con respecto a otros parámetros mecánicos. Finalmente, se plantea una propuesta por correlacionar la resistencia a compresión de los testigos cilíndricos con la de los testigos prismáticos.

TABLE OF CONTENTS

LIST OF FIGURES

LIST OF GRAPHS

LIST OF TABLES

1. INTRODUCTION

1.1. MOTIVATION FOR NUMERICAL ANALYSIS

Masonry is one of the oldest and most widely used construction techniques since ever. Evidences of its early use date back to the Mesolithic Era (9000-8000 BC). The in-situ availability of raw material necessary to the building process, the resistance and high durability of masonry structures and the simplicity of the manufacturing process, are just few of the key-factors contributing to the spread and success of this construction technique that survived till today, being still adopted in many countries. It is widely known that the strength of masonry structures depend, on the strength and the cohesion properties of the units. Among all the others, the compressive strength is doubtless one of the most important parameters describing the mechanical features of this type of constructions. As a consequence, the determination of the compressive strength of masonry structures play a fundamental role. The investigations and experimental works carried out may give us a brief description on how the compressive strength can be determined, but the availability of these data is quite limited. Moreover, no unique method is provided in order to obtain the desired value. This resulted in the possibility to work on the development of different approaches aimed at computing the compressive strength of masonry with sufficient reliability and accuracy. The necessity of going beyond the available techniques and moving forward in this direction is the drive behind the present thesis.

One of the idea being investigated in the research field, recommended by the guidelines of UIC 778-3R (International Union of Railways), is to determine the compressive strength by extracting cylindrical specimens and testing them in the laboratory. The extraction of cylindrical specimens from the wall, and their subsequent testing, makes more sense in computing the strength value, since it truly represents the material. But the challenge is in identifying which part of the wall needs to be extracted for the testing. As a result, different combinations of mortar joints need to be studied and the compressive strength of all the specimens has to be checked, in order to determine the true strength of the wall.

With the purpose of validating the experimental results and understanding the stress distribution, numerical modelling needs to be carried out. In particular, the numerical modelling allows us to understand not only the evolution of the damage and the correspondent

distribution of stresses, but also the failure modes involved in the process and the behavior of units and mortar. All the parameters can be evaluated step by step. Moreover, numerical modelling provides a complementary tool to the experimental activity and helps to understand the complex interaction among the masonry components. In this study both the numerical analysis and part of the experimental activity are carried out, for the purpose stated above.

Particular emphasis is given to the modelling of the cylindrical specimens, first of all selecting the proper type of constitutive model which adequately depicts the real masonry behavior, then comparing the available experimental results on cylindrical specimens, bricks and mortars, and finally discussing the results.

1.2. OBJECTIVE AND FOCUS OF THE THESIS

The main objective of the thesis is numerical modelling of cylindrical masonry specimens to determine the compressive strength. The results from the experimental campaign are modelled using a pre-post processor called GiD and a finite element software called COMET (Cervera et al. 2002), both developed at the International center of Numerical Methods in Engineering (CIMNE, Barcelona, Spain). The concept is based on a new promising technique to determine the compressive strength of existing structures, by extracting cylindrical specimens, according to the guidelines of UIC 778-3R formed by the International Union of Railways.

The work involves modelling of the cylindrical specimens with the results of the experimental campaign already carried out. It helps to understand the behaviour of unit and mortar, the type of stresses acting in them, failure mechanism and ultimate load and also to validate the experimental results. The research is organized on the basis of following steps:

- To gather information on the existing knowledge about the behavior of units and mortar in masonry.
- To determine the compressive strength of masonry using different approaches involving different type of theories.
- To validate the selected constitutive model, by performing benchmark analysis.
- To assess and validate the reliability of the technique by comparing the results with the experimental and through literature review.

- To compare the linear and non-linear analysis results to understand the initiation of damage and stress distribution
- To carry out sensitivity analysis to determine the behaviour of parameters affecting the compressive strength of masonry. To suggest the formula to be used in determining the compressive strength of cylindrical masonry specimens.
- To understand and correlate how better the compressive strength of the cylindrical specimen can be compared to that of the masonry wall.

1.3. OUTLINE OF THE THESIS

The present thesis is divided into six chapters. The first chapter deals with the motivation for numerical analysis, objective and focus of the thesis.

The second chapter deals with the state of art, where an introduction is given on masonry, brick and mortar, along with the compressive strength determination for old and new masonry structures.

In chapter three, the experimental campaign carried out is presented, along with the previous research results on bricks (whole and micro specimens), mortar, masonry prism, two joint cylindrical specimen and three joint cylindrical specimen as these are the input values for the numerical analysis.

Chapter four deals with the numerical analysis carried out. First, an introduction on the constitutive model used is presented. Next, modelling and results of a bench mark analysis carried out to calibrate the model is shown. Finally modelling and results of stack prism along with the comparison of experimental results are discussed.

Chapter five presents the FE modelling, the results and the comparison of cylindrical specimens of two joints and three joints. Firstly the results of linear analysis are presented, next the non-linear analysis of three joint and two joint specimens are shown. Then the comparison of numerical results with experimental results is discussed. Finally, some conclusions are drawn along with the results of sensitivity analysis on masonry prism and cylindrical specimens.

Chapter six concludes the thesis with the summary and outcome of the present research and suggestions for the future work.

2. STATE OF ART

2.1. INTRODUCTION

This chapter deals with the introduction of masonry components, viz. the brick and the mortar, the behaviour of masonry in general, failure criteria of masonry under uniaxial compression and uniaxial tension. The second part deals with the different methods in estimating the compressive strength using the Euro Code, Hilsdorf theory (1969) and finally the new methods.

2.1.1. MASONRY

Masonry is a composite material which involves ordered arrangement of unit and mortar in alternate layers. There are many types of masonry construction even though it involves only two components. Different type of units mainly bricks, stone, adobes, blocks along with different types of mortar like lime, clay, cement, bitumen are used, along with many possible arrangement styles (Figure 2.1) exists.

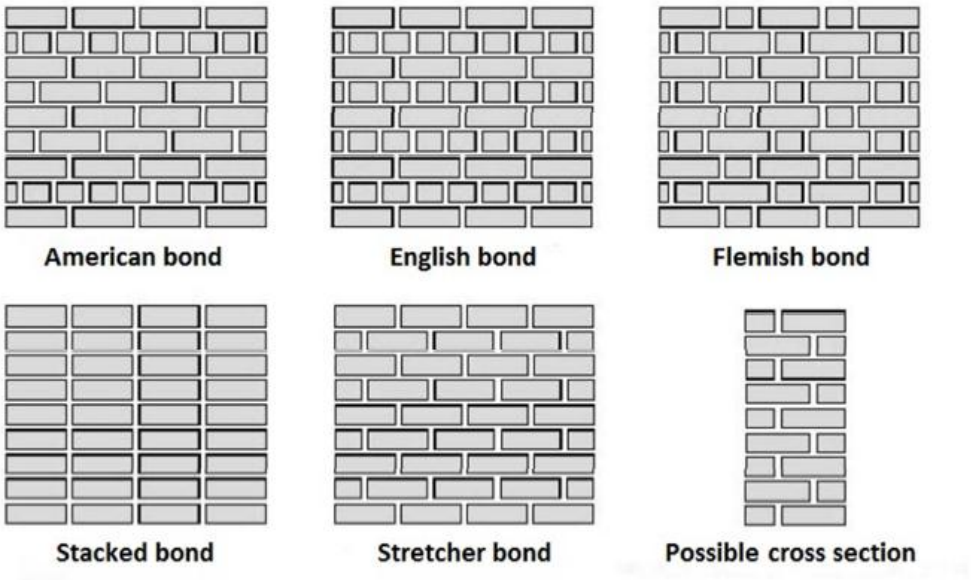

Figure 2.1 Different types of Brickwork

As a result the strength of masonry depends on the geometrical arrangement of units and mortar. The mortar joint acts as a plane of weakness both in horizontal and vertical direction.

Since the interface layer of the unit and mortar has weak bond, the response is strongly dependent on the orientation of joints. There are many other factors which influence the behaviour of masonry. According to Hendry (1990), in general the stress strain behaviour is dependent on

- Units: compressive and tensile strength, type and geometry (solid, perforated, hollow etc) and absorption capacity
- Mortar: strength, thickness, Poisson's ratio
- Unit-mortar interface: bond between the two, direction of stress and local strain.

The features of units are possible to determine during the manufacturing process. But in case of mortar it is subjected to variations, since it depends on the constituent materials. A brief introduction on the behaviour of brick and mortar in masonry is given below.

2.1.2. BRICK

Brick is a single unit or a block made of ceramic material produced under standard size. The strength of brick depends on the way of production whether it is burnt or just pressed and dried, and also on the quality of the material used for the production. It also depends on the availability of the local clay material in the area of production. The brick usually consists of alumina, silica, lime, oxide of iron, magnesia. There are different classes of brick depending on the mode of production. They are also available in different types (Figure 2.2) viz. they may be hollow, perforated or solid bricks. There are large variety of bricks made of different types of materials like clay, lime and sand, concrete, stone etc.

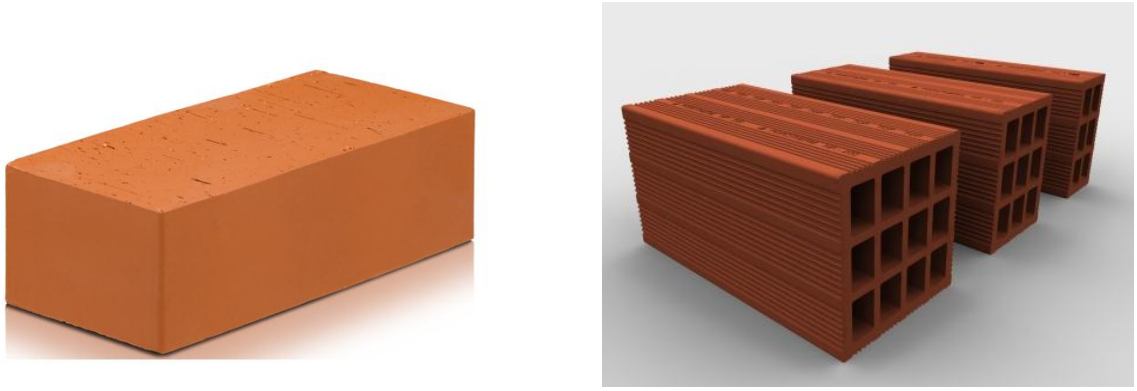

Figure 2.2 Different types of brick

The mechanical parameters may vary within the same bath of bricks. It depends on the duration of burning, the temperature, and manufacturing process. All these contribute to the variation of their properties. There is a large scatter of production, based on the evolution of time. The research has shown that ancient materials have low characteristics in comparison with the modern ones, such as high porosity and absorption, low compressive strength and elastic modulus (Lourenço et al, 2010).

Even though there is scatter of brick properties, the dimension of the brick are almost standard viz., the length is almost twice the shorter side and the shorter side is around 1.5 times the height. The mechanical properties of bricks, in particular the compressive strength, modulus of elasticity and Poisson's ratio are very relevant for the structural behaviour of masonry constructions.

2.1.3. MORTAR

Mortar is a workable paste which holds the units, bricks and concrete together. Mortar becomes hard when it cures, resulting in a rigid aggregate structure. However, the mortar is intended to be weaker than the building blocks and the sacrificial element in the masonry, because the mortar is easier and less expensive to repair than the building blocks. Mortars are typically made from a mixture of sand, a binder, and water. The most common binder since the early 20th century is Portland cement but the ancient binder lime mortar is still used in some new construction.

(a) **(b)**

Figure 2.3 Brickwork with (a) Lime mortar (b) Cement mortar

The important properties of mortar are to fill the joints, impeding the passage of water, to regularize the disposition of bricks and to distribute the load uniformly and to cooperate to lead horizontal stresses until foundations. According to EN 459-1, European standard for building lime (CEN, 2010), the lime mortar can be divided into two categories namely air lime and lime with hydraulic properties, which are sub divided into many categories.
The properties of mortar which effect the masonry are the compressive strength, modulus of elasticity and Poisson's ratio.
The experimental results referred in this thesis are taken from natural hydraulic lime. Natural hydraulic lime is produced by heating limestone that naturally contains clay and other impurities, with no other material added to create hydraulicity.

2.1.4. TYPES OF MASONRY

The combination of brick and mortar can be of two types. The first possibility is when the strength of brick is higher than the strength of mortar. The second case is when the strength of mortar is greater than the strength of brick. Type one is the most common type of construction found in old and also carried out in modern construction. The difference in stiffness between the brick and mortar properties is the main criteria responsible for the failure of masonry as stated by Hilsdorf (1969).
The behaviour of brick and mortar in masonry is shown in Figure 2.4. The mortar is subjected to triaxial compression and the brick is subjected to uniaxial compression and biaxial tension. The triaxial compression on mortar is due to load in one direction and the confinement of brick in the other two direction making the mortar to be in triaxial compression state. The brick is subjected to uniaxial compression in the loading direction and this makes the other two directions of the brick to expand subjecting it to biaxial tension.

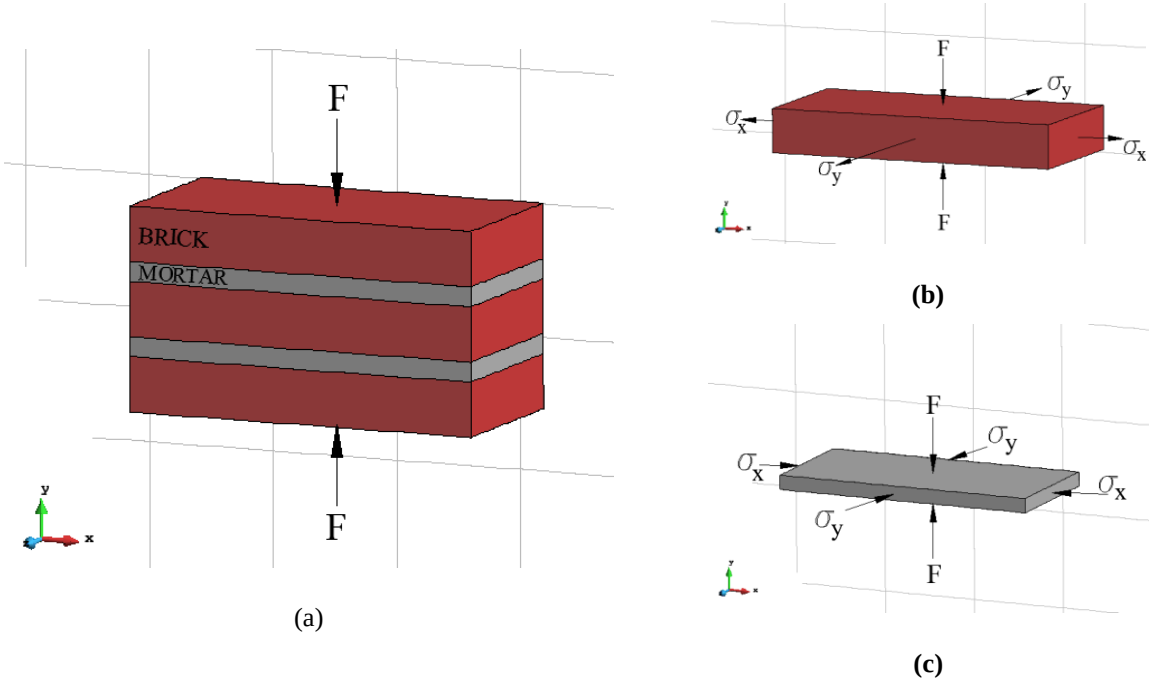

Figure 2.4 Behaviour of (a) Masonry (b) Unit and (c) Mortar

The uniaxial compressive strength of masonry in the direction normal to the bed joint is regarded as the most important property of masonry as it is subjected in reality. The compressive strength in the direction parallel to bed joint has received very less attention, even though it can affect the strength of masonry.

The failure in masonry depends on the strength of the unit and mortar. If the compressive strength of brick is greater than the compressive strength of mortar than the failure of masonry is due to the tensile cracking of units. The uniaxial compressive and uniaxial tensile failure of masonry for different orientation of mortar joints is as shown in Figure 2.5 carried out by Page - 1981.

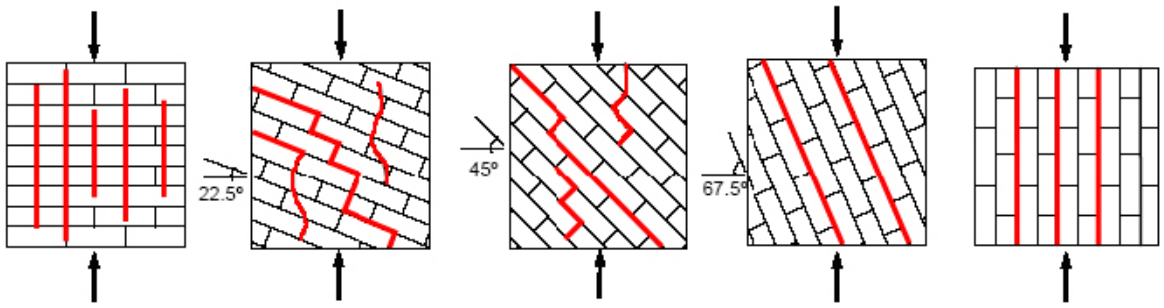

(a)

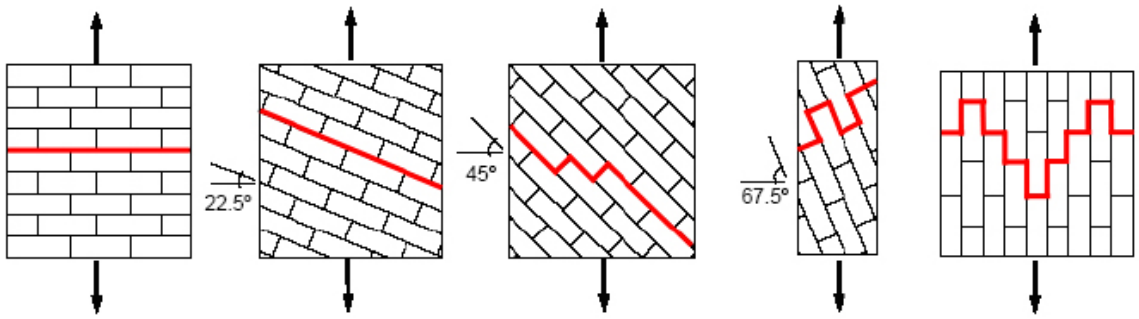

(b)

Figure 2.5 Failure modes of solid clay units under (a) Uniaxial compression (b) Uniaxial tension (Page - 1981, 1983)

In case of biaxial compression-compression the splitting failure occurs in the plane parallel to free surface near the mid span thickness without the influence of the orientation angle. The failure is brittle and starts at one of the edges and propagates to the centre, shown in Figure 2.6.

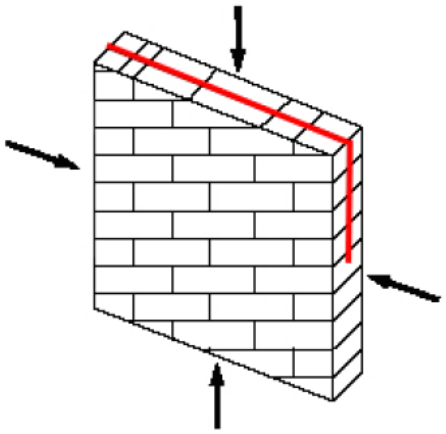

Figure 2.6 Failure mode in solid clay unit under biaxial compression (Page - 1981, 1983)

For tensile loading the failure of masonry is due to debonding between the bed joints and the units for type one viz. the compressive strength of unit is greater than mortar strength. On the contrary the tensile failure is due to the stresses exceeding the unit tensile strength. A study was carried out by Backes (1985) for tensile loading parallel to bed joints. Backes tested wallets under direct tension for both types. For type one, the failure was due to the tensile crack passing through the mortar head joints and for the second type the tensile cracks passed

through the head mortar joints and the centre of the bricks. Both the types of failure are shown in Figure 2.7.

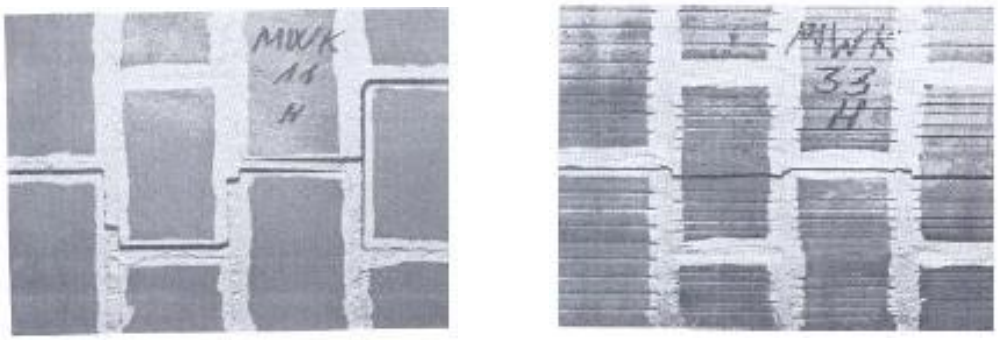

(a) **(b)**

Figure 2.7 Failure mode of masonry wall under direct tensile loading (Backes 1985) (a) Type 1 (b) Type 2

The study of masonry under biaxial state of stress cannot be solely dependent on the uniaxial behaviour of masonry. In order to study the biaxial behaviour a series of tests were carried out by Page (1983) under tension-tension, tension-compression and compression-compression combination. The joints in masonry act as a plane of failure. Therefore the biaxial strength is not only dependent on the principle stresses, it also depends on the orientation of the bed mortar joints. So it is described in a three dimensional diagram with two principle stresses and their orientation angle (θ) to the bed joint (Samarasinghe & Hendry 1980, 1982). The failure modes of biaxial tension-compression of solid clay units are as shown in Figure 2.8.

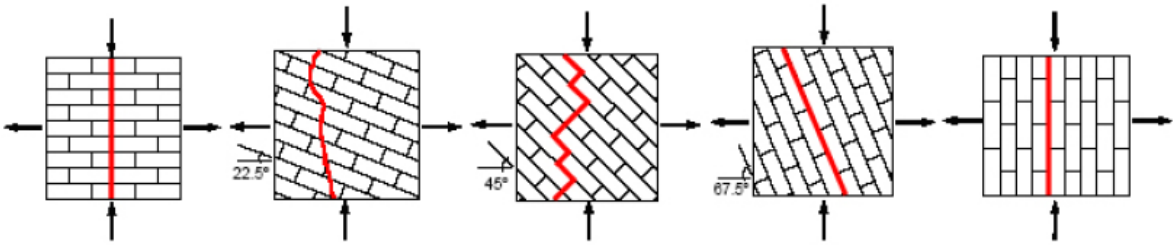

Figure 2.8 Failure modes of solid clay units under biaxial tension-compression (Page - 1981, 1983)

The failure surfaces for different inclination of mortar joints under biaxial tension-compression and uniaxial compression is shown in Figure 2.9. The shape of the failure surface in the biaxial tension-compression is not only influenced by the orientation of the bed joint but also on the shear and tensile bond strength of the mortar joints and the strength of the

brick units. The failure is normal to the plane of loading and is always in the mortar joints alone or in a combined state involving brick and joint.

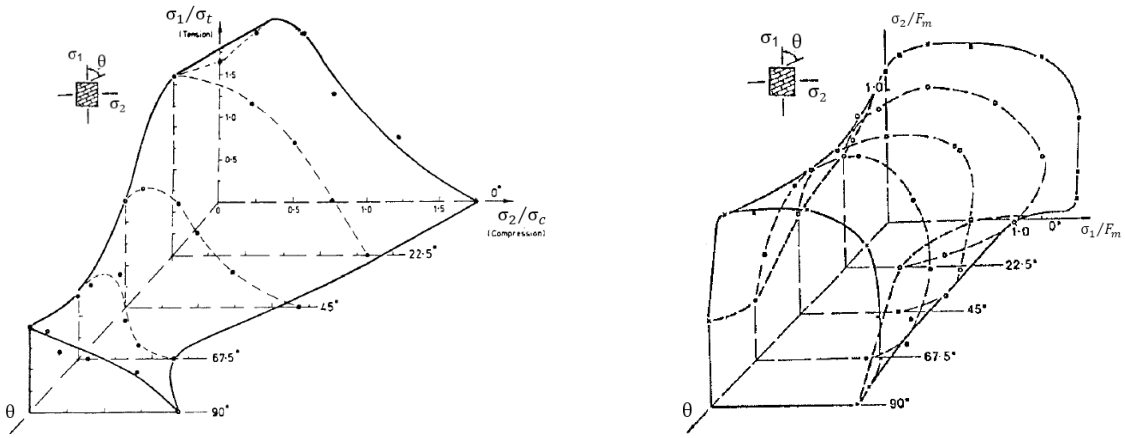

(a) **(b)**

Figure 2.9 Failure surface for different angle of inclination under (a) Biaxial tension-compression and (b) Biaxial compression

In order to estimate the compressive strength of masonry the Euro code 6- Design of masonry structures suggests the equation 2.1 to be used.

$$f_k = K f_b^{\alpha} f_m^{\beta} \qquad \textbf{2.1}$$

Where f_k is the compressive strength of masonry, K is a constant which depends on the type of masonry, f_b is compressive strength of brick, f_m is compressive strength of mortar, α and β are constants. But as seen above the equation does not take into consideration the tensile strength of brick which causes the failure.

So it becomes an important task to take into consideration the tensile strength of brick, since failure does occur due to the tensile failure of the bricks as explained above. As a result there have been many theories proposed by Hilsdorf (1969), Khoo and Hendry (1973, 1975), Ohler (1986) where they take into consideration the tensile strength in evaluating the compressive strength of masonry.

According to Hilsdorf the compressive strength of masonry can be obtained by using Equation 2.2

$$f_u = \frac{f_{bc}}{U_u} \frac{(f_{bt} + \alpha' f_j)}{(f_{bt} + \alpha' f_{bc})} \qquad \textbf{2.2}$$

f_{bc} is the compressive strength of brick, f_{bt} is the tensile strength of brick, f_j is the compressive strength of mortar, α' is the ratio of thickness of mortar joint to thickness of the brick and U_u is coefficient of non-uniformity which Hilsdorf established according to his experimental investigation. This equation was developed based on an assumed linear relation between the lateral biaxial tensile stress and local compressive stress equal to external compressive stress multiplied by the non-uniformity.

Ohler (1986) developed an equation for compressive strength determination of masonry, assuming the tri-linear representation of biaxial failure crack for brick based on the available experimental data.

$$\sigma_y = \sigma_{yom} + \frac{s\sigma_{yos} - \sigma_{yom}}{l + \frac{th_m \sigma_{yos}}{mh_s \sigma_{xos}}} \qquad \textbf{2.3}$$

σ_y is the compressive stress at failure, σ_{yom} is the uniaxial compressive strength of mortar, σ_{yos} is the uniaxial compressive strength of brick, σ_{xos} is the uniaxial tensile strength of brick, h_s and h_m are the thickness of mortar and brick, m is the slope of failure, s and t are the parameters defining unit failure envelope.

2.2. EXPERIMENTAL COMPRESSIVE STRENGTH DETERMINATION

Compressive strength determination can be split into two parts based on the age of masonry structures. One for the new masonry construction, which can be tested along with the construction of new masonry walls and the other for old masonry constructions which requires a method to determine the compressive strength.

2.2.1. NEW MASONRY STRUCTURES

The compressive strength determination for new masonry can be performed by constructing new masonry walls simultaneously and testing them under laboratory conditions. The

European standard EN 1052-1:1998 is followed for the construction and testing procedures. Experimental investigations have been carried out based on this standard for instance by Peverini (2014), and by University of Padova in the framework of the NIKER European project (New integrated knowledge based approaches to the protection of cultural heritage from earthquake induced risk) for the strength determination.

Small masonry stack prisms and wallets are constructed according to Table 2.1 for the specimen dimensions and tested under loading, till the specimen fails. Once the maximum load is obtained the compressive strength is calculated using the equation 2.4, the maximum force divided by the area under loading.

Table 2.1 Specimen sizes for testing the compressive strength of masonry

Face size of unit		**Masonry specimen size**			
l_u (mm)	h_u (mm)	**Length** l_s (mm)	**Height** h_s (mm)		**Thickness** t_s (mm)
≤ 300	≤ 150	$\geq (2\ X\ l_u)$	$\geq 5\,h_u$	$\geq 3\,t_s$ *and* $\leq 15 t_s$ *and* $\geq l_s$	$\geq t_u$
	> 150		$\geq 3\,h_u$		
> 300	≤ 150	$\geq (1.5\ X\ l_u)$	$\geq 5\,h_u$		
	> 150		$\geq 3\,h_u$		

$$f_i = \frac{f_{i,\max}}{A_i} \qquad \textbf{2.4}$$

The experiments conducted by Peverini (2014) on masonry prism is shown in Figure 2.10 compute good results. The average compressive strength of prisms were 8.64 MPa with a maximum force of 320.69 kN. The tests were performed under displacement control to obtain the post peak behaviour.

Figure 2.10 Tests on Prisms by Peverini (2014) at UPC

Before testing the masonry prisms, the brick and the mortar casted at the time of construction can be tested, in order to compare the results with masonry. This is the method used to estimate the compressive strength of new masonries. But to find the compressive strength of historical masonry or old masonry, there have been little investigation and works related to it.

2.2.2. OLD MASONRY STRUCTURES

It is difficult to estimate the compressive strength of existing masonry, since only non-destructive and minor destructive tests need to be carried out. As a result deformation and failure theories are necessary. Many theories have been proposed by Hilsdorf (1969), Khoo and Hendry (1973, 1975), Atkinson (1982) and others, for both theoretical, empherical and failure criteria based on the mechanical parameters of masonry. Since theoretical assumptions do not satisfy the experimental outcomes, there is further research need to be carried out in this field.

UIC 778-3R (International Union of Railways, 1995) proposes to extract cylindrical specimens from the existing masonry to determine their compressive strength. The diameter of the cylindrical specimens is recommended to be 150 mm by UIC and Brencich et al (2004, 2006), since they represent actual brickwork involving a vertical and two horizontal mortar joints. There are experiments carried out on 90-100 mm diametrical cylindrical cores by Sassoni & Mazzotti (2013) to estimate the compressive strength. The specimens are small and represent partially the complex interaction among joints and bricks, therefore more

investigation is necessary for a better correlation between the strength of small cores and that of whole masonry.

Brencich et al (2004, 2006) carried out experiments on cylindrical masonry specimens from 150 year old bridge in Alessandria, Italy. The specimens are shown in Figure 2.11. Three centimetre thick mortar was casted on top and at the bottom of the specimens to apply the load uniformly on the specimen. To compare the results from the experiments, they also carried out numerical analysis using finite element method. The failure of the cylindrical specimens in experiments and the numerical model were almost the same viz. the failure of brick in tension and the vertical mortar joint resulting in the detachment of the lateral parts of the brick. The failure of the specimen in the numerical model is at lower load, resulting in lower compressive strength in comparison to the experimental results. The numerical model is compared with the traditional approaches like flat jack and sclerometer using Schmidt hammer to determine the compressive strength.

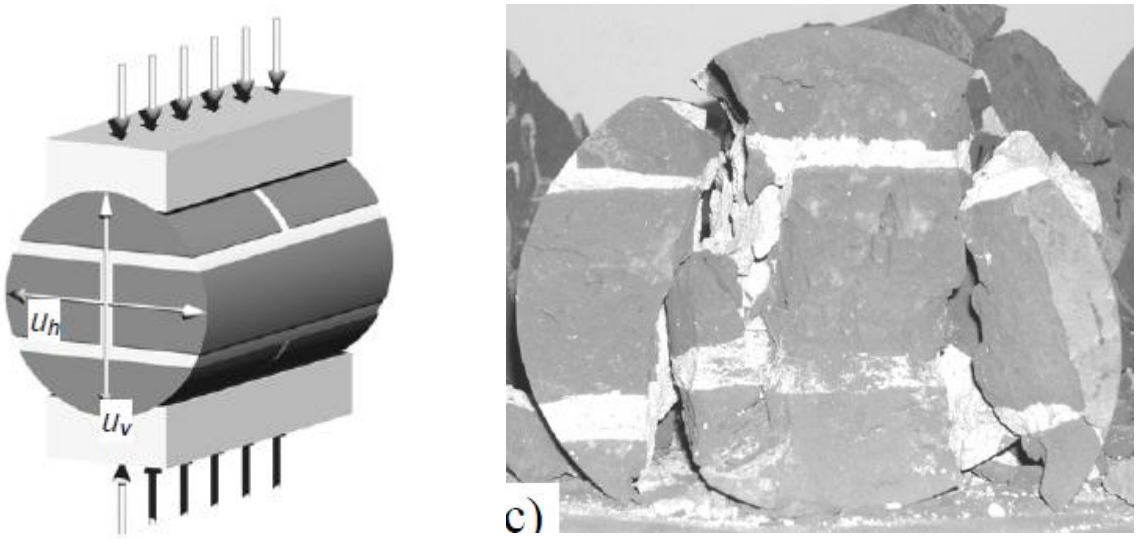

(a) **(b)**

Figure 2.11 (a) Cylindrical specimen with mortar on top and bottom for testing (b) Sand cone shaped failure

The compressive strength is given by the equation 2.5. The area of consideration is the full diametric area of the specimen, which is assumed to resist the applied force. This criterion might lead to underestimations of the masonry strength, since at failure the distribution of vertical stresses should distribute in the sand cone shape in the central part of the specimen.

$$f_c = \frac{F_{coll}}{\phi l} \qquad \textbf{2.5}$$

The finite element models (FEM) helps in understanding the collapse mechanism viz. the evolution of cracking in the specimen. The lower strength of the numerical model is due to the elastic mismatch between the brick and mortar, resulting in the evolution of tensile stresses in the brick near the vertical joint, where the failure initiates.

3. EXPERIMENTAL CAMPAIGN

3.1. INTRODUCTION

This chapter deals with the experimental extraction of cylindrical specimens carried out in the laboratory. Also the results of compressive strength, tensile strength, Young's modulus of elasticity and Poisson's ratio of the mortar, brick, prism and cylinders are presented. The latter experiments were carried out in Technical University of Catalonia, being the objective of master thesis by *Peverini* (2014) and *Usan Cañ o* (2014), and the former was carried out for the present thesis. The results are presented, since they are the values of input for the numerical analysis carried out on prism and cylindrical specimens of two joints and three joints.

The chapter is split into sections dealing individually with cylindrical extraction (present), brick, mortar, prism and cylindrical specimens with reference codes used for respective experimental campaign.

3.2. CYLINDRICAL EXTRACTION

Extraction of cylinders were planned and executed on the newly constructed masonry wall in the laboratory. Two walls were constructed with Spanish brick units and non-hydraulic lime mortar having the total dimension 1537 x 700 x 133 mm^3. The extractions were carried out at the age of 61 days.

The extraction was performed in order to eliminate the drawbacks from the previous experimental work. Namely, before extraction the wall was laid in horizontal direction. The extraction was done by using drilling machine along with water, to reduce the dust and pressure originating from the extraction. As a result five cylindrical specimens of three joints and six cylindrical specimens of two joints were successfully extracted.

Based on this experience, the new extraction was carried out by keeping the wall in vertical direction. An initial pre compression of 3 kPa was applied at four points so as not to lose the integrity during extraction as a whole, or part of the wall. Markings of the cylinders were made on the masonry wall with the necessary joints (three joints, two joints and one joint) before performing the extraction.

The drilling machine was kept in a stable horizontal position by attaching it to the forklift machine, not to produce any movement, resulting in the loss of specimen due to vibration. The end of the drilling machine was fit with the necessary drilling cores of 150 mm and 100 mm during the respective extraction. The machine was also fit with the air compressor to reduce the dust produced during drilling of the specimens. The extraction was carried out from the outer side to the centre of the masonry wall. The final form of the wall before extraction, is shown in Figure 3.1(a) during the extraction in Figure 3.1(b) and the final form after the extraction in Figure 3.1(c).

(a)

(b)

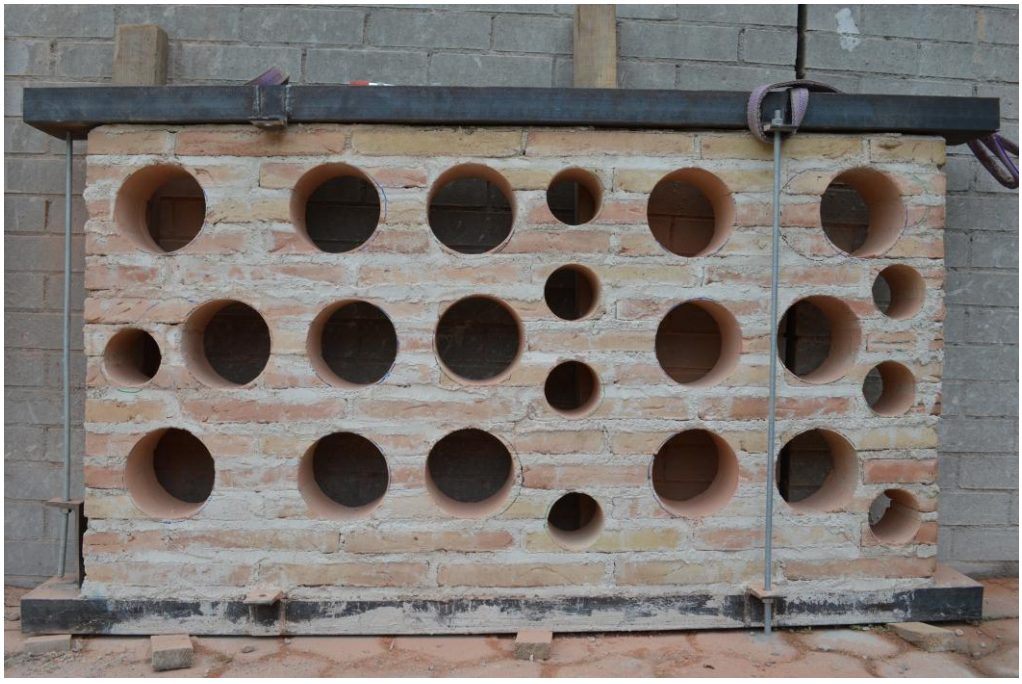

(c)

Figure 3.1 (a) Before extraction (b) During extraction (c) After extraction

Three types of cylindrical specimens were extracted viz., two joint cylinder (with two horizontal mortar joints) of 150 mm, three joint cylinders (with two horizontal and one vertical joint) of 150 mm and a single joint cylinder (with one horizontal joint) of 100 mm.

No problems were encountered during any stages of the extraction. A total of 14 two joint cylinders, 15 three joint cylinders and 22 single joint cylinders were extracted from the two walls.

After the completion of extraction regularization mortar was laid around the cylindrical specimens. This was applied to provide a uniform surface to apply load and to remove any irregularities if present. The mortar used is Sika FastFix, a quick setting mortar. Wooden moulds (Figure 3.2 a) were created to place the cylindrical specimens in the centre, and to pour the quick setting mortar around it. The final specimen after casting the regularisation mortar is shown in Figure 3.2(b).

(a) **(b)**

Figure 3.2 (a) Cylinder in the mould & (b) Final specimen

Unfortunately any of the experiments planned were not executed because of the time constraint. But the specimens will be used to carry out the experimental investigation in the near future.

3.3. BRICK

The experiments carried out on bricks will be presented in two parts. First part dealing with the tests carried out on whole brick specimens and second part with the tests carried out on micro specimens extracted from the bricks.

3.3.1. WHOLE BRICK SPECIMENS

Compressive tests were carried out on whole brick specimens. The surface of the specimen were treated in two ways to remove any irregularities present. In the first type the surface was capped (Figure 3.3 a) and in the other, the brick were polished (Figure 3.3 b) with sulphur mortar layer. The standard UNE-EN 772-1 was followed to perform the tests. The results of the compressive strength are shown in Table 3.1.

Table 3.1 Experimental results of compressive strength of brick

Type	Compressive strength (MPa)
Capped	30.8
Polished	25.5

(a) **(b)**

Figure 3.3 Bricks with surface treatment (a) Capped & (b) Polished

Three point flexural tests were carried out to determine the tensile strength of brick indirectly. The concrete standard UNE-EN 772-6, was used as reference since there is no specific EN standard to determine the tensile strength. Three different types of treatments were carried out on the loading area, viz., neoprene strip, cement mortar and polishing. The average results

obtained from the tests are shown in Table 3.2. The tensile strength was calculated using the equation 3.1 (Model Code 1990).

$$f_{ctm} = f_{ct,fl} \frac{1.5\left(\frac{h_b}{h_0}\right)^{0.7}}{1+\left(1.5\left(\frac{h_b}{h_0}\right)^{0.7}\right)} \qquad \textbf{3.1}$$

f_{ctm} is the mean axial tensile strength, f_{ctm} is the flexural tensile strength, h_b is the depth of the specimen, $h_0 = 100mm$.

Table 3.2 Flexural test on whole brick specimens

Type	Flexural strength (MPa)	Tensile strength (MPa)
Neoprene	3.57	1.17
Mortar	3.74	1.23
Polished	3.68	1.15

3.3.2. MICRO BRICK SPECIMENS

Cylinders were extracted from the bricks and subjected to compressive and Brazilian tests. The extraction was carried out in all the three directions of the specimen viz., along the header, stretcher and bed (Figure 3.4 a). These three directions were selected to study the variation of strength. The extracted cylinders were of diameters of 35 mm and 75 mm.

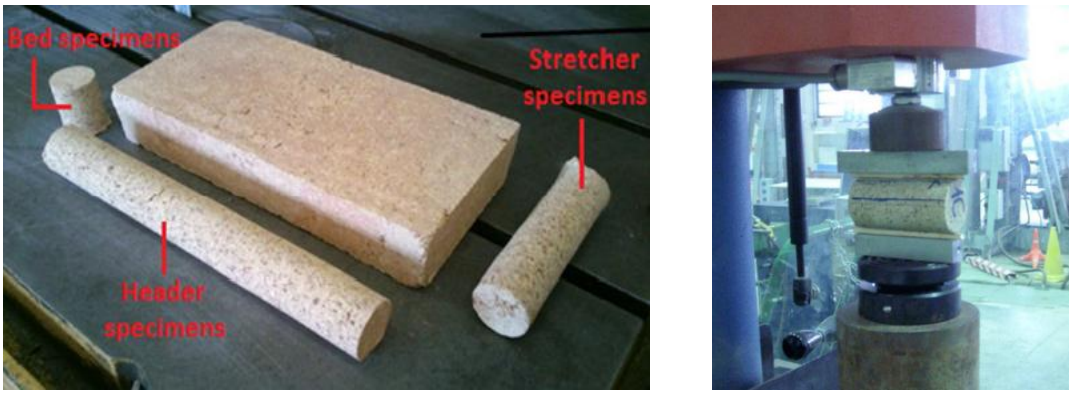

(a) **(b)**

Figure 3.4 (a) Micro specimens of the brick & (b) Experimental set up for Brazilian test

Two ratios were opted to perform the test, with each test having three minimum samples for testing. The ratio 2:1 with the height to diameter and the ratio of 1:1 were carried out. For the bed sample to be tested for 2:1 ratio, two samples were placed one on top of another without any connecting material. Fracture energy was also determined by calculating the area below the stress displacement curve. The modulus of elasticity was found to be 6671.3 MPa. The results of compressive strength and fracture energy are shown in Table 3.3.

Table 3.3 Results of Compressive tests on Bricks of 35 mm diameter specimens

	Compressive strength (MPa)	**Fracture energy (N/mm)**
Header (2:1)	16.17	0.151
Stretcher (2:1)	25.36	0.167
Bed (2:1)	12.41	0.156
Average	**17.98**	**0.158**

The same experiments were carried out on 75 mm diametrical cylinders. The average results of these are presented in Table 3.4.

Table 3.4 Results of Compressive tests on Bricks of 75 mm diameter specimens

	Compressive strength (MPa)	**Fracture energy (N/mm)**	**Poisson's ratio**
Bed	23.62	1.72	0.1

The concrete code UNE-EN 12390-3 was used for the compressive tests and the ASTM standard C496-96 was used for the Brazilian test. The experimental set up of the Brazilian test is shown in Figure 3.4 (b) and the results are shown in Table 3.5.

Table 3.5 Results of Brazilian tests on Brick specimens of 35 mm diameter

	Tensile strength (MPa)
Header (1:1)	3.33
Stretcher (1:1)	3.10
Bed (1:1)	2.07
Header (2:1)	1.90
Stretcher (2:1)	2.07

3.4. MORTAR

The experimental tests on mortar were carried out according to the European standard CEN - 2007 -EN 1015-11 - Methods of test for mortar for masonry - Part 11 Determination of flexural and compressive strength of hardened mortar. The preparation, storage, testing and analysis are all explained in detail in the code. The results were analysed at 7, 14, 28 and 61 days to compare the evolution of strength over the period. The results obtained were comparatively less with respect to the standard lime mortar, hence even the standard for concrete UNE-EN 12390-3 was also referred to evaluate the compressive strength and modulus of elasticity.

Flexural tests were performed on 40 x 40 x 160 mm^3 cube specimens. The results obtained from the flexural test are shown in Table 3.6. Compressive tests were performed on the remaining samples obtained from the flexural test with dimensions 40 x 40 x 40 mm^3. The experimental setup for the flexural test and the compressive test are shown in Figure 3.5. The results of compressive tests and the flexural tests are shown in Table 3.6, which are the average results from three tested samples.

Table 3.6 Experimental results on Mortar flexural and compressive strength

	7 days	14 days	28 days	61 days
Flexural strength (MPa)	0.140	0.505	0.553	0.580
Compressive strength (MPa)	0.736	0.828	1.266	1.600

(a) **(b)**

Figure 3.5 Experimental setup of Mortar for determination of (a) flexural & (b) compressive strength

Cylindrical samples were casted, to perform the tests to determine the modulus of elasticity. The ratio of height to diameter was 2:1 with the dimensions of 150 mm and 75 mm. The loading was performed in cycles of three to five for each sample and maintaining the load for 30 seconds at peak in each cycle. Poisson's ratio was also determined using the same cylindrical specimens, by measuring the displacements in horizontal and vertical directions using extensometric chain. The results obtained are shown in Table 3.7.

Table 3.7 Experimental results of Mortar

Modulus of elasticity (MPa)	429.76
Poisson's ratio	0.196

3.5. STACK PRISM

Three specimens of stack prisms were tested to determine their compressive strength, modulus of elasticity and Poisson's ratio. The dimensions of the tested prism were 276 x 280 x 133 mm^3, all the three samples were measured on the day of testing. The size of the brick units are 276 x 133 x 43 mm^3 and the thickness of the mortar was at an average of 10 mm. A layer of hard mortar (12.5 mm) made of Sika fast fix-130 TP was laid on top and at the bottom of the prism to have uniform surface during load application, eliminating any surface irregularities. All the three samples were tested under displacement control in order to obtain

the post peak behaviour. The brick units and the mortar investigated earlier were used to construct the prisms.

Each prism had five brick units, with four layers of lime mortar and hard layer of mortar on top and in the bottom. The testing was carried out at the age of 61 days. 6 LVDT's were used to measure the displacement in the horizontal and vertical directions, with the aim to determine the Poisson's ratio. The prism was subjected to cyclic loading and unloading for five cycles, to determine the modulus of elasticity.

The Poisson's ratio and the modulus elasticity were not determined in first stack prism, since it was used to perform the pilot test just to obtain the compressive strength. For stack prism 2 and 3 modulus of elasticity and Poisson's ratio were calculated. The loading was applied under displacement control at the rate of 0.003 mm/sec, to obtain the post peak response of the prism. The results of the compressive strength are shown in Table 3.8.

Table 3.8 Experimental results of the compressive test on stack prisms

Specimen	**Area (mm^2)**	**F_{max} (kN)**	**Compressive strength (MPa)**
Stack prism 1	37125	328.28	8.84
Stack prism 2	37125	308.96	8.32
Stack prism 3	37125	324.83	8.75
Average	**37125**	**320.69**	**8.64**

The load displacement graph of prism 1 and prism 2 are shown in Graph 3.1. But unfortunately none of the experiments were able to capture the post peak behaviour, since the LVDT's were either removed or detached from the prism after the maximum load was reached, in order not to damage the measuring instruments.

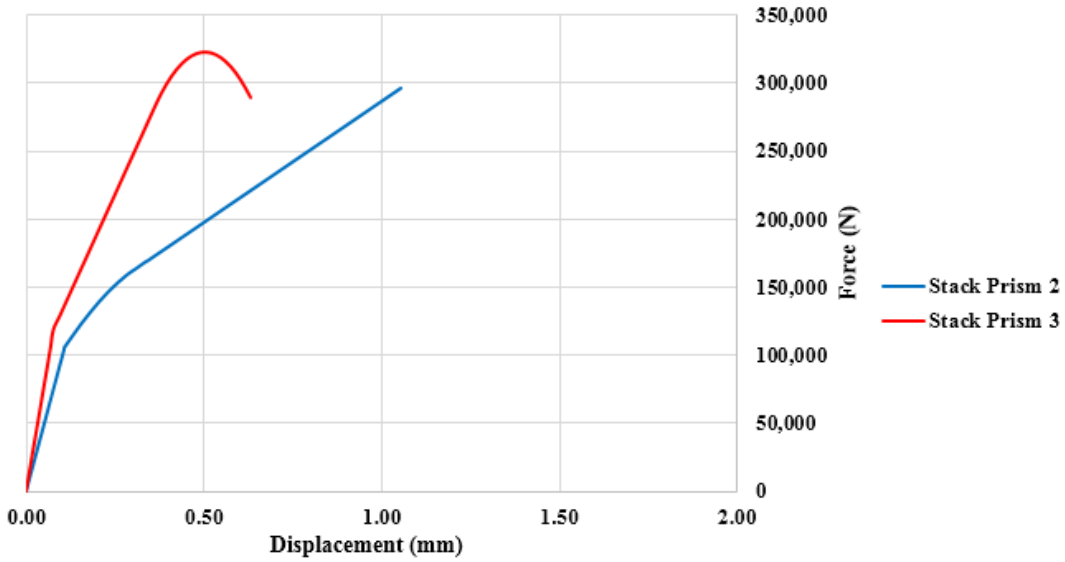

Graph 3.1 Force displacement diagram of Stack prism 1 and 2

The results of the cyclic loading to determine the modulus of elasticity on the prisms are shown in Graph 3.2. It can be seen from the graph that the first cycle of both the graphs has non-linear part, this is due to the settling of the LVDT's for the initial loading. The last cycle was used to calculate the modulus of elasticity and the results are shown in Table 3.9.

Table 3.9 Modulus of elasticity of stack prims

	Range of stress	**Modulus of elasticity**	
		Stack Prism 2	**Stack Prism 3**
E_0	4-10% σ_{max}	2684.24	3968.23
E_1	19-28% σ_{max}	3545.65	5013.36
E_2	3-30% σ_{max}	3073.51	4398.96

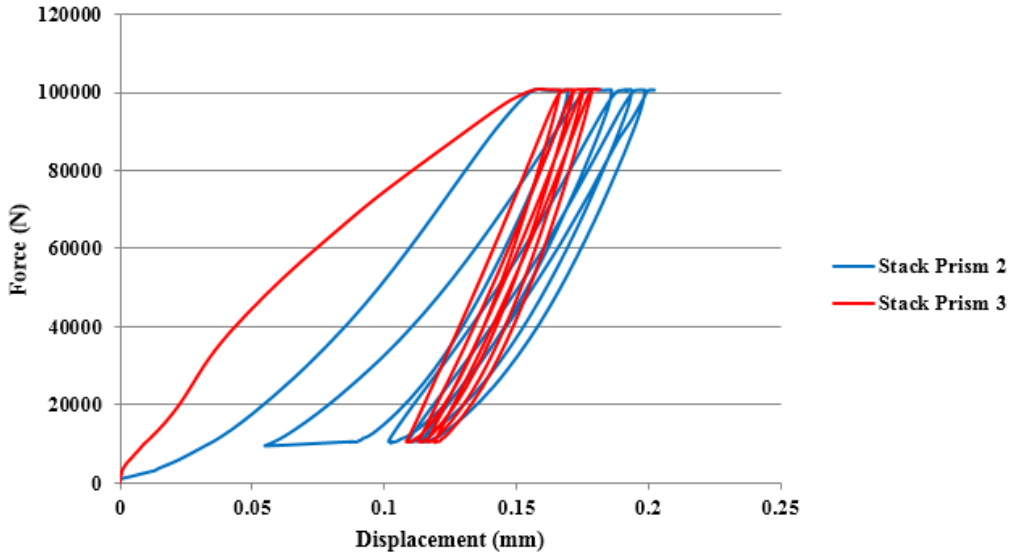

Graph 3.2 Loading and unloading cycle for Stack prisms

Three similar types of failures were observed in the three prisms tested. All the failures occurred in the brick and not in the mortar. The prism was investigated after the failure. The prism as a whole was observed to be very fragile, since the test was continued till the end of the residual strength.

(a) **(b)**

Figure 3.6 Failure of prisms (a)(a) Stack prism 2 & (b) Stack prism 3

In prism one the failure originated in the left quarter of the second brick from the top and propagated throughout the height of the specimen. In the second prism the failure occurred in

the upper and the lower extreme (Figure 3.6 a). Finally the failure in the last prism initiated in the middle of the central brick and propagated throughout the height of the prism (Figure 3.6 b).

3.6. THREE JOINT AND TWO JOINT CYLINDERS

Cylinders were extracted from the wall constructed in the laboratory for the purpose. The extraction was carried out using the drilling machine with water to reduce the dust and the loss of mortar. Five cylinders with three joint (2 horizontal and 1 vertical joint) and six specimens with two joint (2 horizontal joints) were successfully extracted from the masonry each having diameter of 150 mm. The main purpose of the extraction was to determine the compressive strength, modulus of elasticity and Poisson's ratio of the brickwork using a non-standard test. The guidelines of UIC 778-3R (UIC 1995) was used to perform the compressive test is. The same guidelines have been followed by many authors (Gambarotta et al (2001), Brencich et al (2004), Bilello et al (2007)), to determine the compressive strength.

Since the wall was of two leaves, the cylinders were cut into half before testing and after extraction. The test consists of applying the load on the extracted cylinder in the same direction as it receives the load in the original wall. A hard mortar of Sika FastFix-130 TP, is laid around the cylinder to obtain a regularised surface to distribute the load uniformly during the test. The final specimen before testing for compressive strength is shown in Figure 3.7 (a). Four LVDT's were attached to the cylinder (Figure 3.7(b)) to measure the vertical and horizontal displacement, to determine the modulus of elasticity and Poisson's ratio.

(a) **(b)**

Figure 3.7 ((a) Final specimen before testing (b) Specimen with LVDT's placed

Compressive tests were carried out under displacement control instead of load control to capture the post peak behaviour. The force displacement diagrams of the three joint cylinders and two joint cylinders are as shown in the Graph 3.3.

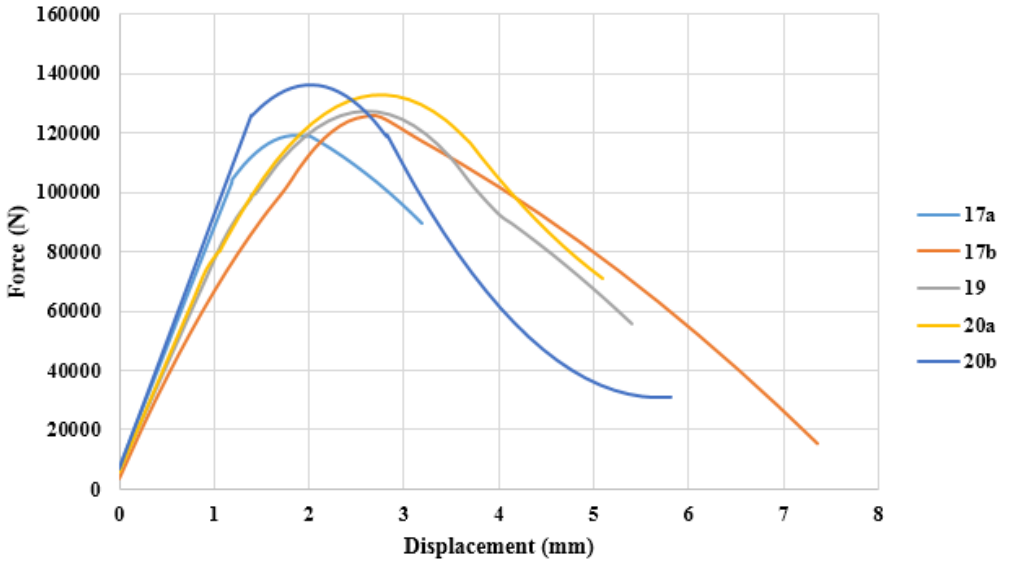

(a)

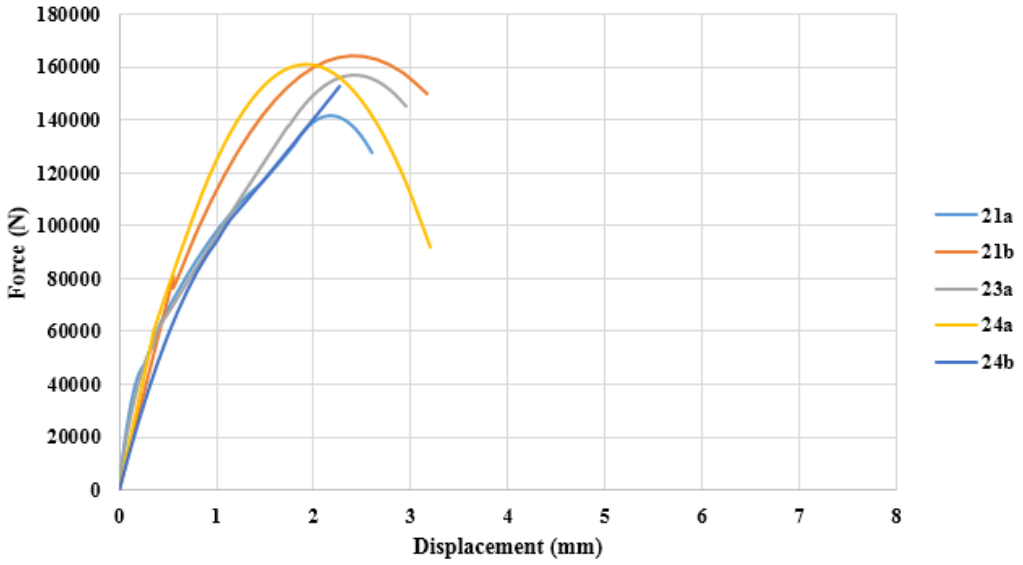

(b)

Graph 3.3 Force displacement diagram (a) Three joint cylinders & (b) Two Joint cylinders

The obtained results were compared with A. Brencich & Sterpi (2006). The main discussion on the analysis of the experimental results was to determine, the area to be considered for compressive strength, which is the aim of the present thesis too. The two areas considered in determining the experimental results are the diametric area of the specimen and the area below the loaded cap. The results are shown in Table 3.10, where F_{max} is the maximum load, A_1 is the diametric area of the specimen and A_2 is the area below the loaded cap .It is clear that if the area of loaded cap is taken into consideration the compressive strength increases by 25%. In order to understand better the distribution of stresses and to finalise the area to be considered for the calculation, numerical analysis is carried out.

Table 3.10 Experimental results of three joint and two joint cylinders

Specimen	F_{max}	**Area (A_1) mm^2**	**Area (A_2) mm^2**	**Compressive strength (MPa)**	**Compressive strength (MPa)**
Three Joint specimens	133.30	19500	15600	6.84	8.55
Two Joint specimens	157.87	19500	15600	8.10	10.12

The initiation of cracks in the experiments were observed in the lateral parts of the cylinder, right below the regularisation mortar. As the load was increased, the cracks increased their width and finally detached from the cylinder, before reaching the maximum load. Apart from these main cracks, several micro cracks were distributed throughout the cylinder by the end of the experiment. The final specimen at the end was a prism with the width equal to regularisation mortar as shown in Figure 3.8.

Figure 3.8 Specimen at the end of the test

The Young's modulus of elasticity was calculated based on equation 3.2. The results are tabulated in Table 3.11 for both three joint and two joint specimens.

$$E = \frac{4}{3}\frac{(F^{0.5} - F^{0.1})}{(u_V^{0.5} - u_V^{0.1})l} \qquad \textbf{3.2}$$

Table 3.11 Young's modulus for three joint and two joint specimens

Specimen	Range of Stress (MPa)	Young's modulus of elasticity (MPa)
Three joint specimens	0-15% σ_{max}	1650.52
Two joint specimens	0-35% σ_{max}	2033.61

4. NUMERICAL ANALYSIS

4.1. INTRODUCTION

Finite element models (FEM) are able to capture some aspects which are unable to be captured in the experimental testing. To perform the numerical analysis it is necessary to know the mechanical parameters of mortar and brick. These parameters are the compressive strength, tensile strength, young's modulus, Poisson's ratio, compressive fracture energy and tensile fracture energy.

Masonry can be modelled in three types. The first type is micro modelling where the brick, mortar and the interface layer is studied individually to access the behaviour of the masonry. The second type is the meso scale modelling where the interface and the units are clubbed together to study as single entity and the brick separately. The final type is the macro modelling where the entities for the brick and mortar is homogenised as a continuum.

To model masonry using finite element technique, three parts need to be carefully examined (1) Behaviour of clay bricks (2) Behaviour of mortar joints and (3) Mechanisms of joint failure (Page - 1978). The numerical modelling is a necessity to study the triaxial compressive state in mortar and the uniaxial compression and biaxial tension state in brick, allowing us to study the stress distribution as a whole. Since mortar joints act as plane of weakness, the structural response of masonry depends on the orientation of mortar joint.

4.2. CONSTITUTIVE LAW

The damage model used is of Faria et al (1998), where they consider the split of stress tensor into tension and compression. It is performed to capture the unilateral behaviour of the material when it passes from tension to compression. The split of effective stress tensor $\bar{\sigma}$ into tension and compression is done according to Ortiz (1985) is presented in equation 4.1 and equation 4.2.

$$\bar{\sigma}^{+} = \sum_{i} \langle \bar{\sigma} \rangle p_i \otimes p_i \qquad \textbf{4.1}$$

$$\bar{\sigma}^{-} = \bar{\sigma} - \bar{\sigma}^{+} \text{、} \qquad \textbf{4.2}$$

Where $\bar{\sigma}_i$ denotes the *i*th principle stress extracted from tensor $\bar{\sigma}$ and p_i corresponds to the unit vector for the associated principle direction. $\langle \bullet \rangle$ Are the Macaulay brackets, which returns the value if positive or zero if negative. The constitutive law is as shown in equation 4.3.

$$\sigma = (1-d^+)\,\bar{\sigma}^+ + (1-d^-)\,\bar{\sigma}^- \qquad \textbf{4.3}$$

The split of the stress is defined according to equation 4.4 and equation 4.5, where equation 4.4 represents the tensile stress and equation 4.5 represents the compressive stresses.

$$\sigma^+ = (1-d^+)\,\bar{\sigma}^+ \qquad \textbf{4.4}$$

$$\sigma^- = (1-d^-)\,\bar{\sigma}^- \qquad \textbf{4.5}$$

This derivation is based on Helmholtz free energy potential of the form

$$\psi(\varepsilon, d^+, d^-) = (1-d^+)\,\psi_0^+(\varepsilon) + (1-d^-)\,\psi_0^-(\varepsilon) \qquad \textbf{4.6}$$

Where $\psi_0^+(\varepsilon)$ and $\psi_0^-(\varepsilon)$ are the elastic free energies, which are defined according to

$$\psi_0^+(\varepsilon) = \frac{1}{2}\bar{\sigma}^+ : C^{-1} : \bar{\sigma} = \frac{1}{2}\bar{\sigma}^+ : \varepsilon \geq 0 \qquad \textbf{4.7}$$

$$\psi_0^-(\varepsilon) = \frac{1}{2}\bar{\sigma}^- : C^{-1} : \bar{\sigma} = \frac{1}{2}\bar{\sigma}^- : \varepsilon \geq 0 \qquad \textbf{4.8}$$

The internal variables consist of plastic strain tensor ε, d^+ and d^- the scalar damage variables linked directly to the tensile and compressive deteriorations assumed as independent variables. Strain tensor is the only single variable admitted.

During any loading process the dissipation of energy is always positive, which states the entropy increases leading to an irreversible process, according to second principle of thermodynamics. The dissipation for an isothermic elasto-damageable process is of the form as shown in equation 4.9, which is according to Clausius-Duhem inequality

$$D = -\dot{\psi} + \sigma : \dot{\varepsilon} = \left(\frac{\partial \psi}{\partial \varepsilon} + \sigma\right) : \dot{\varepsilon} + \psi_0^+ \dot{d}^+ + \psi_0^- \dot{d}^- \geq 0 \qquad \textbf{4.9}$$

To guarantee the positive dissipation, Coleman's method is applied and the constitutive law is obtained as

$$\sigma = \frac{\partial \psi}{\partial \varepsilon} = (1 - d^{+}) \frac{\partial \psi_0^{+}}{\partial \varepsilon} + (1 - d^{-}) \frac{\partial \psi_0^{-}}{\partial \varepsilon} \qquad \textbf{4.10}$$

Since $\psi_0^{+}(\varepsilon)$ and $\psi_0^{-}(\varepsilon)$ are to be positive terms, it can be inferred that the dissipation is according to equation 4.11

$$D = \psi_0^{+} \dot{d}^{+} + \psi_0^{-} \dot{d}^{-} \geq 0 \qquad \textbf{4.11}$$

Which results to satisfy the clausius-Duhem inequality

$$\dot{d}^{\pm} \geq 0 \qquad \textbf{4.12}$$

Considering the equations 4.7 and 4.8, the linear dependency between $\bar{\sigma}$ and ε, the stress split in equation 4.1 and the fact that $\bar{\sigma}^{+}$ and $\bar{\sigma}^{-}$ are first degree homogenous functions of ε, we obtain equation 4.13 and 4.14 according to Euler's theorem .

$$\frac{\partial \psi_0^{+}}{\partial \varepsilon} = \bar{\sigma}^{+} \qquad \textbf{4.13}$$

$$\frac{\partial \psi_0^{-}}{\partial \varepsilon} = \bar{\sigma}^{-} \qquad \textbf{4.14}$$

Substituting equation 4.13 and 4.14 in equation 4.10, we obtain the final form of the constitutive equation (Equation 4.3).For further information regarding the derivation of the constitutive law the reader is advised to refer Faria et al., (1998).

4.2.1. TENSION AND COMPRESSION MODEL

In the present model, Mohr-coulomb failure criterion is used for the tensile and shear failure, and Rui Faria criteria for the compressive failure. The damage surface for both the criterion is shown in Figure 4.1.

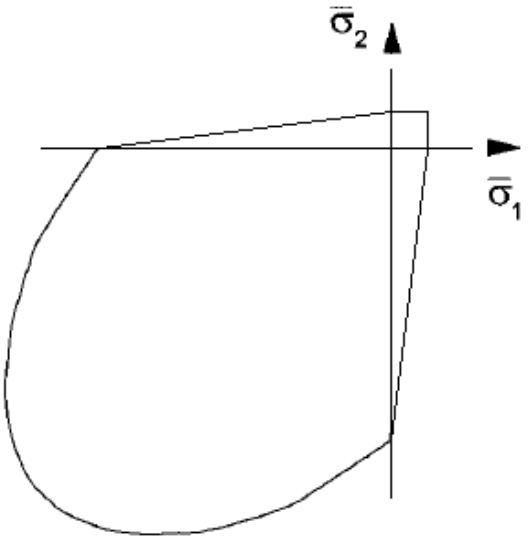

Figure 4.1 Failure criteria for the present model in tension and compression

The Mohr-coulomb failure in terms of shear stress and normal stress is cited in equation 4.15 and in terms of principle stresses is cited in equation 4.16.

$$\tau + \sigma \tan\phi - c_0 = 0 \qquad \textbf{4.15}$$

$$f(\sigma) = \frac{1+\sin\phi}{2}\sigma_{\max}(\sigma) - \frac{1-\sin\phi}{2}\sigma_{\min}(\sigma) - c_0\cos\phi \qquad \textbf{4.16}$$

Similarly the Rui Faria failure condition defining the effective stresses is cited in equation 4.17. Rui Faria failure criterion is similar to Drucker Prager, but the difference is the biaxial failure which can be set in Rui Faria and is unity in Drucker Prager. The effective compressive stresses are dependent on the parameter K, defined according to the equation 4.18. For further information regarding the Rui Faria failure criteria the reader is advised to refer Faria et al. (1998), Pela (2009).

$$\bar{\tau} = \sqrt{3}(K\bar{\sigma}_{oct} + \bar{\tau}_{oct}) \qquad \textbf{4.17}$$

$$K = \sqrt{2}\left(\frac{\bar{f}_{02D} - \bar{f}_0}{2\bar{f}_{02D} - \bar{f}_0}\right) \qquad \textbf{4.18}$$

4.3. BENCH MARK ANALYSIS

An analysis by Berto et al (2005) on the 'Failure mechanism on masonry prism loaded in axial compression' was chosen to perform in COMET software. It was performed in order to validate the software and to check if the constitutive model assumed holds good for the analysis, before running the analysis on the experimental masonry prisms and the cylindrical specimens. This model was chosen as the authors take a similar constitutive model adopted in the present thesis.

Micro modelling is carried out to study the behaviour of masonry under compression. So the brick and the mortar are represented as different elements, where the non-linear behaviour is represented using the isotropic damage model. 3D analysis carried out to capture the out of plane stresses and 2D plane stress analysis to study the differences.

The constitutive model used in Berto et al (2005) is

$$\sigma = (1-d^{+})\,\bar{\sigma}^{+} + (1-d^{-})\,\bar{\sigma}^{-} \qquad \textbf{4.19}$$

Where the evolution of d^{+} and d^{-} the damage variables are expressed in terms as function of $\bar{\tau}^{+}$ and $\bar{\tau}^{-}$

$$d^{+} = 1 - \frac{r_0^{+}}{\bar{\tau}^{+}} e^{\left(A^{+}\left(1-\frac{\bar{\tau}^{+}}{r_0^{+}}\right)\right)} \qquad \textbf{4.20}$$

$$d^{-} = 1 - \frac{r_0^{-}}{\bar{\tau}^{-}}\left(1-B^{-}\right) - B^{-} e^{\left(A^{-}\left(1-\frac{\bar{\tau}^{-}}{r_0^{-}}\right)\right)} \qquad \textbf{4.21}$$

A^{+} depends on the mesh and some characteristics of the material. A^{-} and B^{-} are the material parameters describing the compressive constitutive law.

$$\bar{\tau}^{+} = \sqrt{\bar{\sigma}^{+} : \bar{\sigma}^{+}} \qquad \textbf{4.22}$$

$$\bar{\tau}^{-} = \sqrt{\sqrt{3}(K\bar{\sigma}_{oct}^{-} + \tau_{oct}^{-}} \qquad \textbf{4.23}$$

$$r_0^- = \sqrt{\frac{\sqrt{3}}{3}(K-\sqrt{2})f^-} \qquad \textbf{4.24}$$

The constitutive curves of stress strain for both the uniaxial tension and uniaxial compression is shown in Figure 4.2.

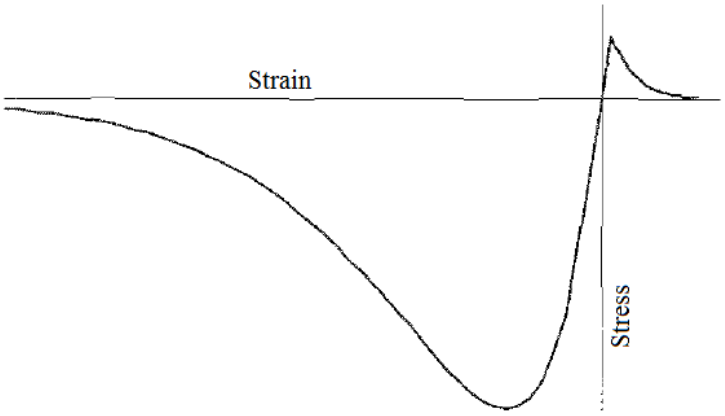

Figure 4.2 Stress strain curve adopted by Berto et al (2005)

A masonry prism with three brick units and two mortar joints was modelled. The dimensions of the brick are 115 x 115 x 60 mm^3 and the mortar joint is 12 mm thick. This resulted in a masonry prism with overall dimension of 115 x 115 x 204 mm^3. The final model for 2D plane stress analysis is shown in the Figure 4.3.

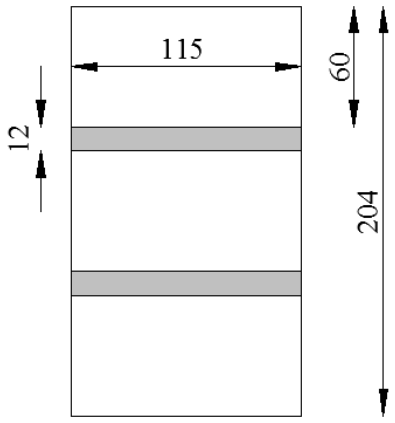

Figure 4.3 Masonry prism

The mechanical parameters assumed for the masonry prism in both the analysis are shown in Table 4.1.

Table 4.1 Mechanical parameter for the prism

	Berto et al (2005)		**Present thesis**	
	Mortar	**Brick**	**Mortar**	**Brick**
Young's Modulus (MPa)	E = 6000	E = 15000	E = 6000	E = 15000
Poisson's Ratio	$\nu = 0.3$	$\nu = 0.1$	$\nu = 0.3$	$\nu = 0.1$
Uniaxial compressive strength (MPa)	$\bar{f}_{1D}^{-} = 5$	$\bar{f}_{1D}^{-} = 14.9$	$\bar{f}_{1D}^{-} = 5$	$\bar{f}_{1D}^{-} = 14.9$
Uniaxial tensile strength (MPa)	$\bar{f}_{0}^{+} = 1.3$	$\bar{f}_{0}^{+} = 1.4$	$\bar{f}_{0}^{+} = 1.3$	$\bar{f}_{0}^{+} = 1.4$
Tensile fracture energy (N/mm)	$G_f = 0.06$	$G_f = 0.08$	$G_f = 0.081$	$G_f = 0.108$
Compressive fracture energy (N/mm)			$G_C = 0.845$	$G_C = 10$
Compression parameter A^-	$A^- = 1$	$A^- = 0.9$	-	-
Compression parameter B^-	$B^- = 1.1$	$B^- = 1.6$	-	-
Ratio $\frac{\bar{f}_{2D}^{-}}{\bar{f}_{1D}^{-}}$	$R_0 = 1.25$	$R_0 = 1.1$	$R_0 = 1.25$	$R_0 = 1.25$
Compressive damage threshold/ Compressive strength ratio	-	-	0.3	0.3

As shown in the table most of the values are same as taken in Berto et al (2005). The only variations of mechanical parameters are the values of compressive fracture energy and the tensile fracture energy. Berto et al assume the fracture energy only below plastic zone of stress displacement diagram. But the present software COMET assumes the fracture energy as the area below the stress displacement graph under both the elastic and the plastic zone. As a result the values for G_f and G_C have higher values than the model in Berto et al (2005). This increment was calculated based on an analysis by trial and error method. The analysis was carried out on a simple triangular element assuming the same mechanical parameters until the stress strain graph of both the models matched. Once the graphs were matched the area below the stress displacement graph was calculated and taken as the fracture energy for both the

tensile and compressive cases in the model. The ratio of compressive damage threshold to the compressive strength ratio, defines the initial linearity of the stress strain curve.

4.3.1. 2D ANALYSIS

Once all the mechanical parameters were assigned to the model, a structured 4 node quadrilateral mesh was created. The size of each mesh was 3 mm in both X and Y direction, resulting in 2652 elements. The final mesh of both the models is shown in Figure 4.4. The mesh was more refined in the present case with respect to 340 elements as in the reference model.

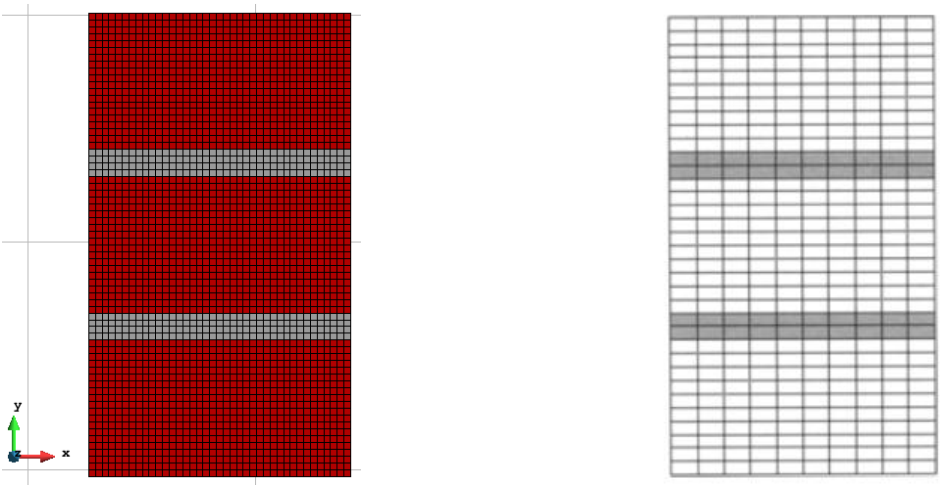

(a) **(b)**

Figure 4.4 2-Dimensional mesh (a) Present model (b) Berto et al (2005)

The bottom of the masonry prism was fixed in both X and Y direction, the only boundary constraint in the model. Load was applied in terms of displacement on top instead of applying the force directly. This was performed to obtain the post peak behaviour. The results obtained from the analysis are shown in Figure 4.5, where the comparison of the tensile damage and the compressive damage are shown.

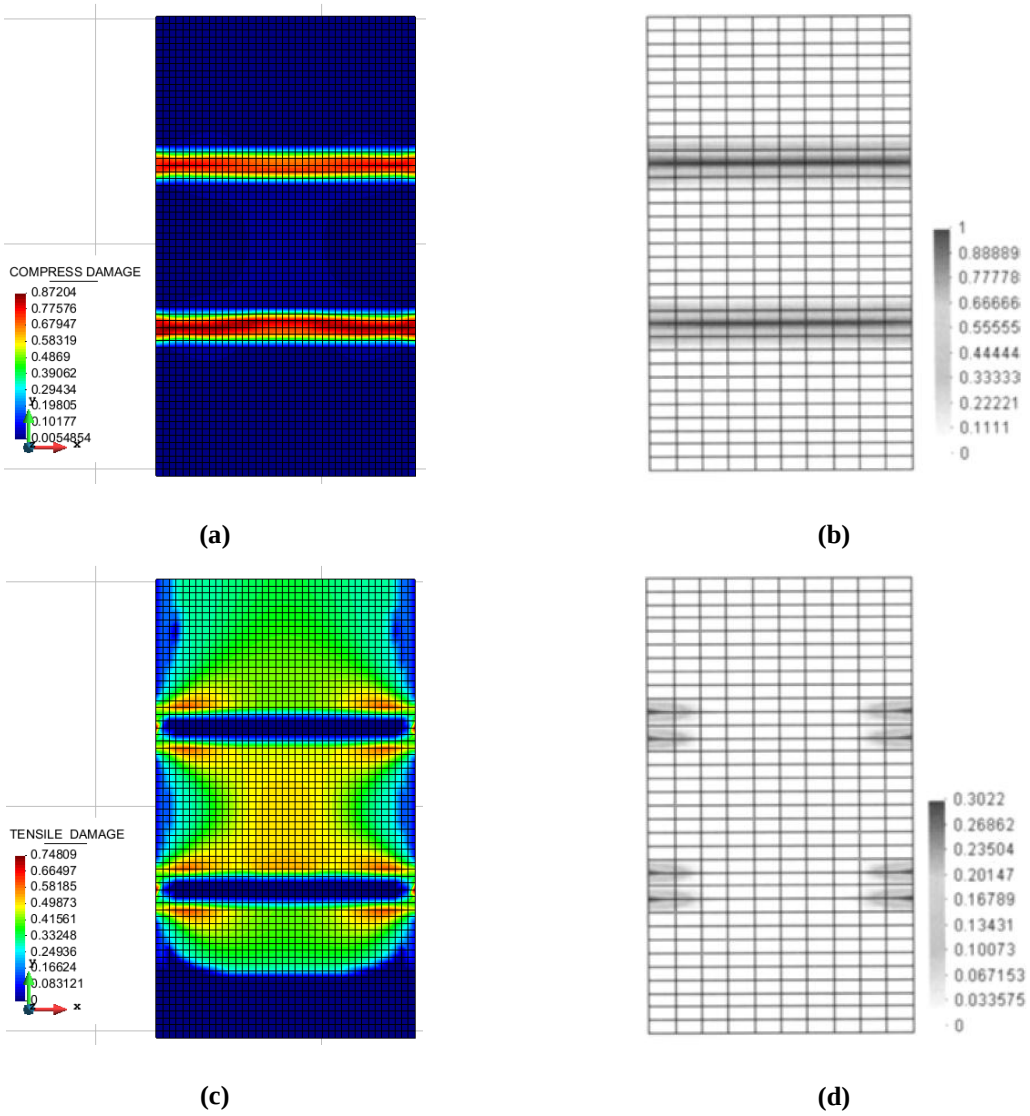

Figure 4.5 2D Plane stress analysis: contours of the damage variable at failure (a) & (b) Compressive damage d^- of present and Berto model (c) & (d) Tensile damage d^+ of present and Berto model

As it can be seen from the figures, the failure is due to the compression in mortar joints than the tensile damage of the brick. The tensile damage is concentrated near the edges of the mortar joint and in the middle of the central brick, even though the damage in the central brick is half of the mortar damage. This is due to, the plane stress analysis which is unable to capture the real behaviour of the masonry in compression viz. the confining effect of the stresses in the out of plane direction of the prism. This results, in underestimation of the compressive strength of the mortar and delays the failure of the bricks in tension.

The maximum compressive stress obtained from the analysis is 5.88 MPa, corresponding to a displacement of 0.12 mm and the tensile stress is 0.6 MPa. The tensile stress and the compressive stresses at this peak is shown in Figure 4.6.

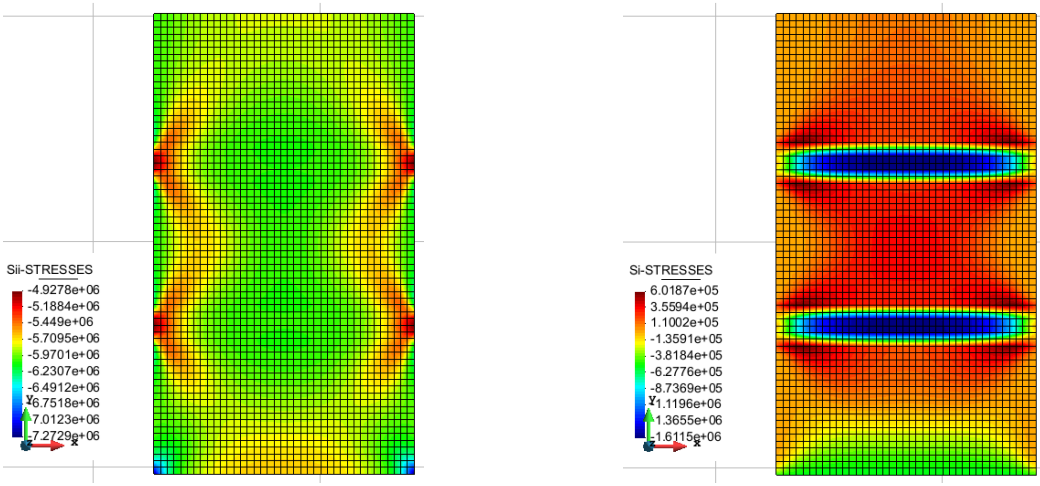

(a) **(b)**

Figure 4.6 2D Plane stress analysis (a) Compressive stress distribution & (b) Tensile stress distribution

The stress strain distribution is shown in Graph 4.1. It can be clearly seen from the graph that both the analysis gives almost the same results. The Berto analysis does not give any softening curve. This is due to the fact that the compressive fracture energy of mortar is just sufficient enough to cause the failure and obtain a slightly inclined straight line.

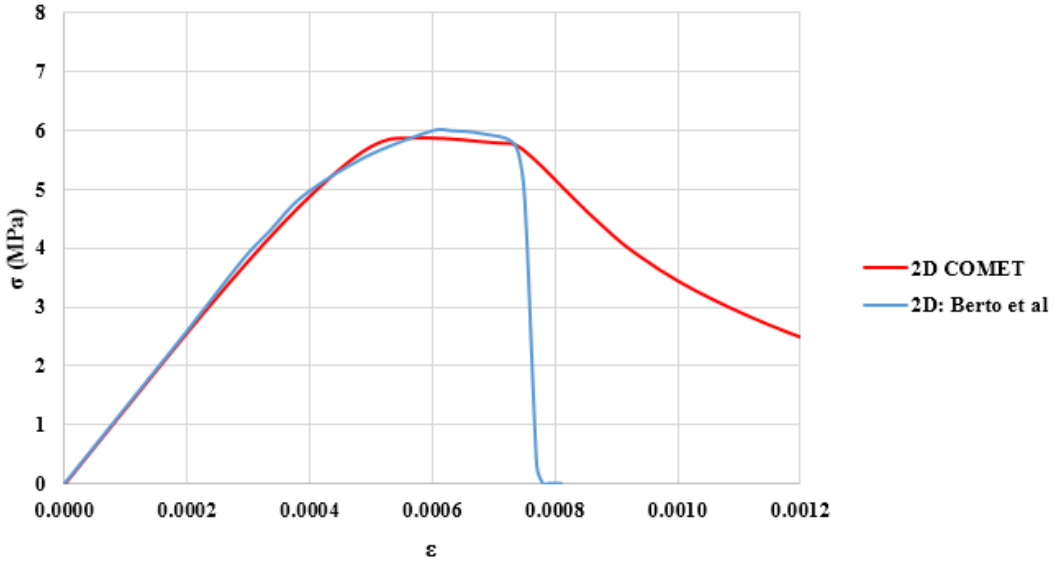

Graph 4.1 2D Plane stress analysis: Stress strain diagram

The plane stress analysis results in the failure of mortar in compression. In order to evaluate if the plane stress analysis gives the proper results, 3D analysis is carried out which is performed as below.

4.3.2. 3D ANALYSIS

Same properties as in the case of 2D plane stress analysis were assigned to the materials in this case. The mesh element is a structured 4 node tetrahedron with 8.5 x 8.5 x 16.5 mm^3 being the dimension of each tetrahedron, resulting in a total of 6762 elements with respect to 3400 elements of 3D Berto model. The final meshes of both the models are shown in Figure 4.7.

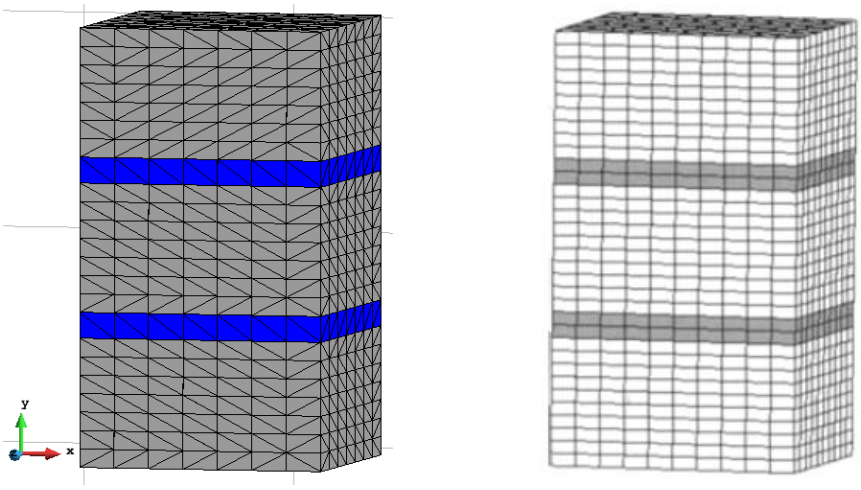

(a) **(b)**

Figure 4.7 3D Model (a) Present Model (b) Berto Model

The bottom surface of the model is fixed in all directions, the only boundary condition assigned to the model. The loading is applied on top surface in terms of displacement to capture the softening curve. The results obtained from the analysis are shown in Figure 4.8.
As it can be seen from the figure, the failure is governed by the tensile failure of the brick rather than the compressive failure of the mortar as in 2D plane strain analysis. This is due to the consideration of stresses acting in the z-direction, which contributes to the tension of brick in the direction. The tensile stresses acting on the brick produces confinement effect on mortar in both x and z-direction, as a result the mortar is subjected to triaxial compression. The compressive failure can be seen only in the edge of the mortar layer (Figure 4.8 (a) and (b)).

The splitting tensile failure is in the middle of the central brick, which is the usual mode of failure for masonry with the combination of weak mortar joint and stronger bricks.

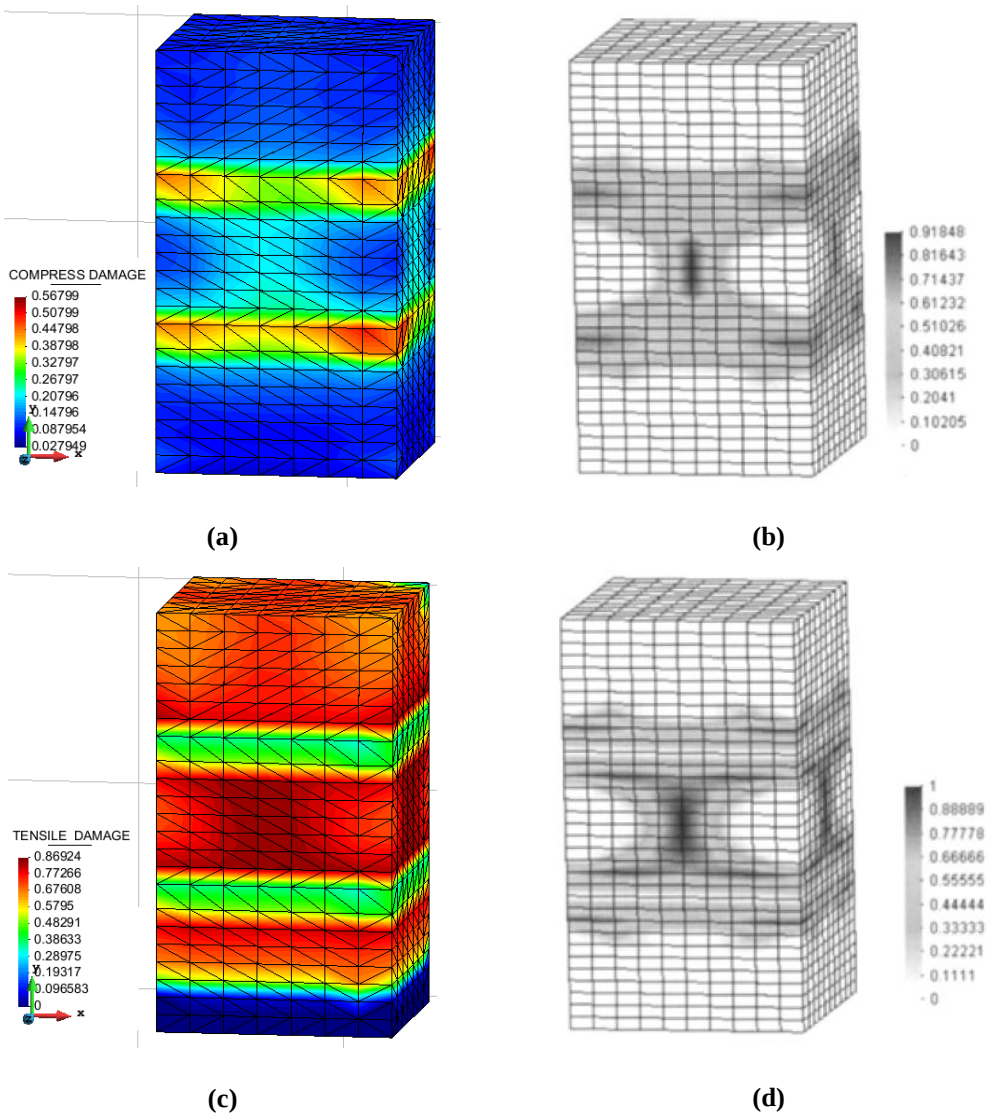

Figure 4.8 3D Model (a) & (b) Compressive damage of present 3D and Berto model (c) & (d) Tensile damage of present 3D and Berto model

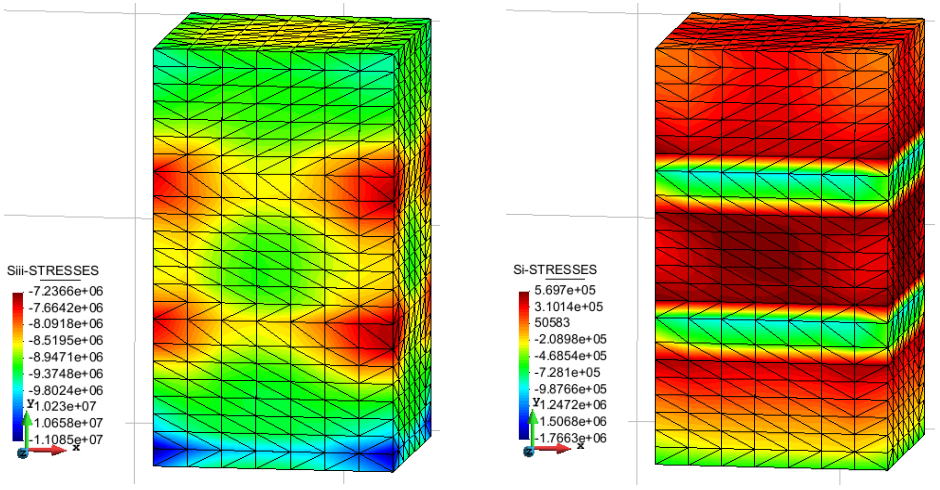

(a) **(b)**

Figure 4.9 3D Model: Stress distribution at peak (a) Compression & (b) Tension

The maximum compressive stress obtained from the analysis is 8.88 MPa and the maximum tensile stress is 0.7 MPa, which are closer to the values obtained by the analysis carried out in Berto et al (2005). The compressive and the tensile stress distributions at peak in the present analysis are shown in Figure 4.9 along with the reference model graph. The stress strain distribution is show in Graph 4.2.

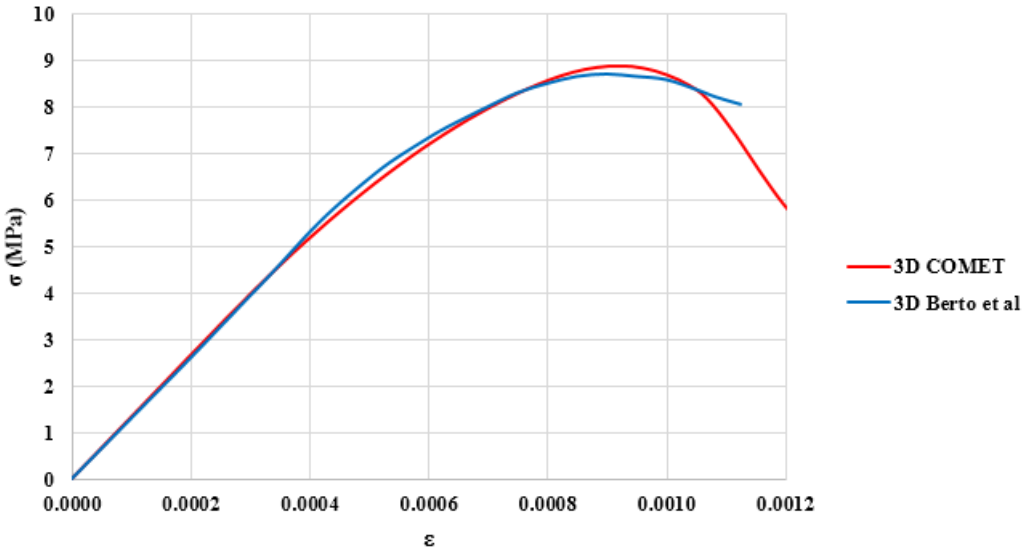

Graph 4.2 3D Model: Comparison of stress strain distribution

4.3.3. RESULTS AND DISCUSSION

The stress strain diagrams in 2D and 3D analysis are shown in Graph 4.3. The compressive strength of the prism obtained from the present 3D analysis is 8.88 MPa in comparison to the compressive strength obtained from 2D analysis with 5.80 MPa, with an error of 34.68%. But the strength is lower than the strength of brick (14.9 MPa) and greater than the strength of mortar (5.0 MPa), is as expected from a weak mortar and strong brick combination. The 2D plane stress analysis results not only in lower compressive strength but also in wrong failure mode of the model viz. the compressive failure of the mortar than the tensile failure of the brick.

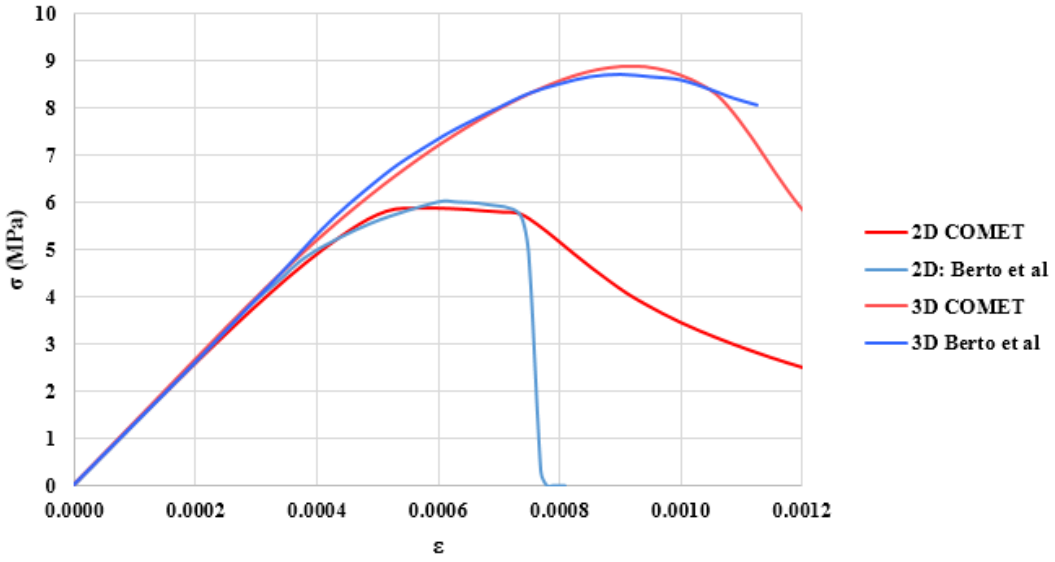

Graph 4.3 Comparison of Stress strain graph by GiD and Berto et al (2005)

The main purpose here was to compare the results obtained from the analysis carried out by Berto et al (2005) and the results from the present analysis carried out in COMET. It can be concluded that after comparing the results of tensile damage, compressive damage, tensile stress distribution and the compressive stress distribution the results match almost in perfect. The only modification which was needed to be carried out is the estimation of fracture energy for tension and in compression. With the results compared, it can be concluded that the software is validated for the prism and cylindrical analysis to be carried out.

4.4. MODELLING OF STACK PRISM

A 3 dimensional masonry prism was modelled with the same dimensions as tested in the laboratory. The dimension of brick is 277 x 133 x 43 mm^3 and the thickness of mortar joints as 10 mm. The prism consisted of five stacked units with four layers of mortar in between. Two layers of mortar were laid on top and at the bottom in the experiments to reduce the effect of the loading beam on the prism. This layer is modelled with the same properties of brick, to reduce the confining effect of the mortar acting on the brick.

The overall dimension of the masonry prism is 276 x 280 x 133 mm^3, including the top and bottom mortar layer with 12.5 mm each. Since the prism is symmetrical in all the directions, only one eight of the prism is modelled to get more refined mesh. The dimension of the modelled prism is 138 x 140 x 66.5 mm^3.

The mechanical properties assigned to the brick and the mortar is shown below in Table 4.2.

Table 4.2 Mechanical properties of Masonry prism

	Masonry prism	
	Mortar	**Brick**
Young's Modulus (MPa)	1500	6671
Poisson's Ratio	0.196	0.1
Uniaxial compressive strength (MPa)	5.5	30.8
Uniaxial tensile strength (MPa)	1	1.18
Tensile fracture energy (N/mm)	0.3	0.5
Compressive fracture energy (N/mm)	1.75	40

Initially the same properties of the experimental tests were assigned to brick and mortar. But the results were very low compared to the experimental values. As a result sensitivity analysis and curve fitting is carried out to understand which parameter affects the results and to match with the experimental results.

In general, sensitivity analysis is a method to determine the effects of individual parameters acting on the model and curve fitting is a process of matching an analytical function or mathematical expression to empirical data or vice versa. As the failure of the prism in this case is due to tensile strength of brick and the compressive strength of mortar, these values

affected the results according to the sensitivity analysis. The tensile fracture energy of brick and the compressive fracture energy of the mortar plays a role, controlling the failure and the softening curve. The Young's modulus of mortar was improved from 500 MPa to 1500 MPa, since the experimental value is very low. This is probably due to the errors in estimating the Young's modulus of elasticity. The final mechanical properties assigned to the 3D model are shown in Table 4.2.

After assigning the mechanical parameters, a structured 8 node hexahedron mesh was created with 11760 elements. The size of each hexahedron is 5 x 5 x 5 mm^3. The final mesh is shown in Figure 4.10. The boundary constraints were assigned to the three planes representing the axis of symmetry in XY, YZ and XZ plane to represent the continuity of the prism in the respective directional planes. Instead of applying force on top of the surface, the displacement is applied in negative Y direction.

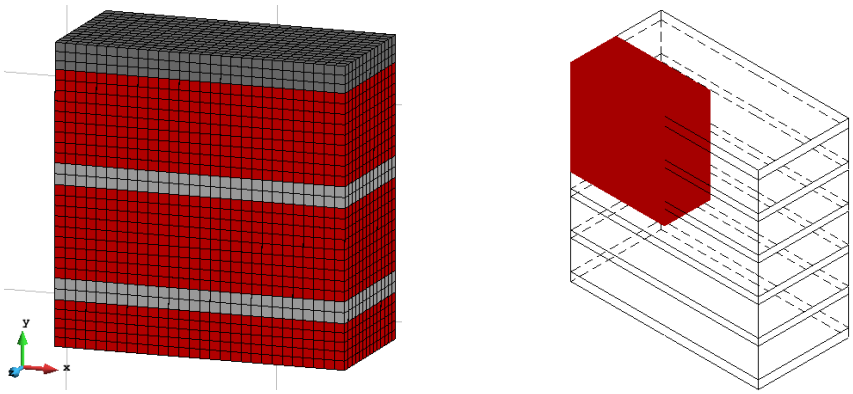

Figure 4.10 3-Dimensional mesh and modelled part of the masonry prism

4.4.1. RESULTS

The results of tensile damage, compressive damage, tensile stress distribution, compressive stress distribution and the vector distribution of stresses are shown from Figure 4.11 to Figure 4.15. The force displacement diagram of the numerical analysis is shown in Graph 4.4. Points 1, 2, 3 and 4 are the different steps showing the distribution of results for different values of force and displacement (Table 4.3). Point 1 and 2 lie in the elastic part, point 3 is the peak value of the analysis and point 4 is just after the peak.

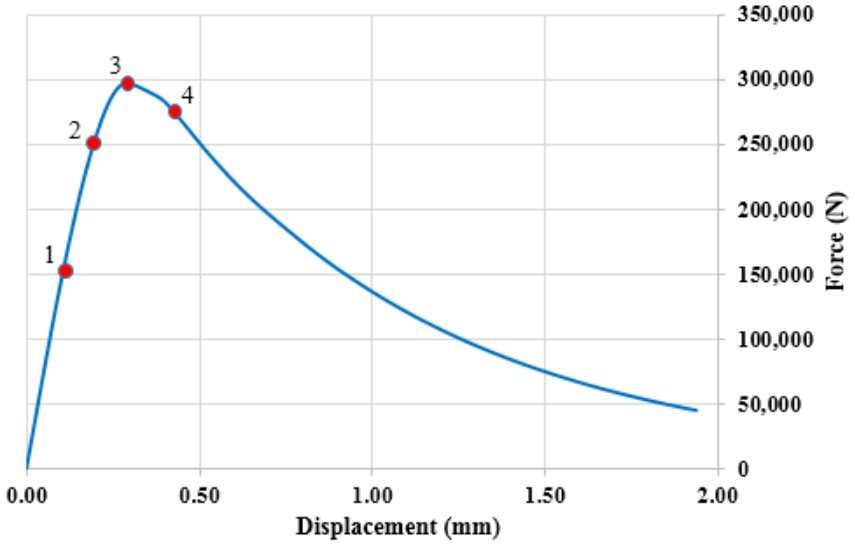

Graph 4.4 Force displacement diagram of masonry prism

The displacement of the prism is measured at the same points as the experimental results were measured, viz., from the centre of the second brick to the centre of the fourth brick. It is based on the code EN 1052-1:1998, Determination of compressive strength. The relative displacements are plot in both the cases. The displacements were also compared from the central top of the first brick to the central bottom of the bottom brick, to compare if there are any major differences in the results. But the difference of only 0.01 mm was obtained and hence the results are not shown.

Table 4.3 Description of points, presented in the force displacement graph

Point Number	Force (N)	Displacement (mm)
1 – Step 14	152000	0.106
2 – Step 25	254000	0.200
3 – Step 34	297000	0.287
4 – Step 39	283000	0.400

The evolution of tensile damage in prism is summarised as shown along the four points in Figure 4.11. It can be seen that the tensile damage initiates in the edges of brick on the external part, and the damage being only 11%. There is no tensile damage found in the mortar throughout the analysis. As there is increment in force, the tensile damage originates in the brick and reaches a high value of damage in short intervals. The damage is distributed in all the bricks with the 2nd, 3rd and the 4th bricks undergoing maximum damage. The damage in

central part of brick initiates at 66% (196 kN) of the maximum load, sustains the load up to a displacement of 0.05 mm from it and finally fails at 297 kN with a total displacement of 0.287 mm.

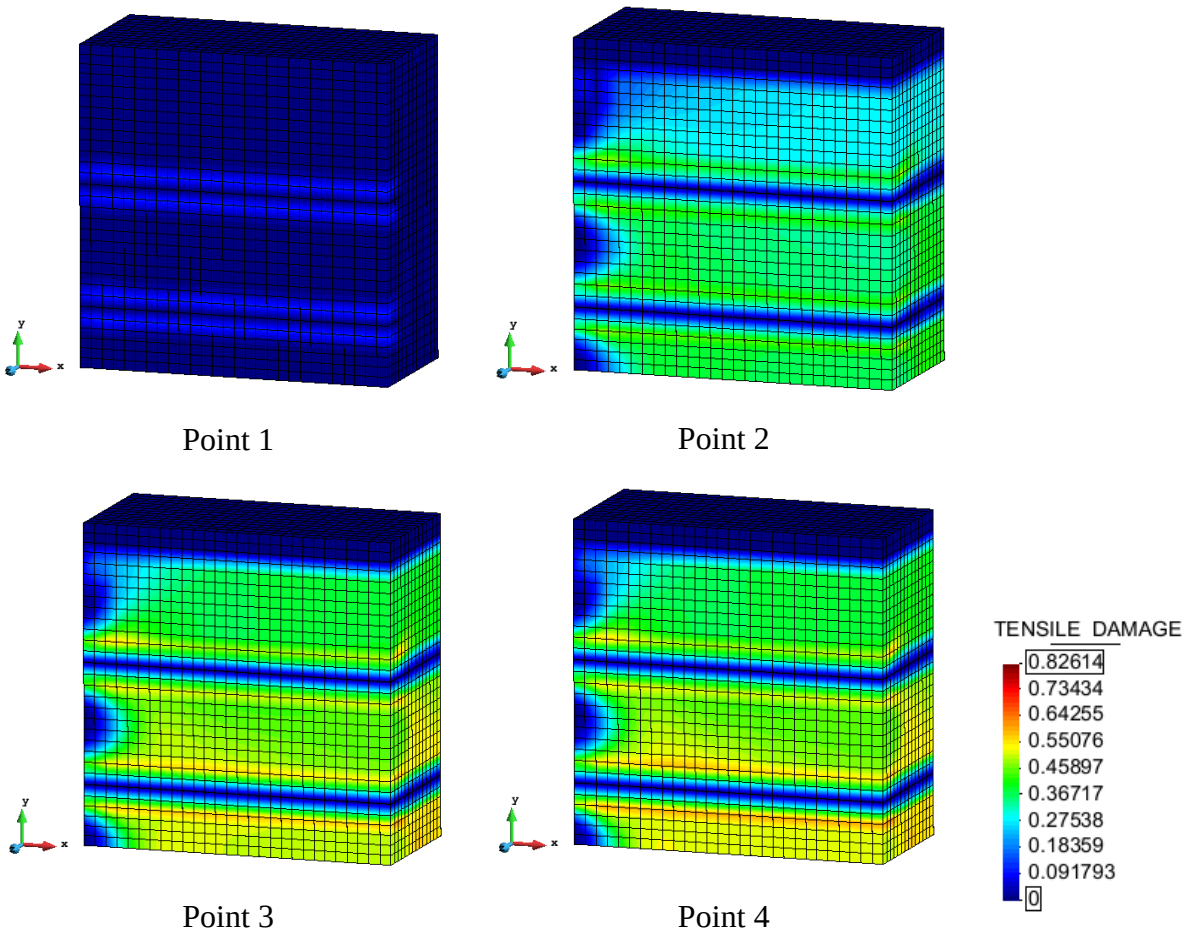

Figure 4.11 Tensile damage evolution

The evolution of compressive damage is shown in Figure 4.12. The compressive damage originates in the very initial stages in the mortar. In the first point, the compressive damage is around 11%, and in second point it reaches 35%. Finally at the peak strength, the damage is equal to 63%. There is no compressive damage found in brick throughout the analysis, as can be seen in Figure 4.12. It is due to the high compressive strength of brick with respect to mortar.

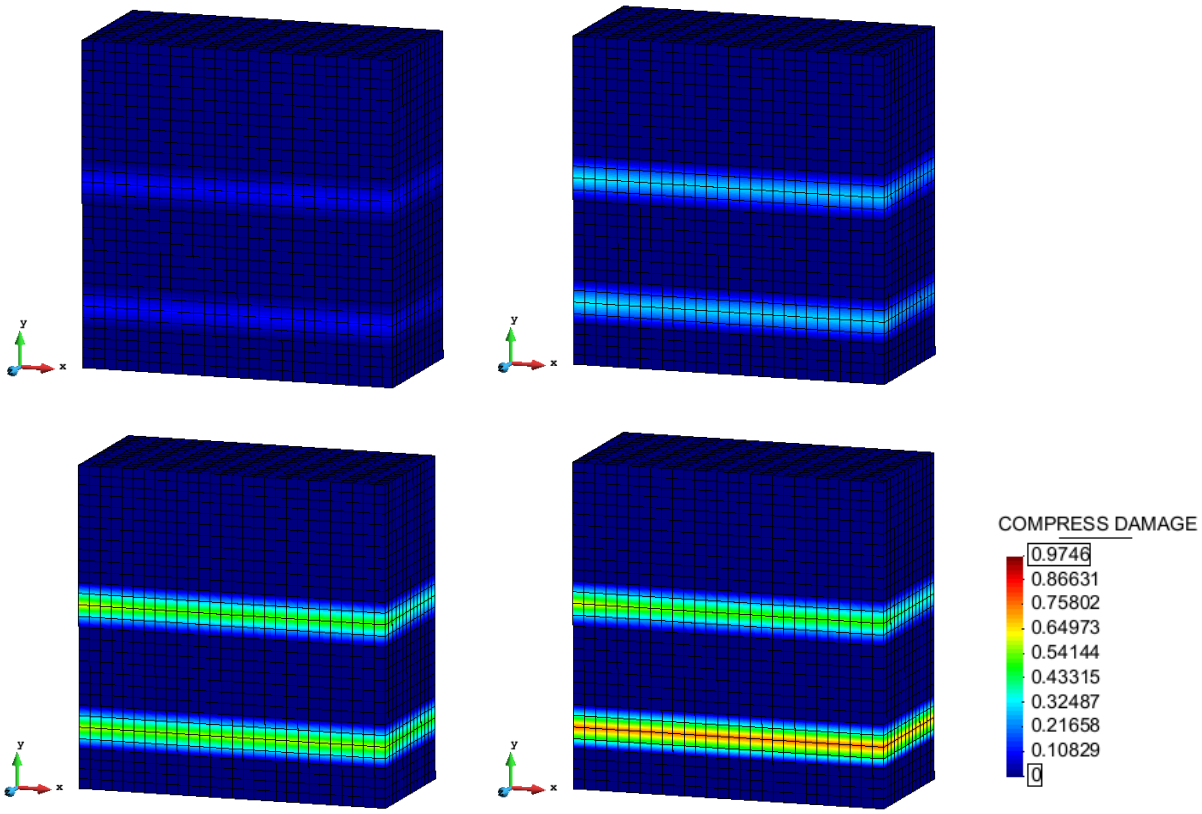

Figure 4.12 Compressive damage evolution of masonry prism

The principle tensile stress distribution is almost the same trend of tensile damage along with the stress values. In the elastic phase the tensile stresses are in the range of 0.36 MPa, as the loading continues the stresses increase to 0.53 MPa in the second point and 0.62 MPa at peak strength of masonry at point 3. But the maximum tensile stresses are obtained at point 4 with a value of 0.67 MPa, at which there is complete failure of the brick and the masonry as a whole (Figure 4.13).

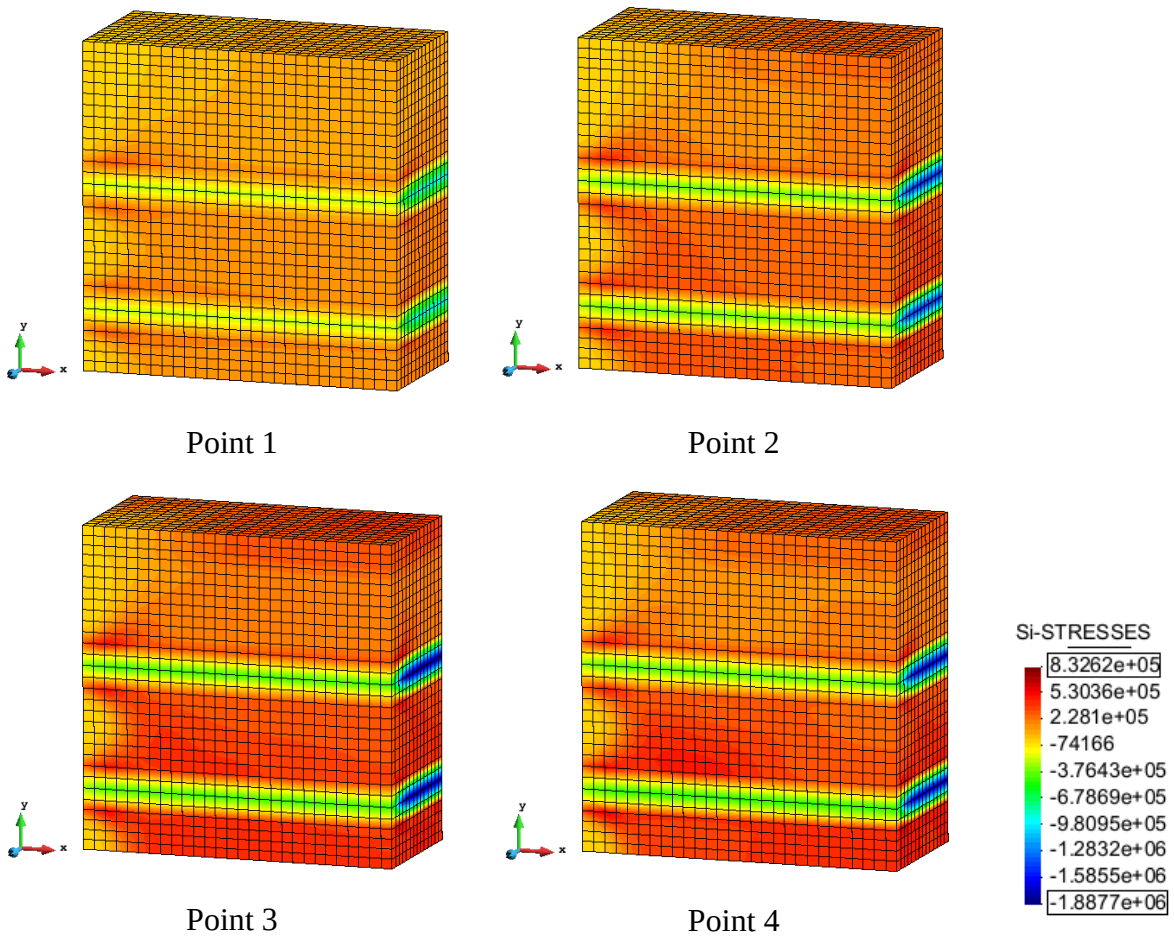

Figure 4.13 Principle tensile stress distribution in Masonry prism

The principle compressive stress distribution of the masonry prism is shown in Figure 4.14. The mortar is subjected to compression right from the initial stages of loading. The maximum elastic compressive stress of prism is 0.56 MPa (second point) and peak stress is 0.57 MPa (third point), both being in mortar. At point 4 the strength of masonry decreases to 0.53 MPa where it is in the softening part.

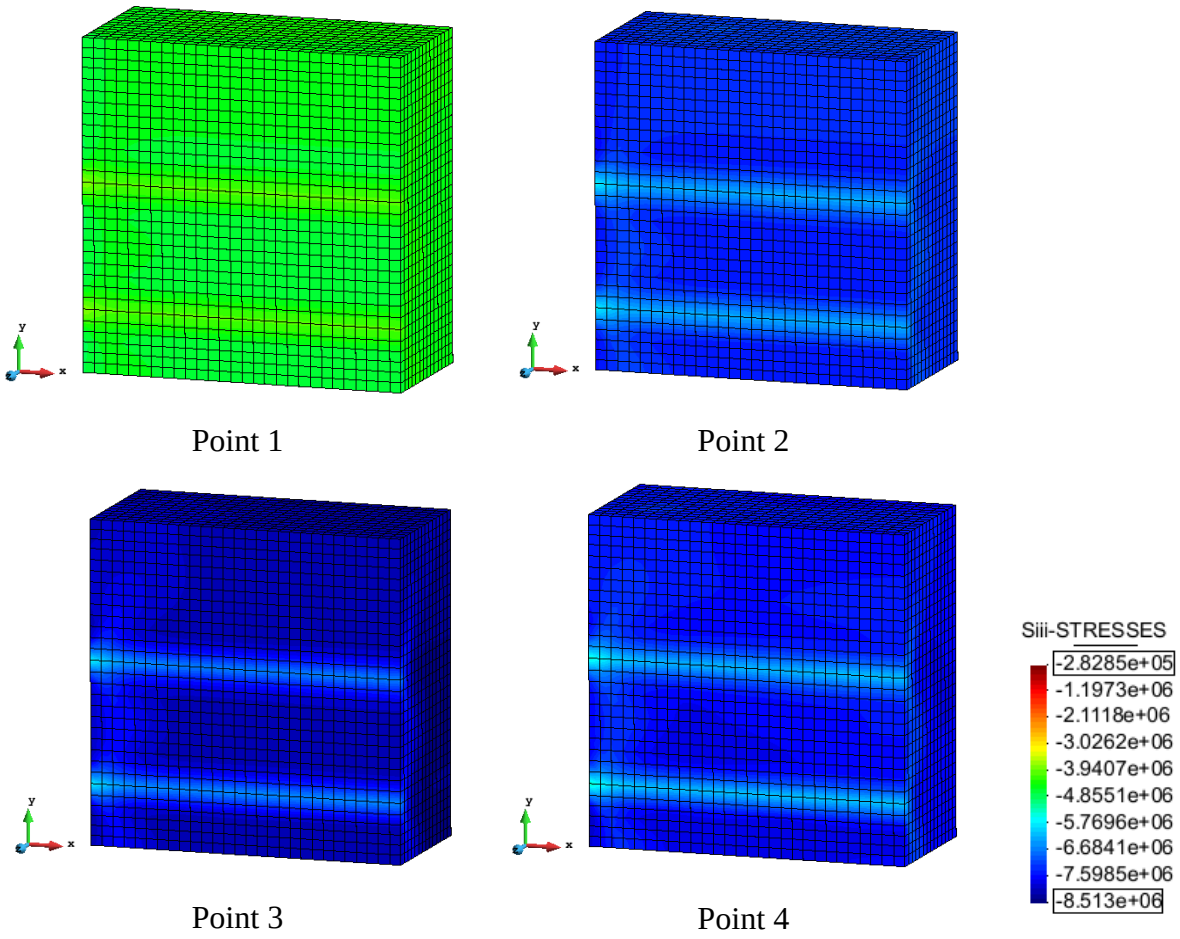

Figure 4.14 Principle compressive stress distribution in Masonry prism

The tensile and the compressive stress distribution are better represented in vector form. Vector stress distribution at peak strength (point 3) is shown in Figure 4.15. The compressive stress distribution is in the loading direction and the tensile stress distribution can be seen in both X and in Z direction.

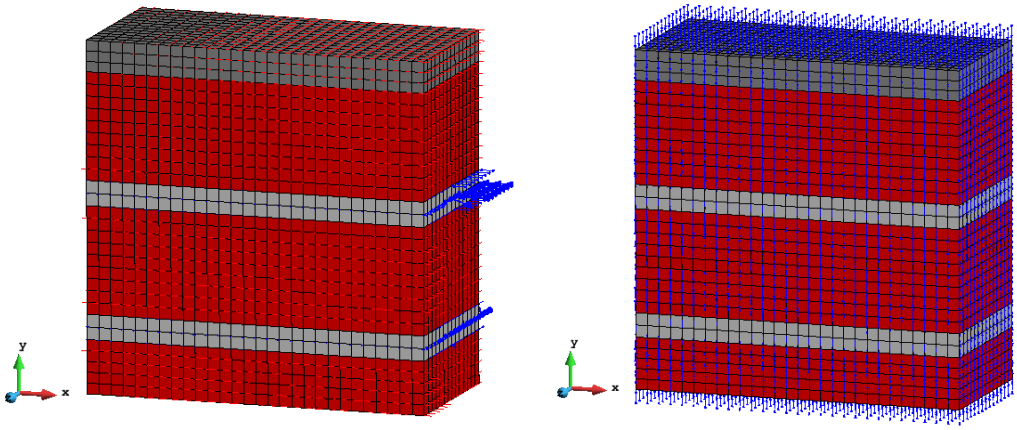

Figure 4.15 Vector distribution of stresses in Masonry prism

4.4.2. COMPARISON OF RESULTS

In the first point, both the tensile (brick) and compressive (mortar) damage are in the range of 11%. As the loading increases and the second point is reached, the tensile damage is 52% and the compressive damage is at 35%. But it is in third point, when the peak strength of masonry is reached, both the compressive damage of mortar and the tensile damage of brick reach 63% of damage. At this point there is failure of masonry.

This proves that the tensile damage acting on the brick governs the failure than the compressive damage acting in the mortar. As seen from the numerical analysis the compressive fracture energy dominates until the peak of masonry is reached. Once the peak strength of masonry is achieved, then the tensile fracture energy of the brick takes over, controlling the softening curve. This draws us to the conclusion that the compressive fracture energy of mortar and the tensile fracture energy of brick plays an important role in achieving the peak strength of masonry and controlling the post peak behaviour of masonry.

The maximum tensile strength is 0.62 MPa, whereas the tensile strength of brick is 1.52 MPa and of mortar is 1 MPa. The compressive stress is almost the same due to equilibrium. This is due to the fact that the tensile failure of brick corresponds to a lower tensile stress than in 1D case, as there is vertical compression and biaxial tension acting in brick. The peak compressive stress of masonry prism obtained from the results of numerical analysis is 8.10 MPa. The compressive strength of the prism falls in between the compressive strength of brick (30.8 MPa) and mortar (5.5 MPa).

The comparison of force displacement diagram of the numerical analysis along with the experimental results is shown in Graph 4.5. The curves of the experimental results are cleaned for better representation and comparison. The blue line represents the numerical curve, the red and yellow line represent the two experimental curves of stack prism 2 and stack prism 3. The softening curve of the experimental results are not obtained since the LVDT's used to measure the displacements were removed not to damage the measuring instruments.

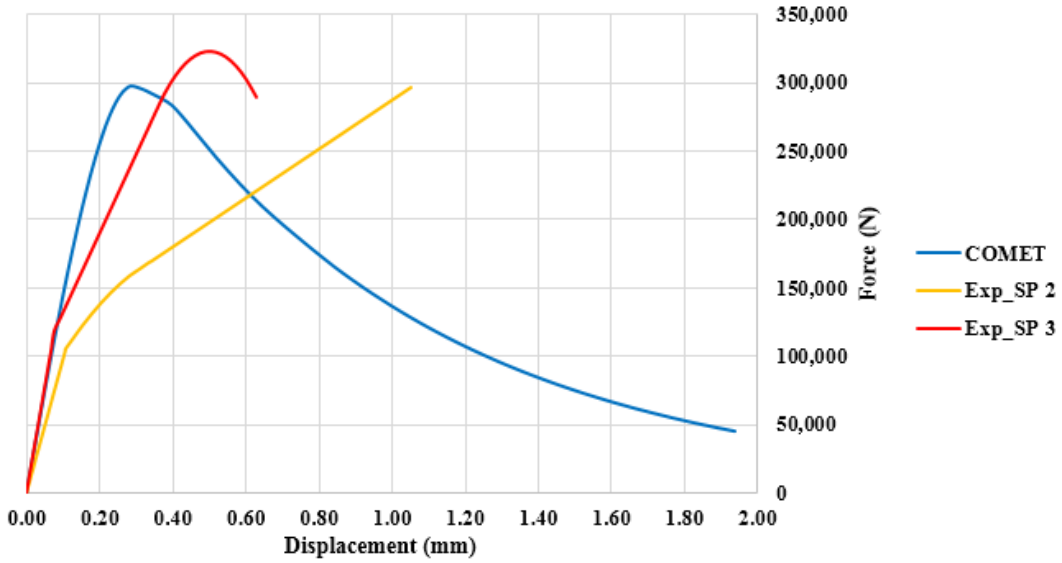

Graph 4.5 Comparison of Force displacement diagram of numerical analysis with experimental results

The initial stiffness of numerical curve and the experimental stack prism 3, match almost in perfect. The average compressive stress of the masonry prism obtained from the experimental result is 8.34 MPa and that of the numerical analysis is 8.10 MPa with an error of 2.87%. The comparison is shown in Table 4.4.

Table 4.4 Comparison of Experimental and numerical results of masonry prism

	Experimental (Average)	**Numerical**	**Percentage difference (%)**
Compressive stress (MPa)	8.34	8.10	-2.87
Modulus of Elasticity (MPa)	3780.3	4139.5	9.50

5. MODELLING OF CYLINDRICAL SPECIMENS

A 3 dimensional model with the same dimensions as tested in the laboratory is modelled in the finite element software COMET. The cylinder has a diameter of 150 mm, with the regularization mortar of height 30 mm at the centre and a width of 100 mm, the overall thickness of the specimen is 133 mm. The cylinder consists of four parts of bricks, two horizontal and a vertical mortar joint. Thickness of mortar layer is 15 mm. Because of symmetry only one quarter of the specimen is modelled to have more elements for finer mesh. Axis of symmetry is assigned to XY plane and XZ plane representing the continuity of the model.

8 noded hexahedron mesh elements are used, with average size of each hexahedron being 4 x 4 x 7 mm^3. The model consists of 8208 elements and is shown in Figure 5.1. The mechanical parameters assigned to units and the bricks are shown in Table 5.1.

Table 5.1 Mechanical properties of cylindrical three joint specimen

	Cylindrical specimen	
	Mortar	**Brick**
Young's Modulus (MPa)	1500	6671
Poisson's Ratio	0.196	0.1
Uniaxial compressive strength (MPa)	5.5	30.8
Uniaxial tensile strength (MPa)	1	1.52
Tensile fracture energy (N/mm)	0.3	0.5
Compressive fracture energy (N/mm)	4	10

The properties assigned to the model are similar to the properties of the masonry prism. Since the sensitivity analysis was carried out to validate the model of masonry prism. Loading is applied in terms of displacement to capture the post peak behaviour. For further details regarding the properties assigned, the reader is advised to refer section 4.4.

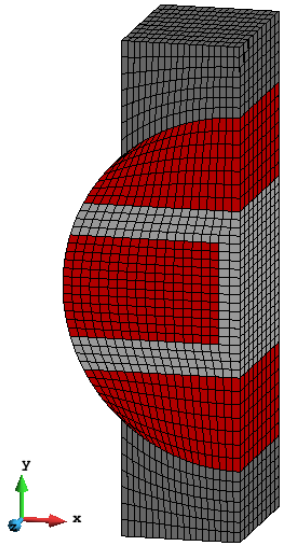

Figure 5.1 Final mesh of the three joint cylindrical specimen

Before performing the non-linear analysis, linear analysis is carried out to validate the numerical model by using experimental results and to understand the initiation of damage. For this reason, first the results of linear analysis are presented and then the non-linear analysis. The explanation for the evolution of damage is discussed throughout the results of non-linear analysis.

5.1. LINEAR ANALYSIS: THREE JOINT SPECIMEN

As linear analysis is performed there is no damage in tension and in compression. The tensile and compressive stresses distribution for a force of 20,000 N is shown in Figure 5.2.

It can be seen in the figure the presence of tensile stresses are closer to mortar in the top and bottom bricks and also distributed throughout the central brick. The compressive stresses assume higher values in the central part of the specimen, according to a sand glass shape, with peaks along the vertical side of the intermediate brick.

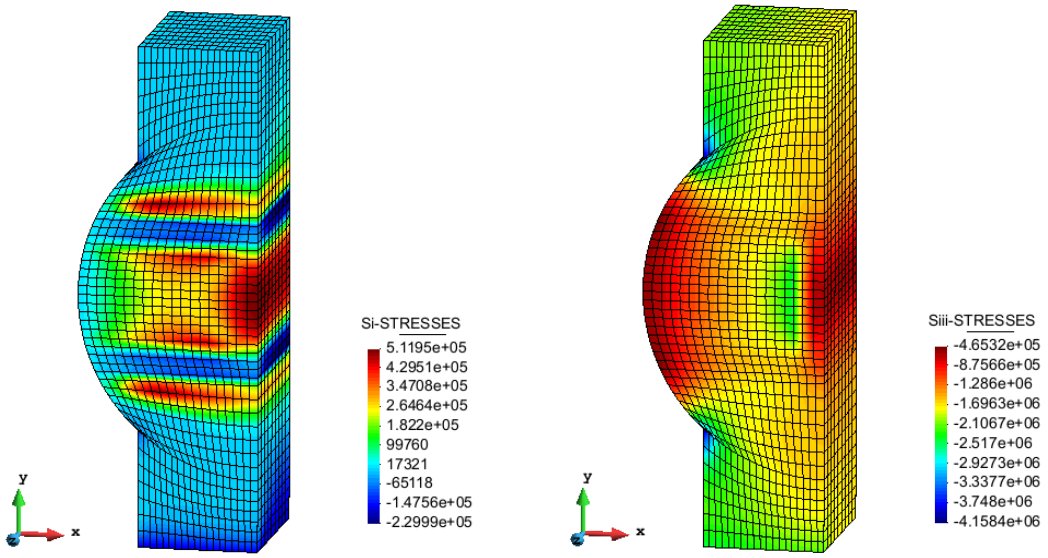

Figure 5.2 Principle tensile and principle compressive stress the in elastic range

For the stresses shown above, a comparison of stress distribution along X, Y and Z are shown from Figure 5.4 to Figure 5.6. Three surfaces chosen are the central surface of the top brick, central surface of the top horizontal mortar and the central surface of the central brick (center of the cylinder) shown in Figure 5.3. In all the three figures the stress in 'x' direction is represented by red line (and surface), the stress in 'y' direction by blue and 'z' in green. If the stresses are above the reference plane then it is tensile stress and if below, compressive stress.

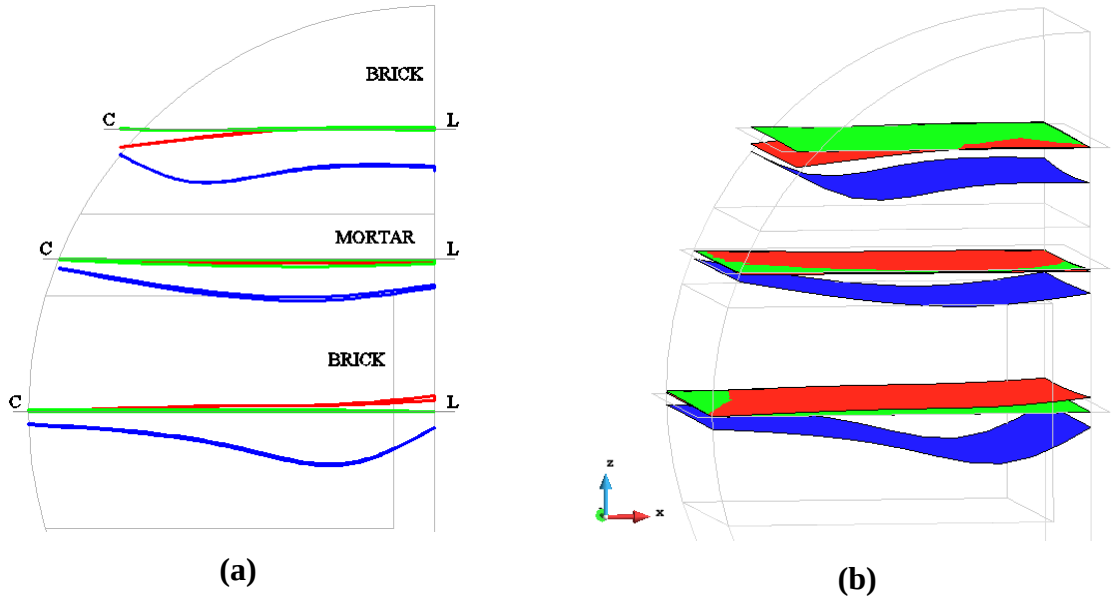

(a) **(b)**

Figure 5.3 Stress distribution along different layers σ_{xx} (red), σ_{yy} (blue) and σ_{zz} (green) (a) 2D (b) 3D

In the center of the top brick shown in Figure 5.4, the compressive stresses are maximum at one quarter on the left side. This is due to concentration of stresses by the regularization mortar above it. The compressive stress is in the range of 1-2 MPa. In the other parts of the plane the stresses in 'x' and 'z' vary from tension to compression. Where the stresses in 'x' are from +0.01 MPa to -0.70 MPa. In 'z' direction the tensile stresses increase from the outer surface towards the central core of the specimen. The increment is from -5.0 kPa to 85 kPa at the center. In the central line of the top brick surface the average stress distribution can be summarised as $\sigma_{xx} = 0.224\sigma_{yy}$ and $\sigma_{zz} = -0.04\sigma_{yy}$

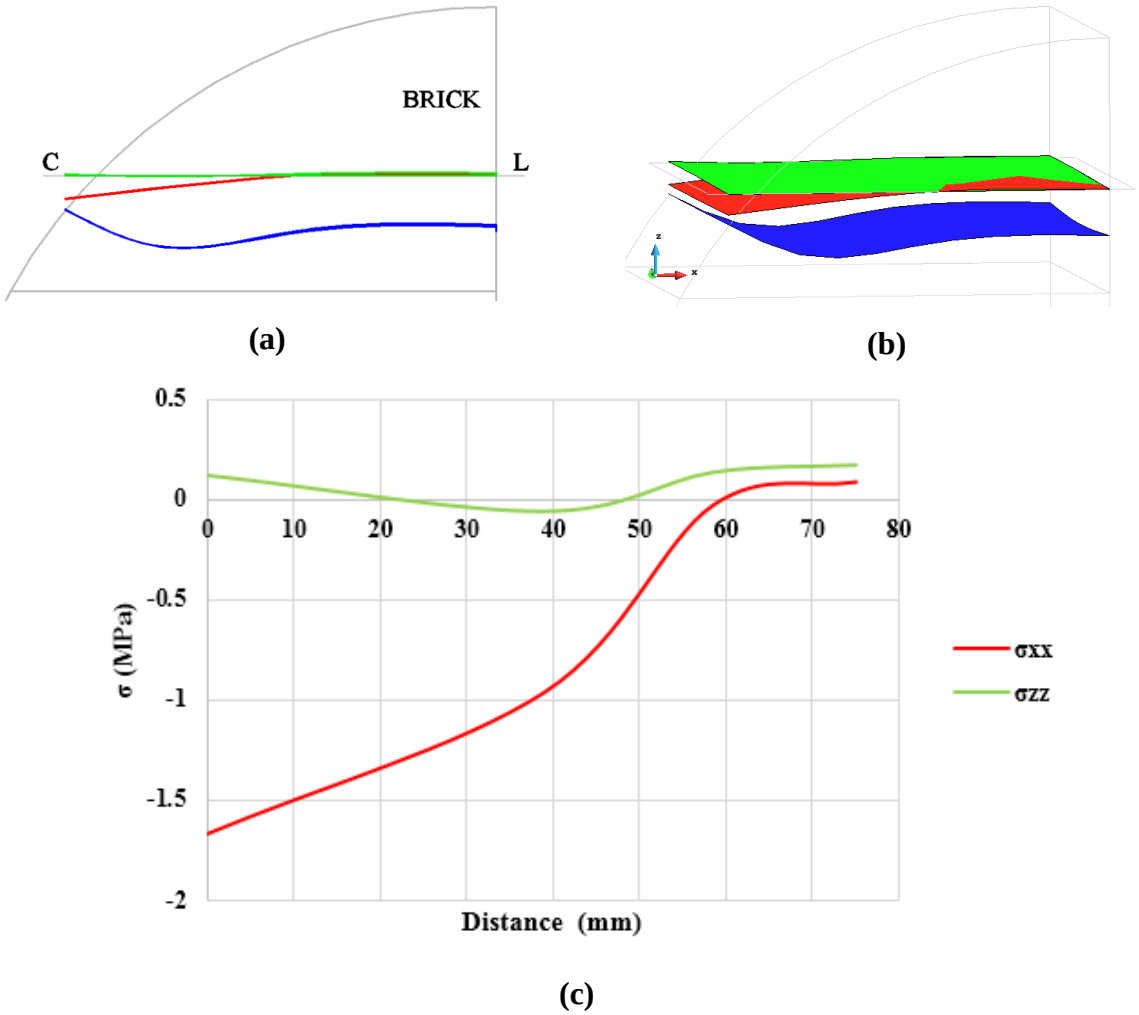

Figure 5.4 Stress distribution in (a) 2D and (b) 3D in the center of the top brick & (c) σ_{xx} and σ_{zz} along the central line of top brick surface, σ_{xx} (red), σ_{yy} (blue) and σ_{zz} (green)

In the central mortar surface the stresses are in compression throughout, where the stresses in 'y' direction are dominating due to the load (0.4-1.8 MPa). In 'x' the stress in compression varies from 0.05-0.25 MPa and in 'z' varies from 0.07-0.34 MPa. In the central line of the top mortar surface the average relation of stresses in 'x', 'y' and 'z' is $\sigma_{xx} = 0.15\sigma_{yy}$ and $\sigma_{zz} = 0.17\sigma_{yy}$. The 2D and 3D representation of the stresses are shown in Figure 5.5.

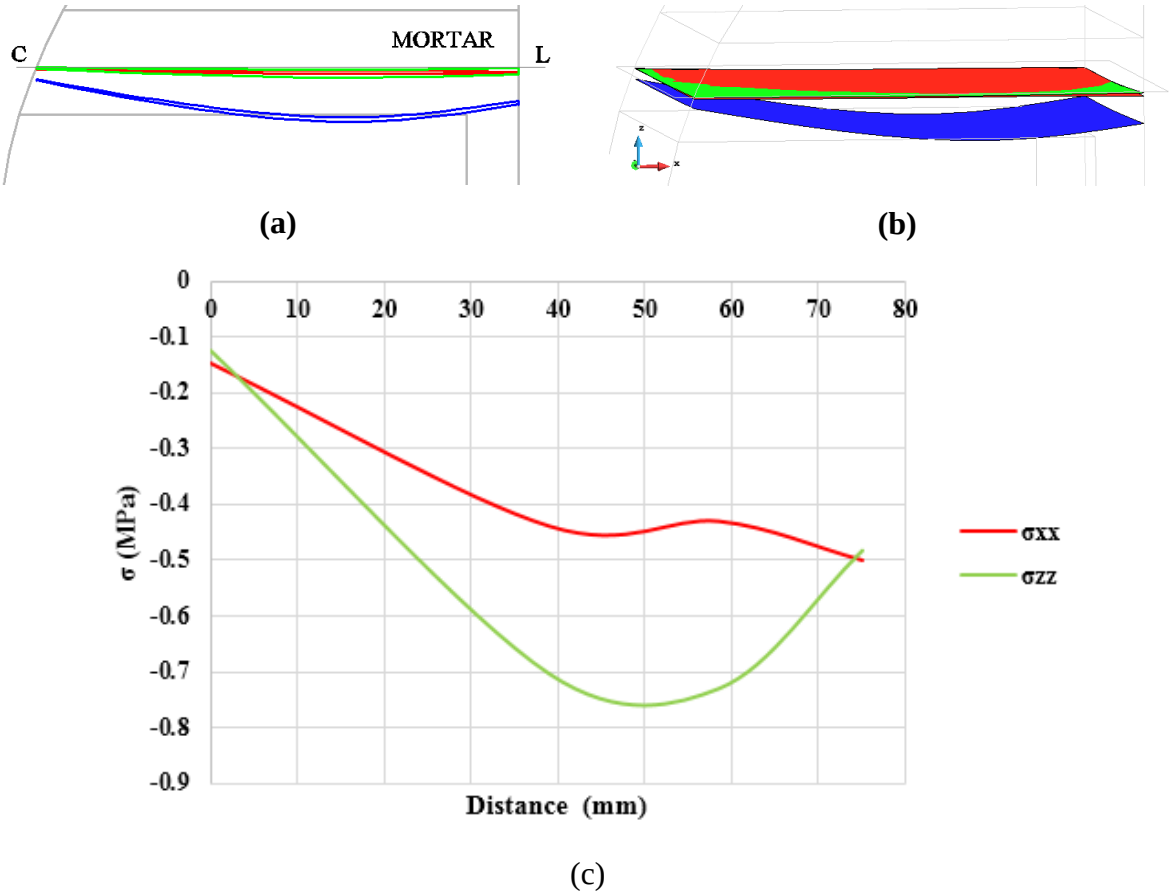

Figure 5.5 Stress distribution in (a) 2D (b) 3D in the center of the top horizontal mortar & & (c) σ_{xx} and σ_{zz} along the central line of top mortar surface, σ_{xx} (red), σ_{yy} (blue) and σ_{zz} (green)

The stress distribution in the interface layer between the mortar and the brick (top) is shown in Graph 5.1. It can be seen that the σ_{xx} stress is almost in tension thorughout. The peak tension is at the joint between the brick and the mortar. σ_{yy} is completely in compression due to the load applied in the direction and σ_{zz} also contributes in compression.

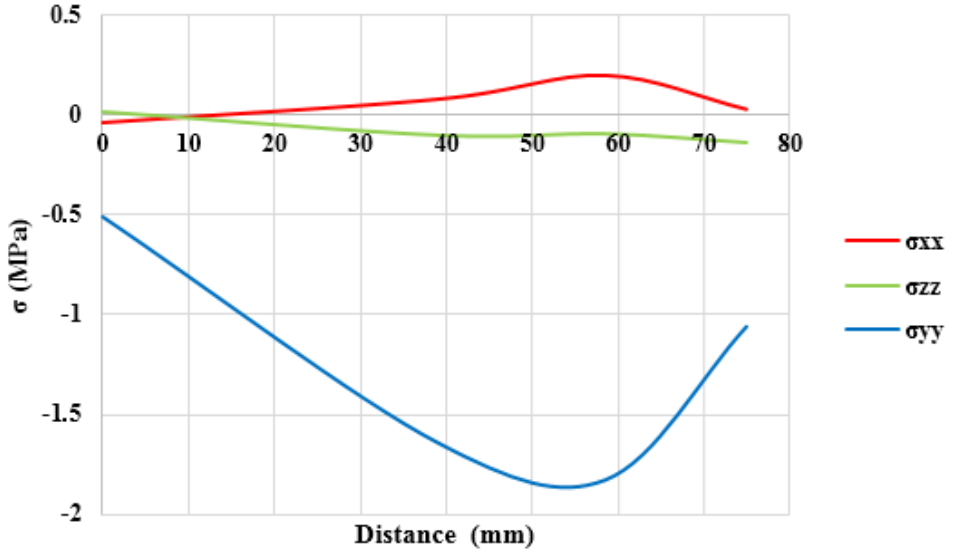

(a)

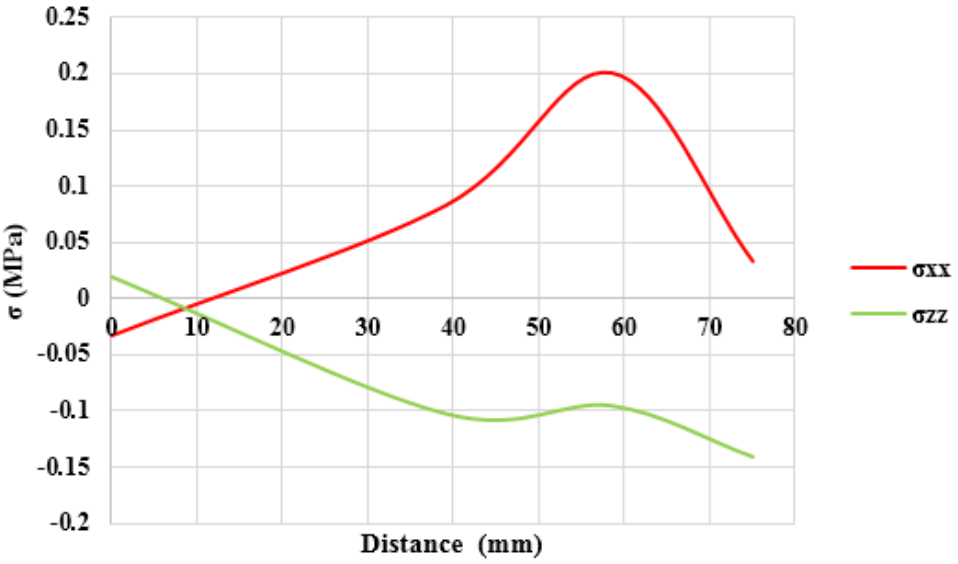

(b)

Graph 5.1 Stress distribution in the interface layer between mortar and brick (a) σ_{xx} (red), σ_{yy} (blue) and σ_{zz} (green) (b) σ_{xx} (red) & σ_{zz} (green)

The stress distribution in the central surface of the specimen is shown in Figure 5.6. The compressive stresses of 'y' are maximum, acting in the range of 0.5-2.5 MPa. The stress in 'x' and 'z' are acting in tension throughout the surface. The average relations between the stresses are: $\sigma_{xx} = -0.30\sigma_{yy}$ and $\sigma_{zz} = -0.10\sigma_{yy}$ along the central line of the specimen. From the center to the outer edge, the stresses in all the direction decreases as shown in the

following figure. This is due to the concentrataion of forces below the regularization mortar and distribution of stresses in the sand glass shape.

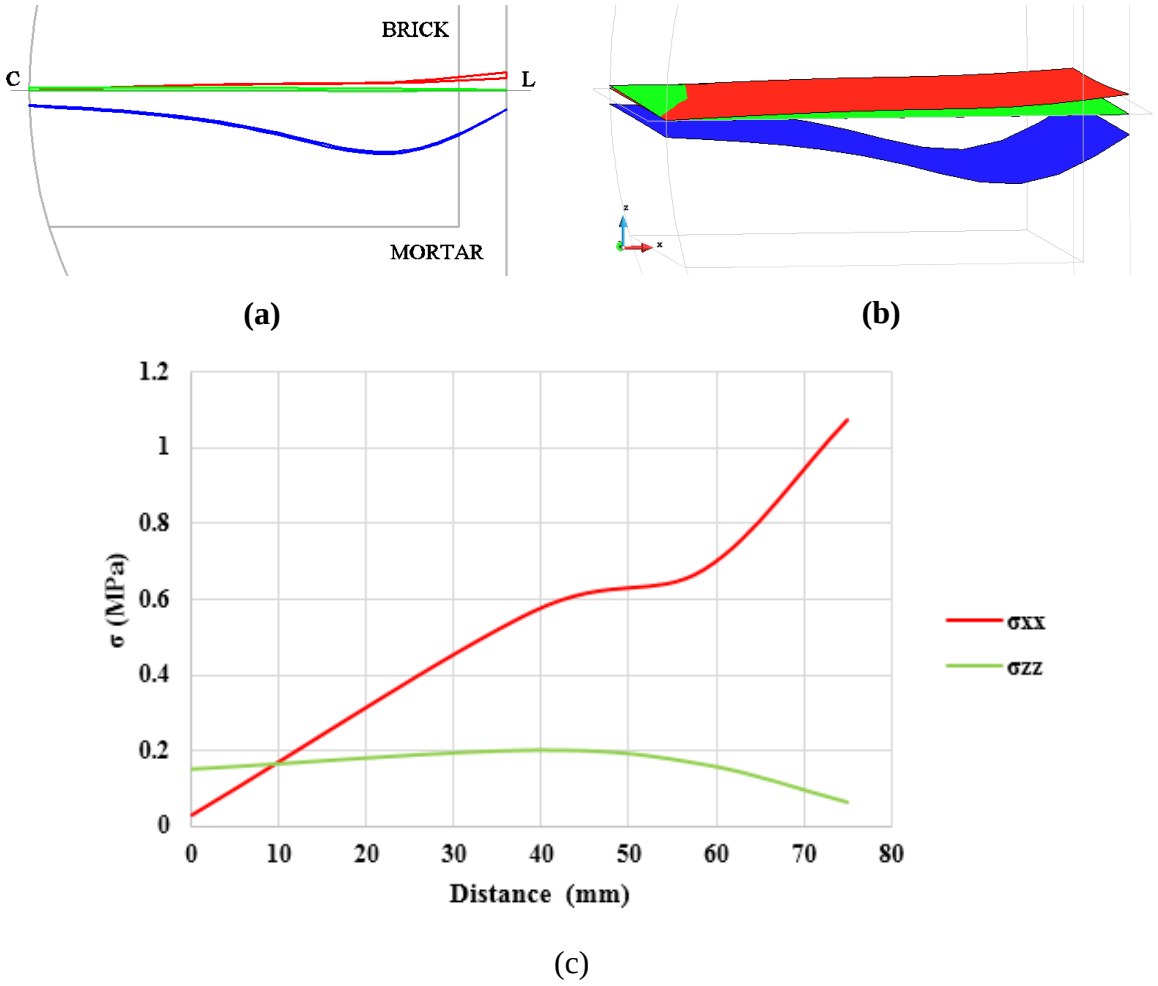

Figure 5.6 Stress distribution in (a) 2D (b) 3D in the center of the cylinder (central brick) & & (c) σ_{xx} and σ_{zz} along the central line of specimen, σ_{xx} (red), σ_{yy} (blue) and σ_{zz} (green)

5.2. LINEAR ANALYSIS: TWO JOINT SPECIMEN

A linear analysis was also performed on two joint cylindrical specimen. The tensile and the compressive stress distribution for a force of 20,000 N is shown in Figure 5.7. The tensile stresses are concentrated in the central brick and near the mortar, in the top and the bottom brick. The tensile stresses are in the range from 0.3 MPa to 0.47 MPa. The compressive stresses take a shape of sand glass, concentrating more in the middle of the specimen, with the external part of the brick receiving the minimum stresses.

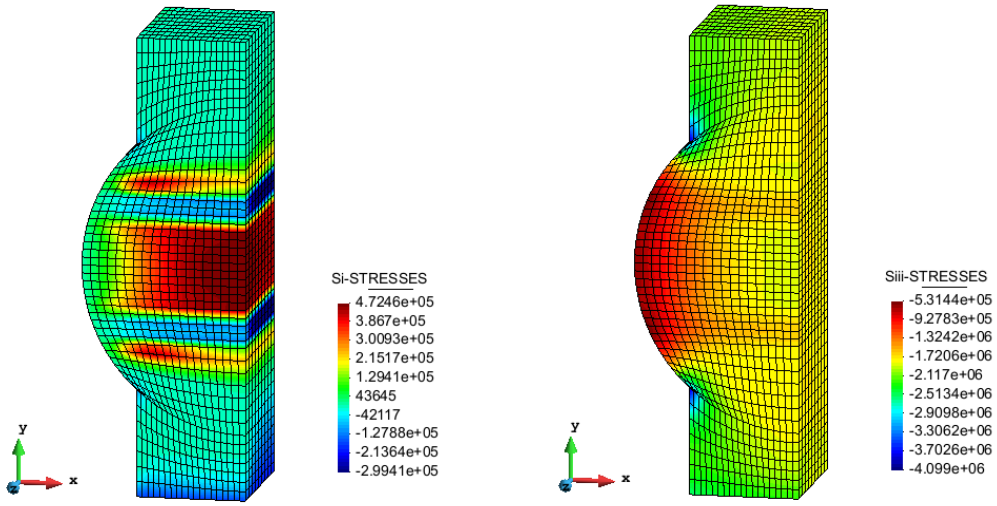

(a) **(b)**

Figure 5.7 Principle (a) tensile & (b) compressive stress in the elastic range

The tensile and compressive stress distribution along a horizontal central line for the specimen, in σ_{xx} (red), σ_{yy} (blue) and σ_{zz} (green) are shown from Graph 5.2 to Graph 5.7. The lines are in the centre of the top brick, centre of the mortar, the interface between the mortar and brick, and at the centre of the specimen.

The stress distribution in the top central brick is shown in Graph 5.2. The stresses in σ_{yy} are dominating in compression due to the applied load in the direction. σ_{zz} stresses are completely in tension and σ_{xx} varies from tension in the centre of the specimen to compression towards the external part of the cylinder. Form the results obtained, the average relation between the stresses are $\sigma_{xx} = 0.18\sigma_{yy}$ and $\sigma_{zz} = -0.04\sigma_{yy}$.

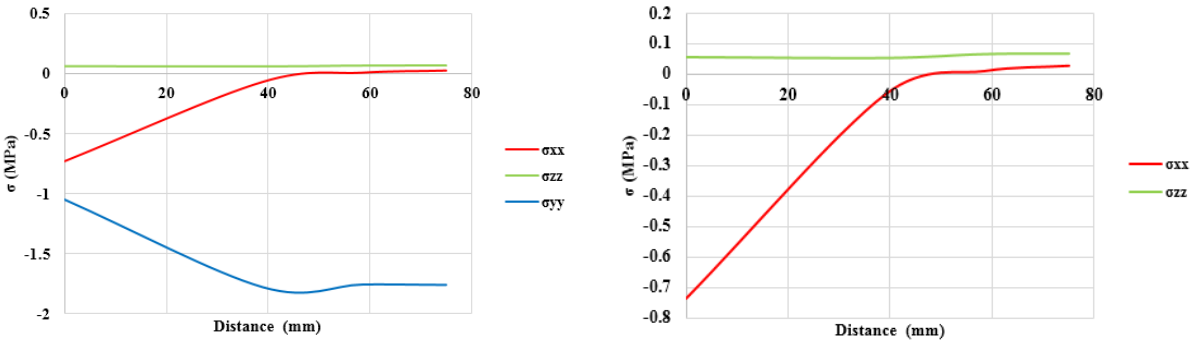

(a) (b)

Graph 5.2 Stress distribution of (a) σ_{xx} (red), σ_{yy} (blue) and σ_{zz} (green) in the central line of the top brick (b) σ_{xx} (red) and σ_{zz} (green)

The variation of stresses along the central line in the middle of the mortar is shown in Graph 5.3 (a) and (b). σ_{xx} (red), σ_{yy} (blue) and σ_{zz} (green) stresses are in compression throughout. $\sigma_{xx} = 0.15\sigma_{yy}$ and $\sigma_{zz} = 0.18\sigma_{yy}$ are the relation between stresses in 'x', 'y' and 'z' directions for average values.

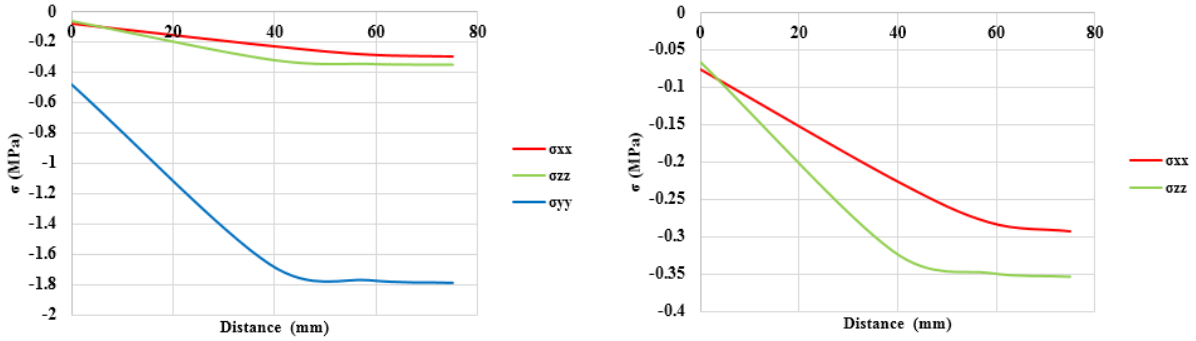

(a) (b)

Graph 5.3 Stress distribution of (a) σ_{xx} (red), σ_{yy} (blue) and σ_{zz} (green) in the central line of the top mortar (b) σ_{xx} (red) and σ_{zz} (green)

At the interface between the brick and the mortar, the stresses along 'x' varies from tension in the central core of the specimen to compression at the external end. The stresses along 'z' acts opposite to stresses in 'x' varying from compression in the centre towards tension in the external end, shown in Graph 5.4(b). Based on the stress distribution in σ_{xx}, σ_{yy} and σ_{zz} the following relation can be summarized $\sigma_{xx} = -0.01\sigma_{yy}$ and $\sigma_{zz} = 0.05\sigma_{yy}$ (for average values).

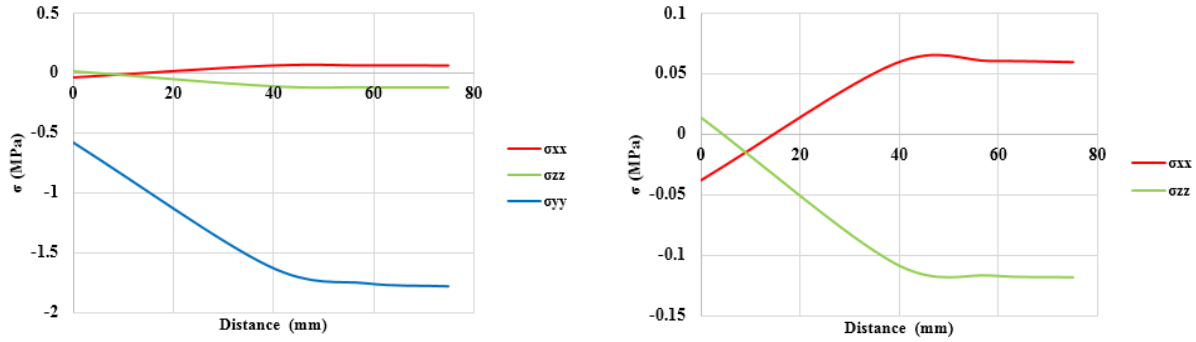

(a) (b)

Graph 5.4 Stress distribution of (a) σ_{xx} (red), σ_{yy} (blue) and σ_{zz} (green) at the interface between the brick and the mortar (b) σ_{xx} (red) and σ_{zz} (green)

The distribution of stresses in ‘x’, ‘y’ and ‘z’ in the centre of the specimen (along the central line) is shown in Graph 5.5. The stresses in ‘x’ and ‘z’ act in tension, with σ_{xx} contributing four times σ_{zz}, the relation $\sigma_{xx} = -0.20\sigma_{yy}$ and $\sigma_{zz} = -0.07\sigma_{yy}$ can be oobtained from the average results of stress distribution in ‘x’, ‘y’ and ‘z’ directions.

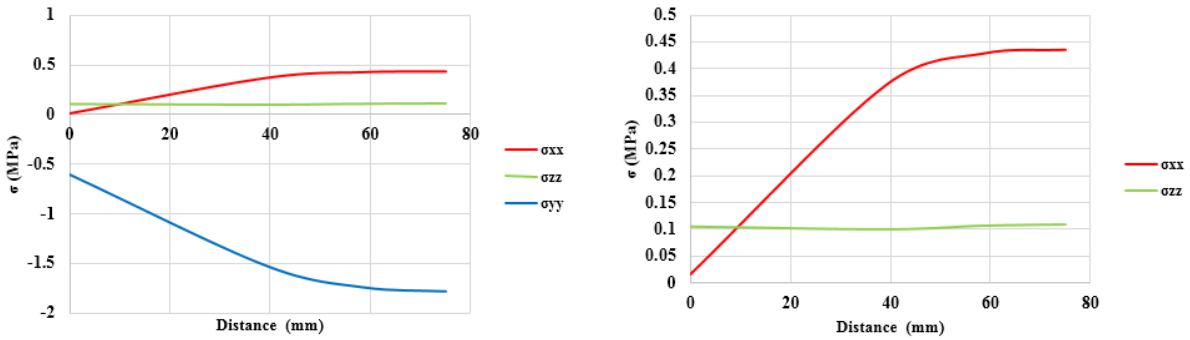

(a) (b)

Graph 5.5 Stress distribution of (a) σ_{xx} (red), σ_{yy} (blue) and σ_{zz} (green) in the central line of the specimen (b) σ_{xx} (red) and σ_{zz} (green)

5.3. NON-LINEAR ANALYSIS: THREE JOINT CYLINDERS

The force displacement graph of the analysis is shown in Graph 5.6. The displacement measured, is the relative displacement between the top central node of the cylinder to the bottom central node. The relative displacement of the whole specimen from the topmost point to the bottom most point was also calculated and since the difference is in the order of one by ten thousandth of a millimetre, the results are not shown.

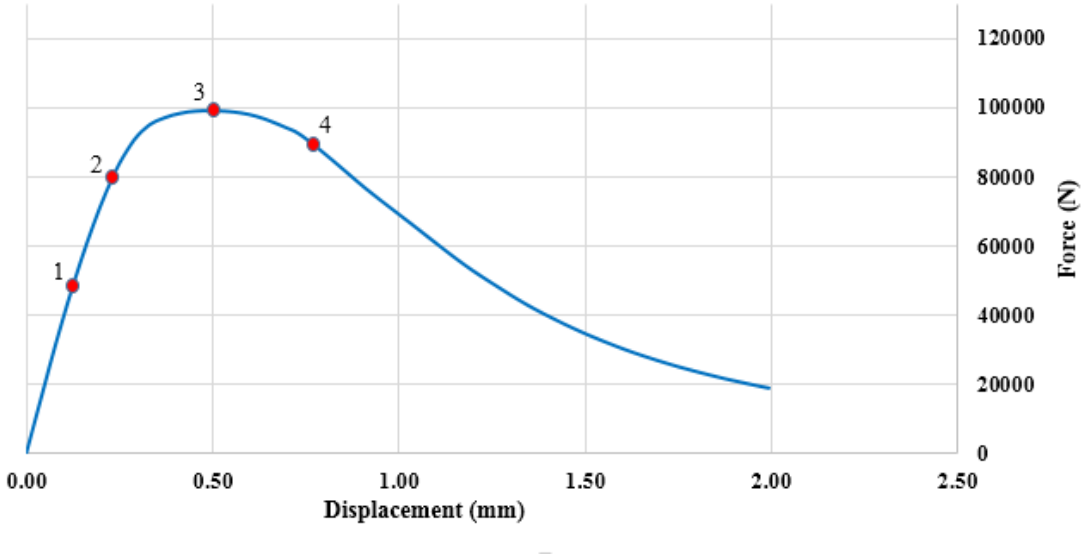

Graph 5.6 Force displacement graph of three joint cylindrical specimen

Four points are chosen in the graph to explain the initiation of tensile damage, compressive damage, tensile stresses and compressive stresses. The details of these points are given in the Table 5.2.

Table 5.2 Description of points, referred in the force displacement graph of three joint cylinder

Point Number	Force (N)	Displacement (mm)
1 – Step 06	32000	0.080
2 – Step 15	80000	0.234
3 – Step 28	99000	0.495 (peak)
4 – Step 41	90000	0.763

The evolution of tensile damage is shown in Figure 5.8, along the points shown in the above table. The first point is initiation of the non-linear behaviour of the cylinder, where the tensile damage originates at the internal interface between the brick and the mortar, and spreads across the mortar. The damage initiates simultaneously at the top and at the bottom. The second point is in between the peak strength and the initiation of the non-linear behaviour, having a tensile damage of 92% in the central mortar. It can be clearly observed that the tensile damage is also present in brick and is distributed throughout in the range of 60-80%. In the third point, the peak strength of masonry, the tensile damage in the vertical mortar joint and in the brick is 98.6%. Fourth point is after the failure of cylindrical specimen.

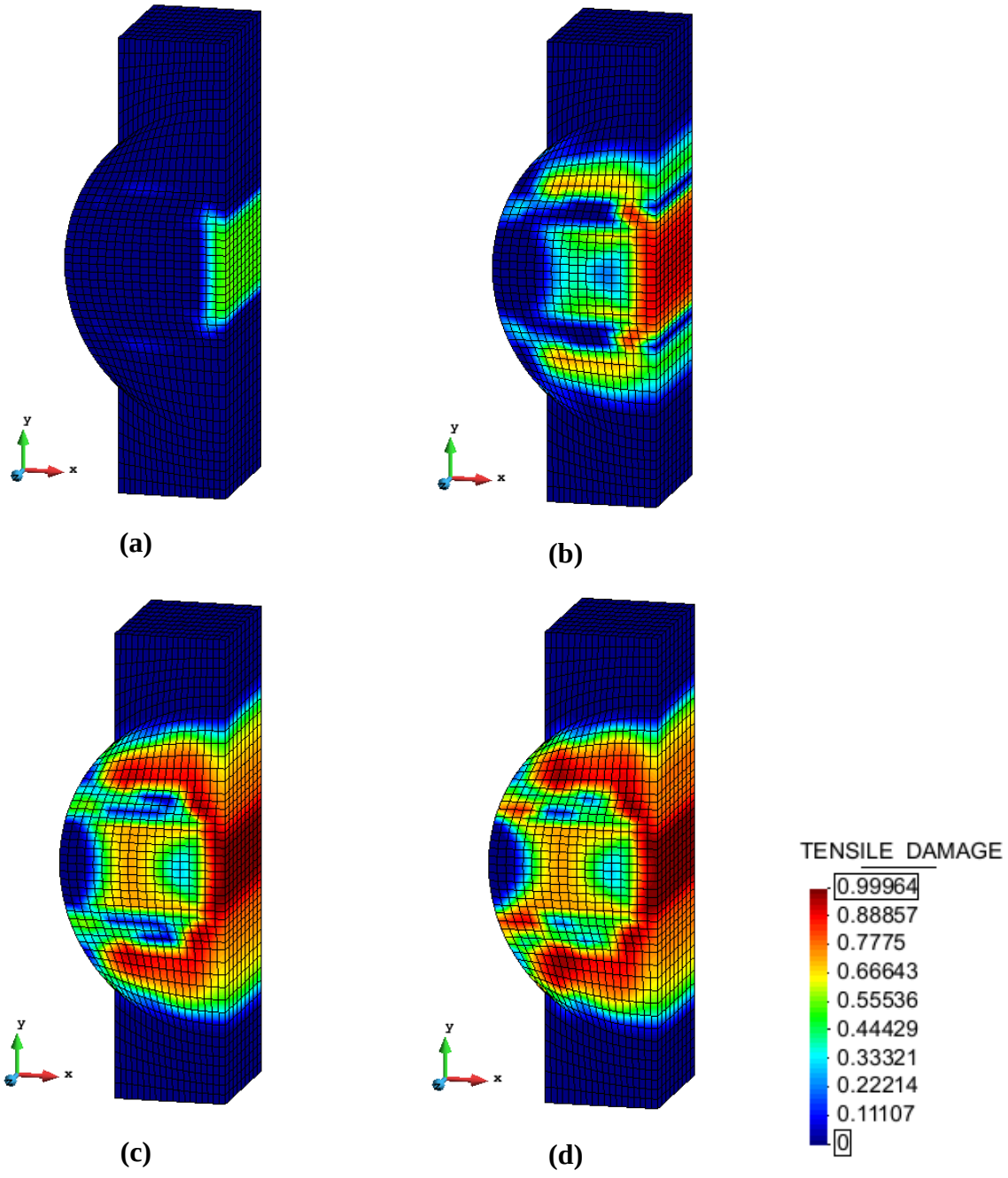

Figure 5.8 Evolution of tensile damage in three Joint cylinder (a) Point 1 (b) Point 2 (c) Point 3 and (d) Point 4

The compressive damage evolution is shown in Figure 5.9. The damage initiates closer to the internal interface layer between the brick and the mortar, both at the top and bottom simultaneously. In the second point, the compressive damage spreads from the vertical mortar joint towards the horizontal mortar joint at both top and bottom (91%). Point 3 shows the damage at peak strength and finally in fourth point the damage moves towards the end of the

regularization mortar. Comparing the tensile damage and compressive damage it can be seen that at peak strength the tensile damage is 98.6% and the compressive damage is 91%.

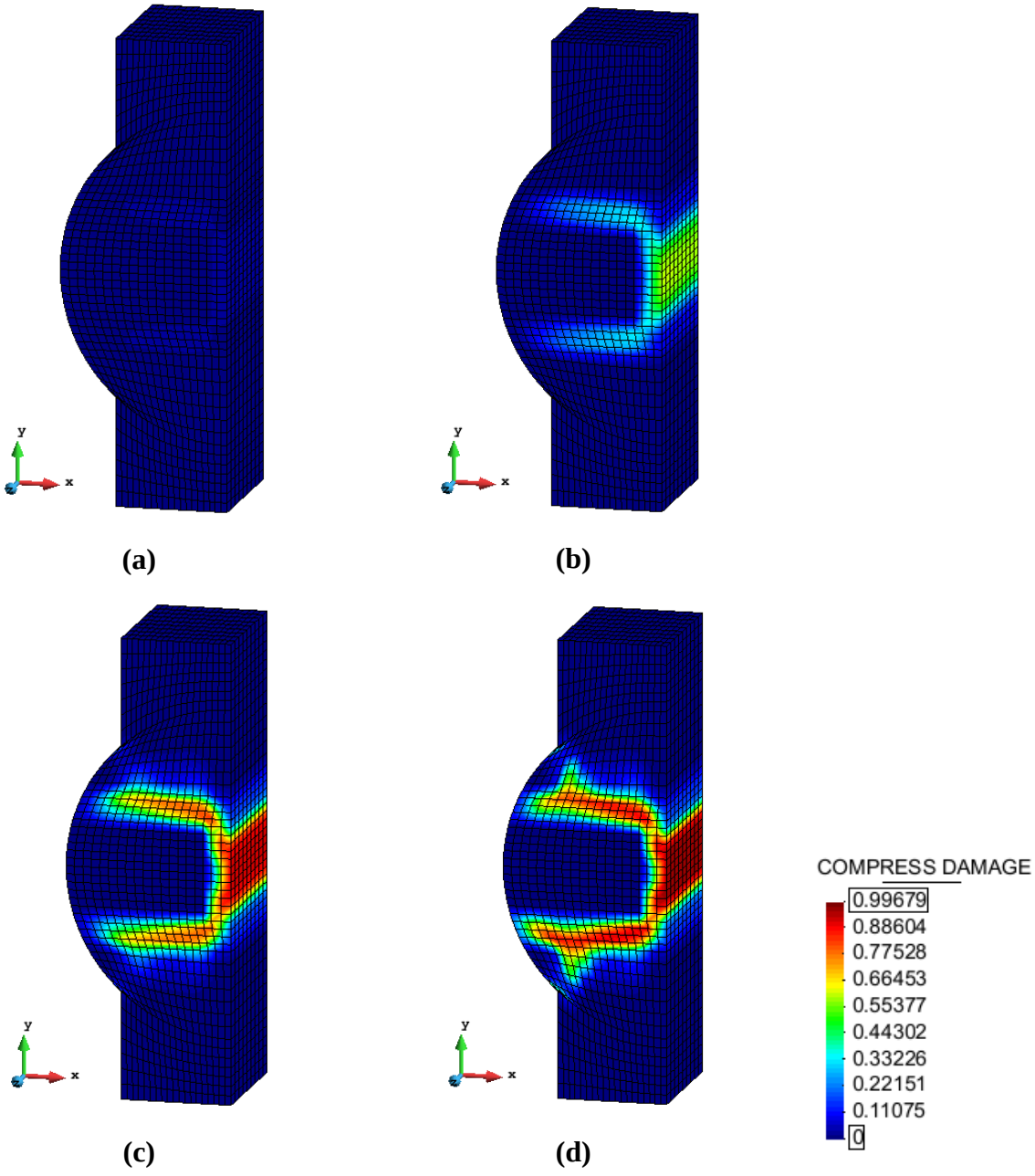

Figure 5.9 Evolution of compressive damage in three joint cylinder (a) Point 1 (b) Point 2 (c) Point 3 & (d) Point 4

The principle tensile stress distribution gives us a clear idea about the failure taking place in the specimen (Figure 5.10). The stresses are in the range of 0.6-0.8 MPa in the first point. It can be observed in the first figure that the initiation of tensile stresses in the brick is around

the mortar. The tensile stress reaches a maximum of 1.37 MPa at the peak strength (point 3) lies in between the tensile strength of brick (1.52 MPa) and tensile strength of mortar (1 MPa). The cracking in brick is reached slightly before the uniaxial tensile strength value is reached, due to the combined effect of vertical compression according to the Mohr-Coulomb criterion. It can be clearly seen the distribution of tensile stresses are dominated in the brick throughout.

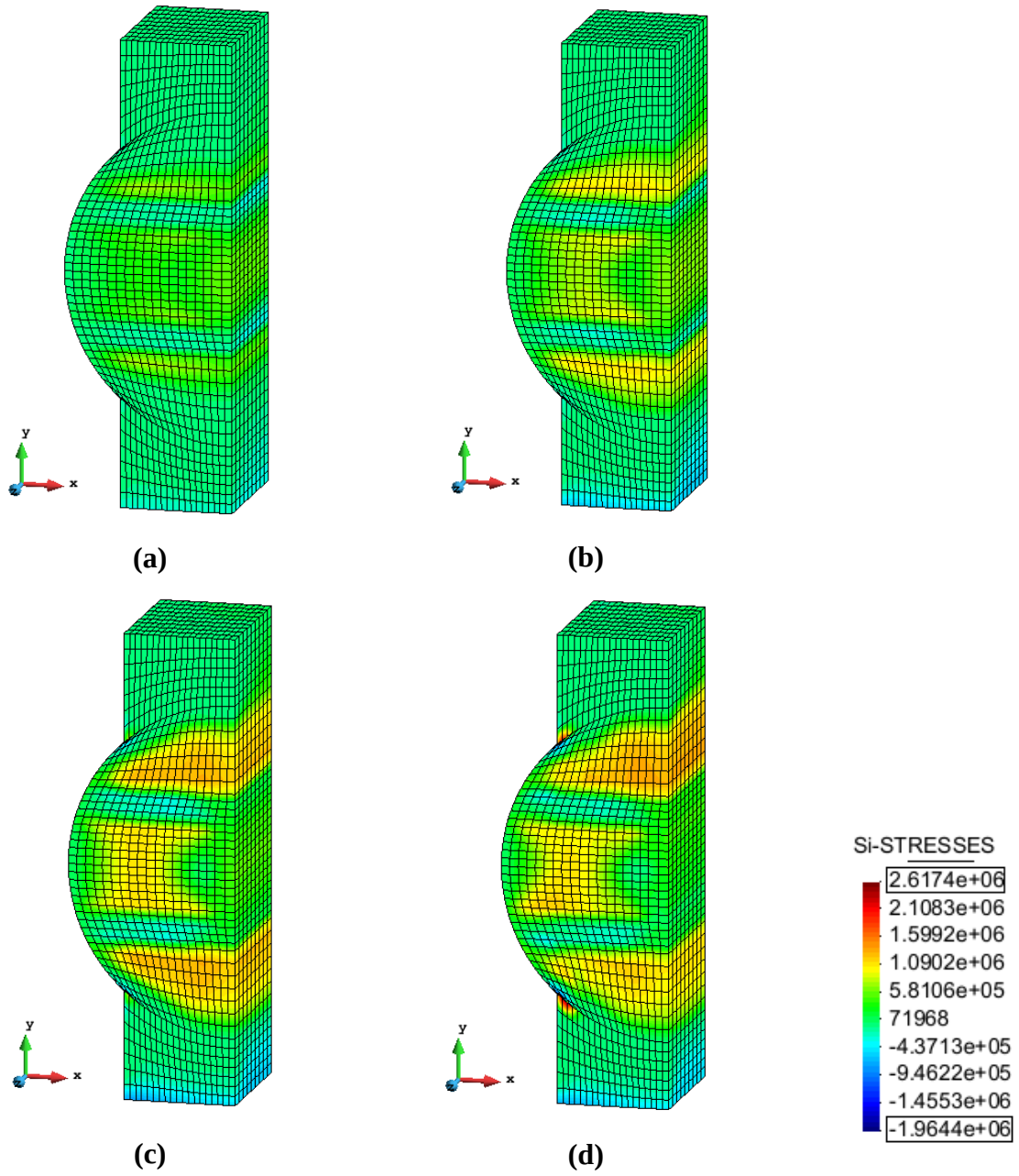

Figure 5.10 Principle tensile stress distribution in three Joint cylinder (a) Point 1 (b) Point 2 (c) Point 3 & (d) Point 4

The principle compressive stress distribution is found both in mortar and in brick throughout the analysis (Figure 5.11). At peak strength most of the cylindrical specimen is subjected to compressive stresses and is in the range of 5 MPa. Major damage is not observed in the brick except the external part, since the compressive strength of brick is 30.8 MPa.

It can be observed from the results the sand glass shaped central core, bearing the applied load. The rest of the cylinder specially the external part of brick outside the capped area, receives the minimum compressive stress. As a result a failure surface is created along the sand glass shape, resulting in the separation of the external part before the failure of the specimen.

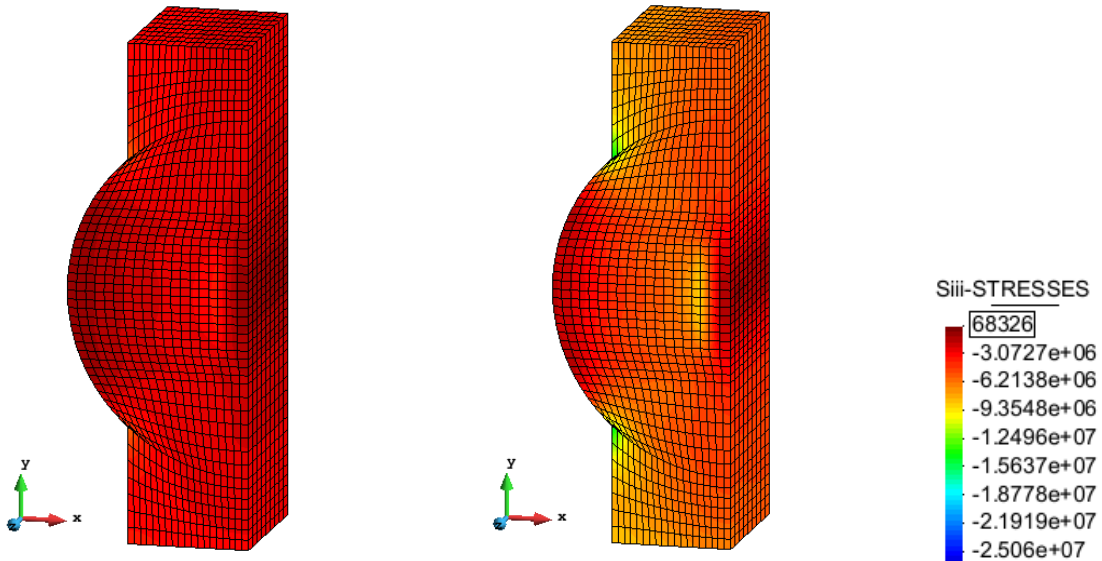

(a) **(b)**

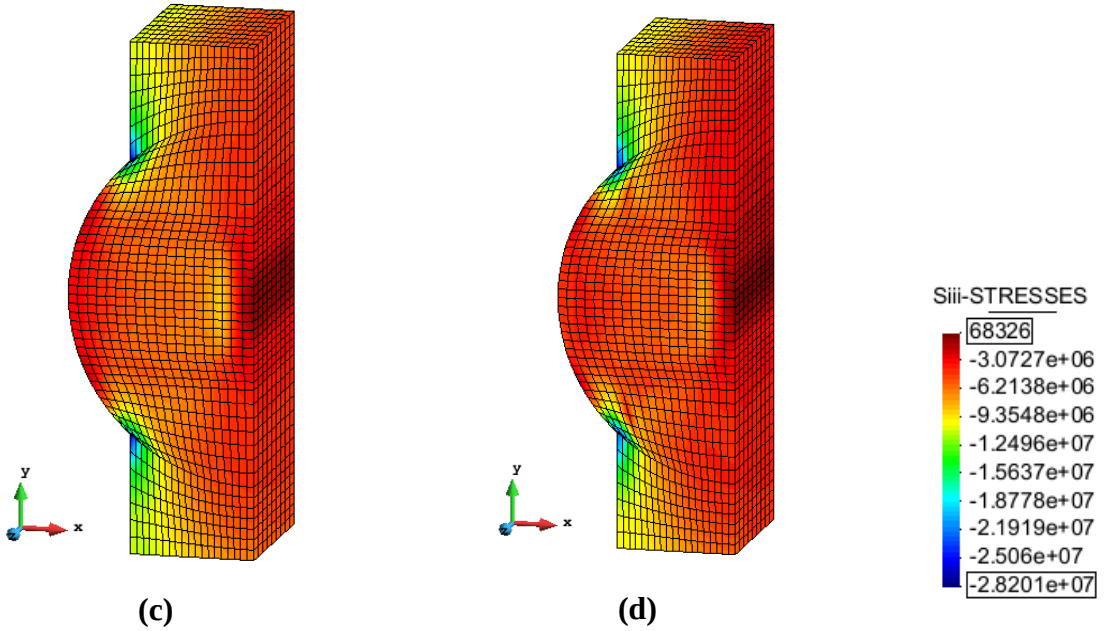

Figure 5.11 Principle compressive stress distribution in three Joint cylinder (a) Point 1 (b) Point 2 (c) Point 3 & (d) Point 4

The vector distribution of tensile and compressive stress at peak strength is shown in Figure 5.12. It gives a clear idea of the stress distribution. The tensile stresses are dominating in X and Z direction in the brick. The compressive stress being distributed throughout the specimen especially in the area of loaded cap.

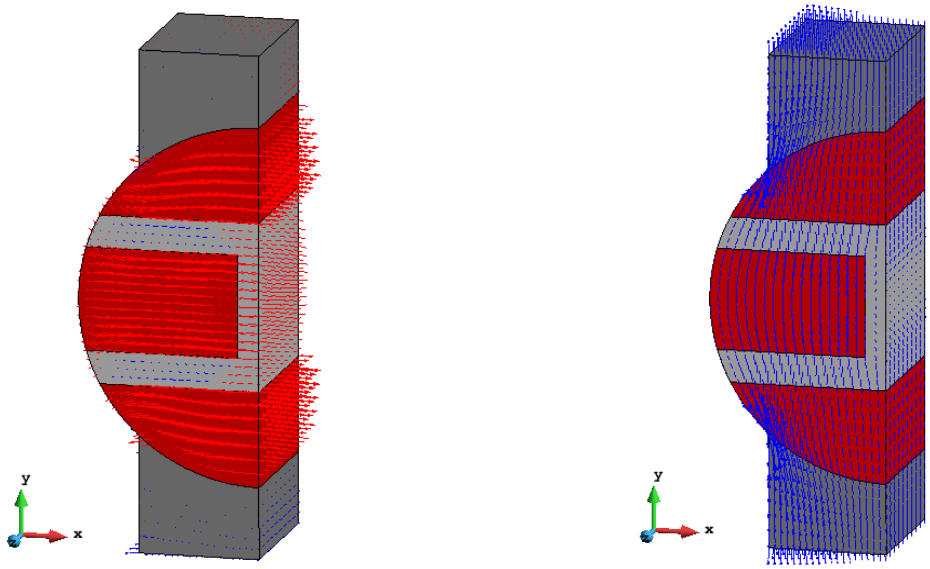

Figure 5.12 Vector distribution of stresses in three joint cylinder at peak

Figure 5.13 Experimental failure of three joint specimen

From Figure 5.12 and Figure 5.13 it can be observed that the failure is same in both numerical analysis and the experimental testing.

5.4. NON-LINEAR ANALYSIS: TWO JOINT CYLINDERS

A two joint cylinder is modelled with the exact same properties mentioned in the beginning of the chapter 5. The only difference is the absence of the vertical joint. 8 nodded hexahedron mesh elements are assigned to the model with the dimension of each hexahedron being 4 x 4 x 7 mm^3. A total of 8208 elements are created. The final mesh is shown in Figure 5.14.

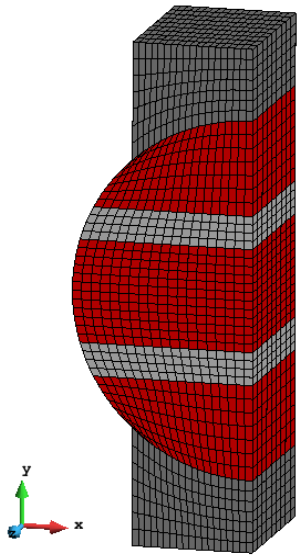

Figure 5.14 Final mesh of two joint cylindrical specimen

The force displacement graph of the two joint cylindrical specimen is shown in Graph 5.7. The displacement measured is the relative displacement from top central node of the brick to the bottom central node of the brick. It follows almost the same trend of Graph 5.6 (three joint cylindrical).

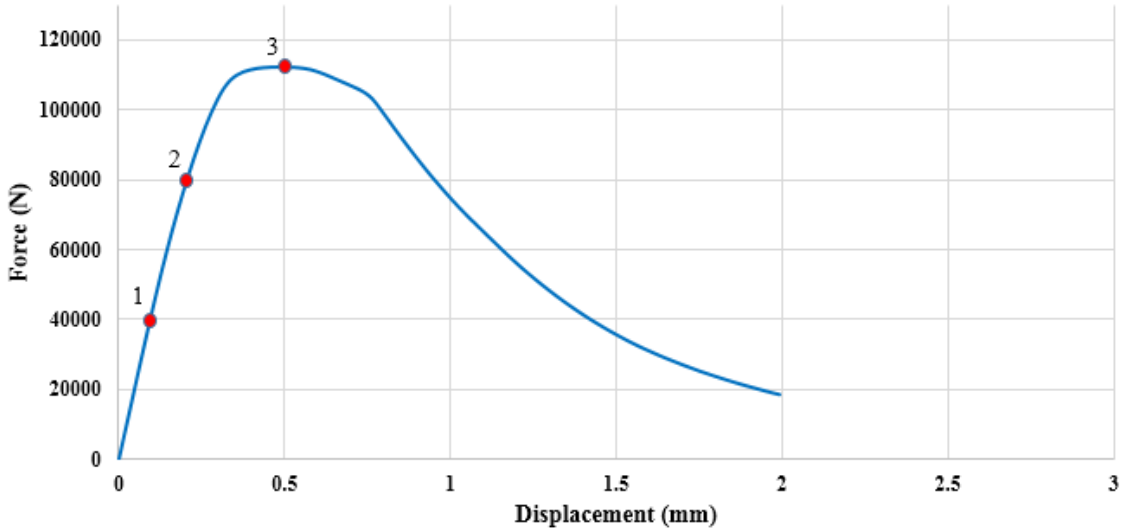

Graph 5.7 Force displacement graph of two joint cylindrical specimen

Three points are chosen to explain the initiation of damage and stress distribution. The details of the points are shown in Table 5.3.

Table 5.3 Description of points, referred in the force displacement graph of two joint cylinder

Point Number	Force (N)	Displacement (mm)
1 – Step 7	40000	0.095
2 – Step 14	81000	0.209
3 – Step 29	112000	0.496 (peak)

The evolution of tensile damage is shown in Figure 5.15. It can be seen that initiation of damage takes place in the central brick at 35% of the maximum load. At 72% of the maximum load, the damage is spread throughout the central brick and in the top and bottom of the brick near the mortar. At peak even the mortar has tensile damage right below the edge of regularization mortar.

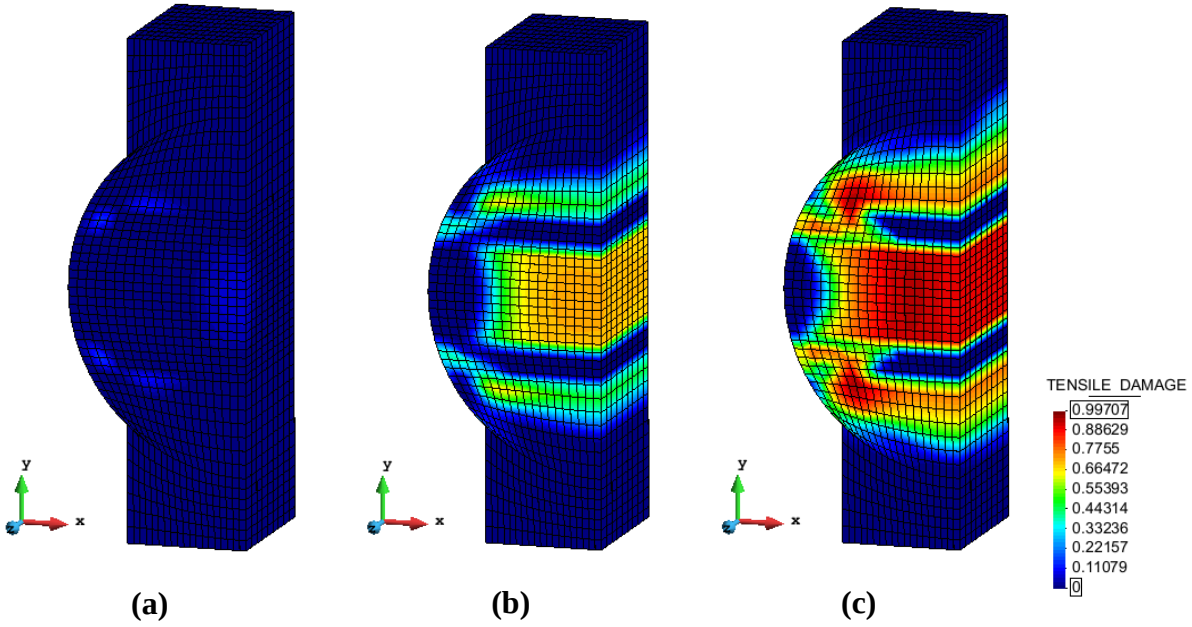

Figure 5.15 Evolution of tensile damage in two Joint cylinder (a) Point 1 (b) Point 2 & (c) Point 3

The compressive damage evolution is shown in Figure 5.16. The damage initiates in the mortar due to the low compressive strength till the peak strength. Only at peak there is slight damage present in the brick. The maximum damage is 76% (mortar) whereas it is 95% in the tensile damage (brick).

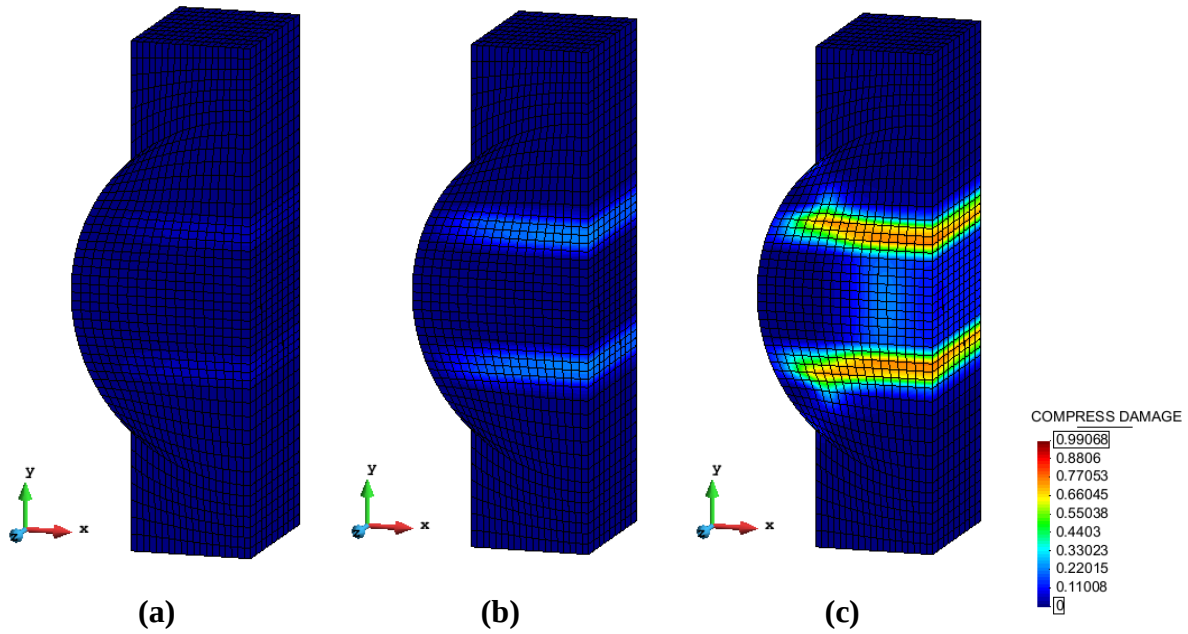

Figure 5.16 Evolution of compressive damage in three joint cylinder (a) Point 1 (b) Point 2 & (c) Point 3

The principle tensile stress distribution is shown in Figure 5.17. In the first step the tensile stress is 0.8 MPa. In second step the tensile stress is 1.12 MPa, reaching a maximum of 1.34 MPa in the third point.

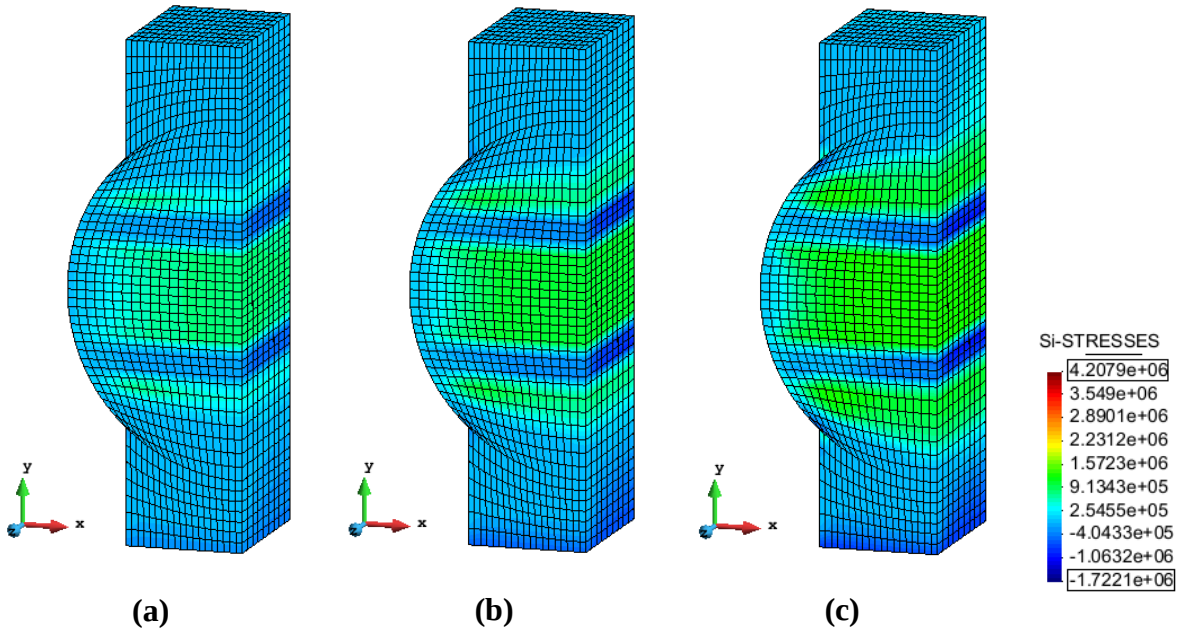

Figure 5.17 Principle tensile stress distribution in two Joint cylinder (a) Point 1 (b) Point 2 & (c) Point 3

The principle compressive stress distribution is shown in Figure 5.18. The stresses are in the range of 3-6 MPa from first point to the second. At peak strength the stresses are at a maximum, ranging from 5-7 MPa. The external part of the cylinder outside the loading cap, receives the minimum compressive stress throughout. It can be observed from the results the sand glass shaped core, receiving the maximum compressive stresses until the failure.

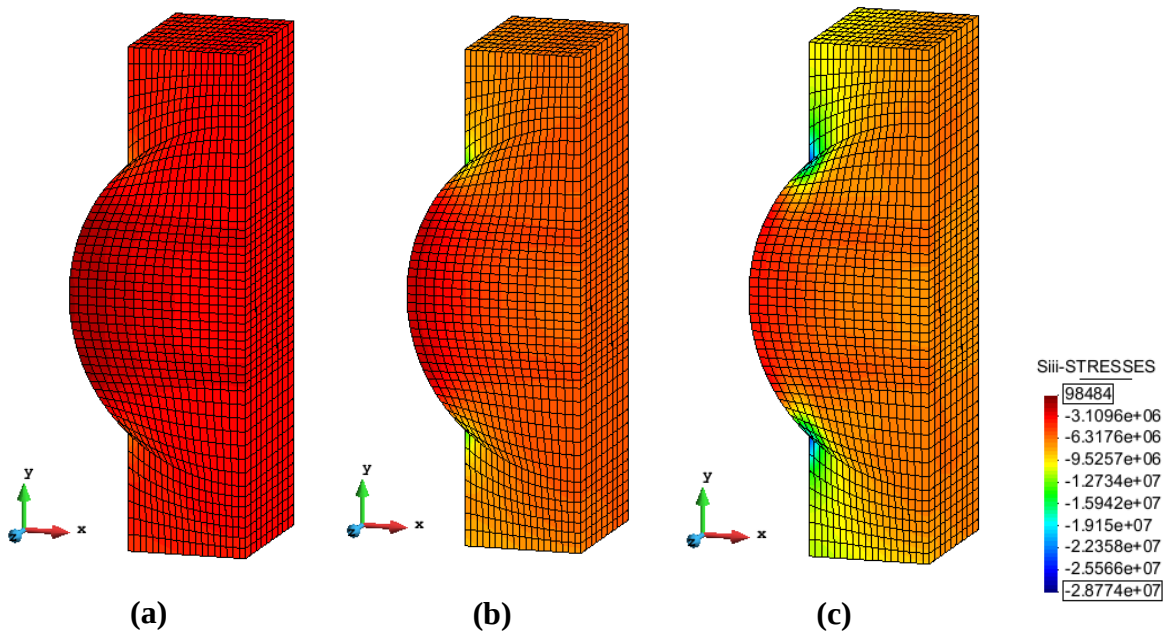

Figure 5.18 Principle compressive stress distribution in two Joint cylinder (a) Point 1 (b) Point 2 & (c) Point 3

Figure 5.19 shows the principle tensile and principle compressive stress distribution, showing the presence of tension in brick and compression in mortar. Figure 5.20 shows the failure of experimental tests. From both the figures it can be concluded, that the failure is same in numerical and experimental testing.

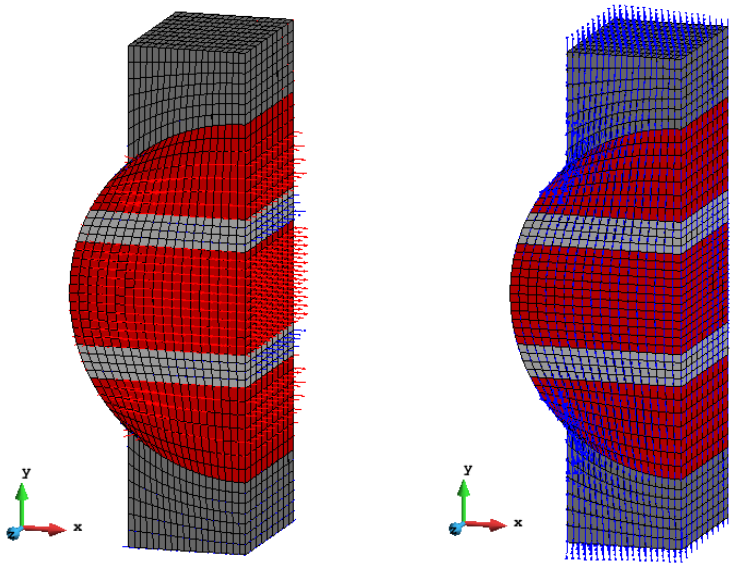

Figure 5.19 Vector distribution of principle stresses

Figure 5.20 Experimental failure of two joint specimen

5.5. COMPARISON OF RESULTS

5.5.1. NON-LINEAR: THREE JOINT AND TWO JOINT CYLINDER

In this section the comparison of three joint and two joint numerical results are presented. The force displacement diagram is shown in Graph 5.8. For both the models, with the same mechanical properties, it shows that the two joint specimen has higher resistance. It is due to

the presence of the vertical mortar joint in three joint cylinder, causing failure of the specimen earlier than two joint cylinder.

The comparison of force, displacement and stresses are shown in Table 5.4. The results show that the three joint specimen has 11.7% lower value than two joint for the maximum load and almost the same displacement at failure in both the cases.

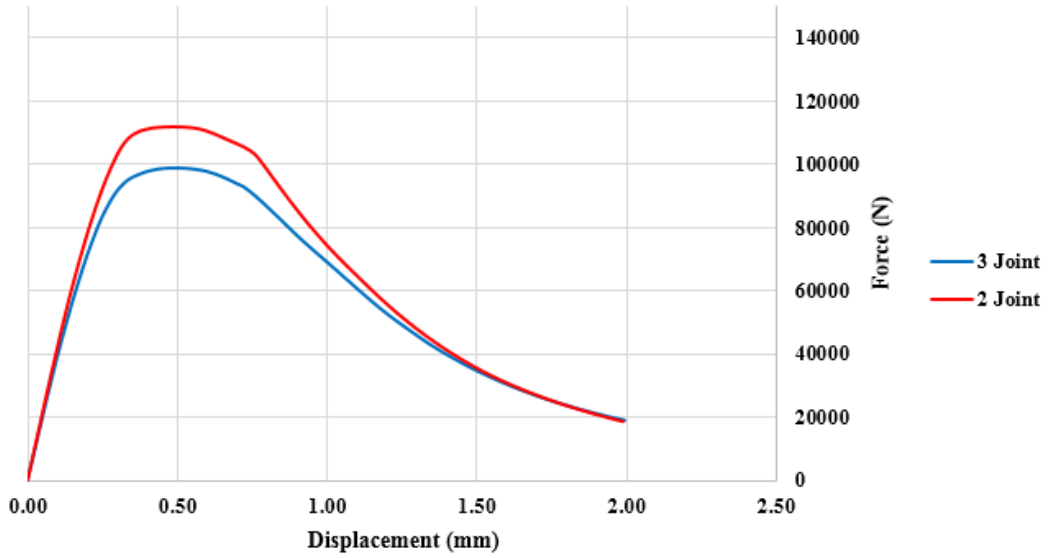

Graph 5.8 Comparison of force displacement diagram of three joint and two joint cylinder (Numerical)

Table 5.4 Comparison of three joint and two joint numerical results

Specimen	Max. Force (kN)	Δ at max F (mm)	Stress (Diametric area)	Stress (Area below loaded cap)	Percentage variation
Two Joint cylinder	112.03	0.496	5.62	7.02	-
Three Joint cylinder	98.91	0.495	4.96	6.20	11.68%

Similarly the comparison of modulus of elasticity for both the cases is shown in Table 5.5.

Table 5.5 Comparison of modulus of elasticity

Specimen	Modulus of elasticity (diametric area)	Modulus of elasticity (Area below loaded cap)	Percentage variation
Two joint cylinder	3210	4012	-
Three joint cylinder	3020	3775	-5.90

Graph 5.9 shows the comparison of stress strain diagram for three joint and two joint specimens. Graph 5.9(a) shows the variation considering the diametric area of cross section and Graph 5.9(b) considering area below the loaded cap. In both the graphs, the stress values are more when resisting area is considered, which is obvious due to considering the reduced area. The three joint specimen results are lower than the two joint by 11.7%.

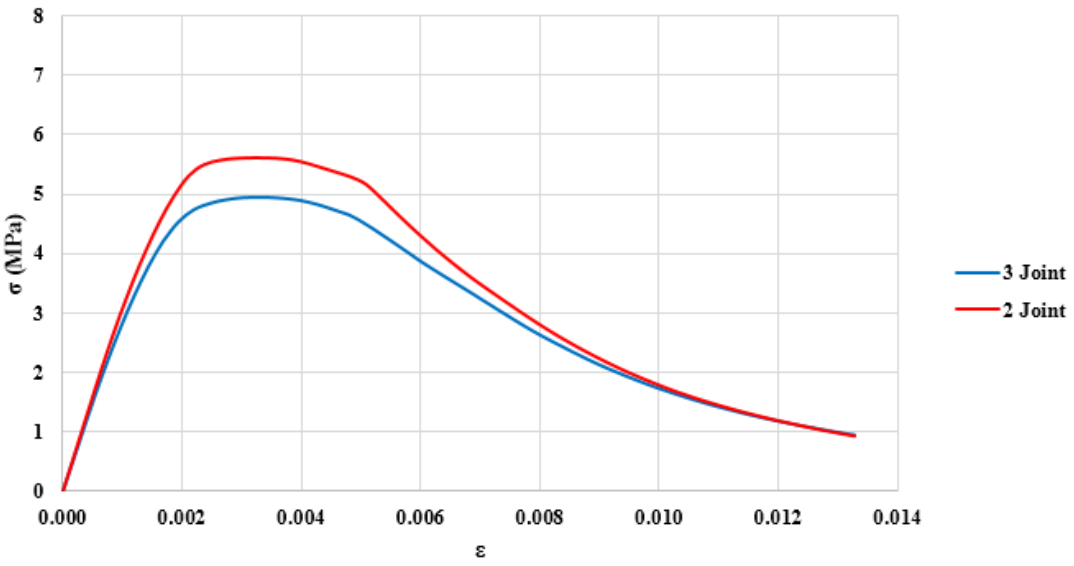

(a)

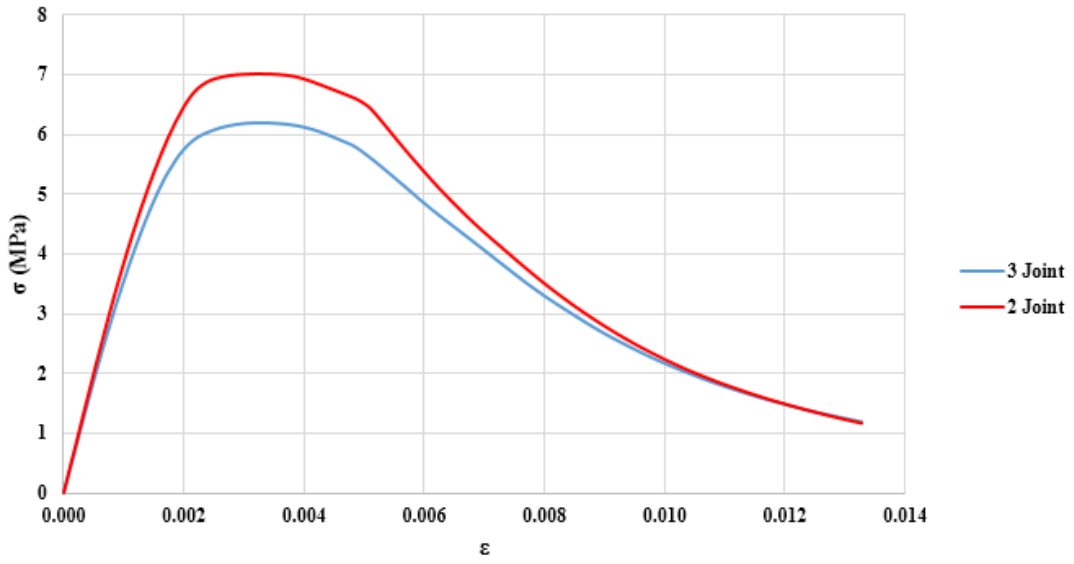

(b)

Graph 5.9 Comparison of stress strain diagram (a) considering diametric area (b) considering area below loaded cap

Since there is difference in values of strength and force considering different specimens from the same masonry wall. There is a need to carry out more research regarding the relation to evaluate the compressive strength. Based on the results obtained, the following relation can be established between three joint and two joint specimen.

Table 5.6 Relation between experimental and numerical results

	Compressive strength	Modulus of elasticity
Experimental	$f_c^{2\,joint} = 1.18 f_c^{3\,joint}$	$E^{2\,joint} = 1.23 E^{3\,joint}$
Numerical	$f_c^{2\,joint} = 1.13 f_c^{3\,joint}$	$E^{2\,joint} = 1.06 E^{3\,joint}$

5.5.2. NUMERICAL AND EXPERIMENTAL THREE JOINT CYLINDER

In this section the numerical analysis and the experimental tests are compared. The force displacement diagram of experimental and the numerical analysis is shown in Graph 5.10. It is seen that the displacements of experimental tests are in the range of 2-6 mm, which is very unusual. The displacements of the masonry prism shown in Graph 4.5, has a displacement of

0.50 mm at the peak strength and the results obtained from the numerical analysis for the same, matched almost in perfect. However in this case there is no match of experimental and numerical results.

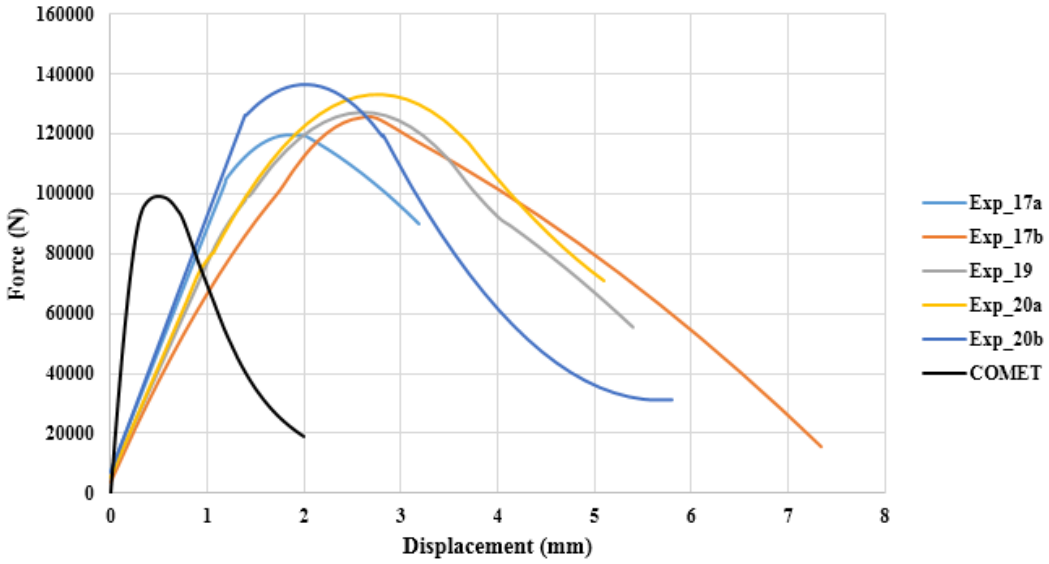

Graph 5.10 Force displacement diagram of experimental tests and numerical analysis (three Joint cylinders)

In order to evaluate this, the experimental results of the cylindrical specimens were analyzed to find any errors. But there were no notable errors found in the calculation. It was finally concluded that, there have been some errors during the collection of the data or some error in the measuring instruments during the experimental testing. So the experimental results had to be corrected i.e. by decreasing the displacement by five times. The corrected experimental results along with the numerical result are shown in Graph 5.11. Comparison of force, displacement, modulus of elasticity and compressive strength for numerical and experimental for two combinations viz., considering diametric area and the area below the loaded cap is shown in Table 5.7.

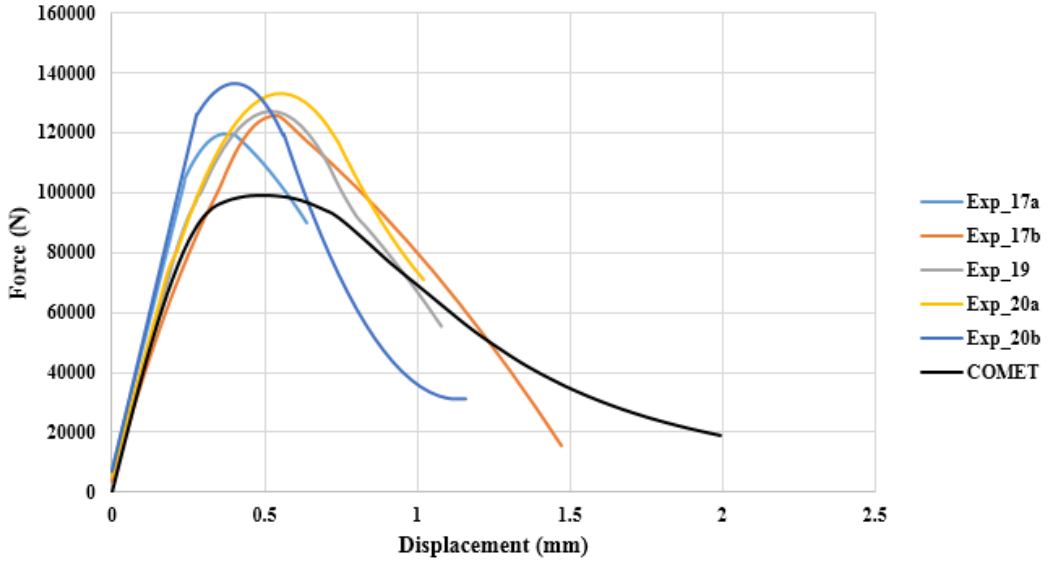

Graph 5.11 Corrected experimental results along with the numerical results (three joint cylinders)

Table 5.7 Comparison of experimental and numerical results (three joint cylinders)

	Avg. Exp. (Diametric area)	**Avg. Exp. (Area below loaded cap)**	**Num. (Diametric area)**	**Num. (Area below loaded cap)**
Max. Force (kN)	123.95	123.95	98.91	98.91
Displacement at max force (mm)	0.47	0.47	0.50	0.50
Modulus of Elasticity (MPa)	2888	3610	2956	3695
Compressive strength (MPa)	6.84	8.55	4.96	6.20
Variation of compressive strength	-	+25%	-28.36%	-9.35%

The numerical analysis predicts lower compressive strength with respect to experimental results in both the cases (Brencich et al., (2004), Bilello et al., (2007), A Brencich et al., (2006)). The comparison of stress strain diagram for experimental and numerical analysis is shown in Graph 5.12 (a) and (b). (a) Is considering the diametric area of cross section and (b)

is considering the area below the loaded cap. Even though the graphs are completely similar, the values are different in both results.

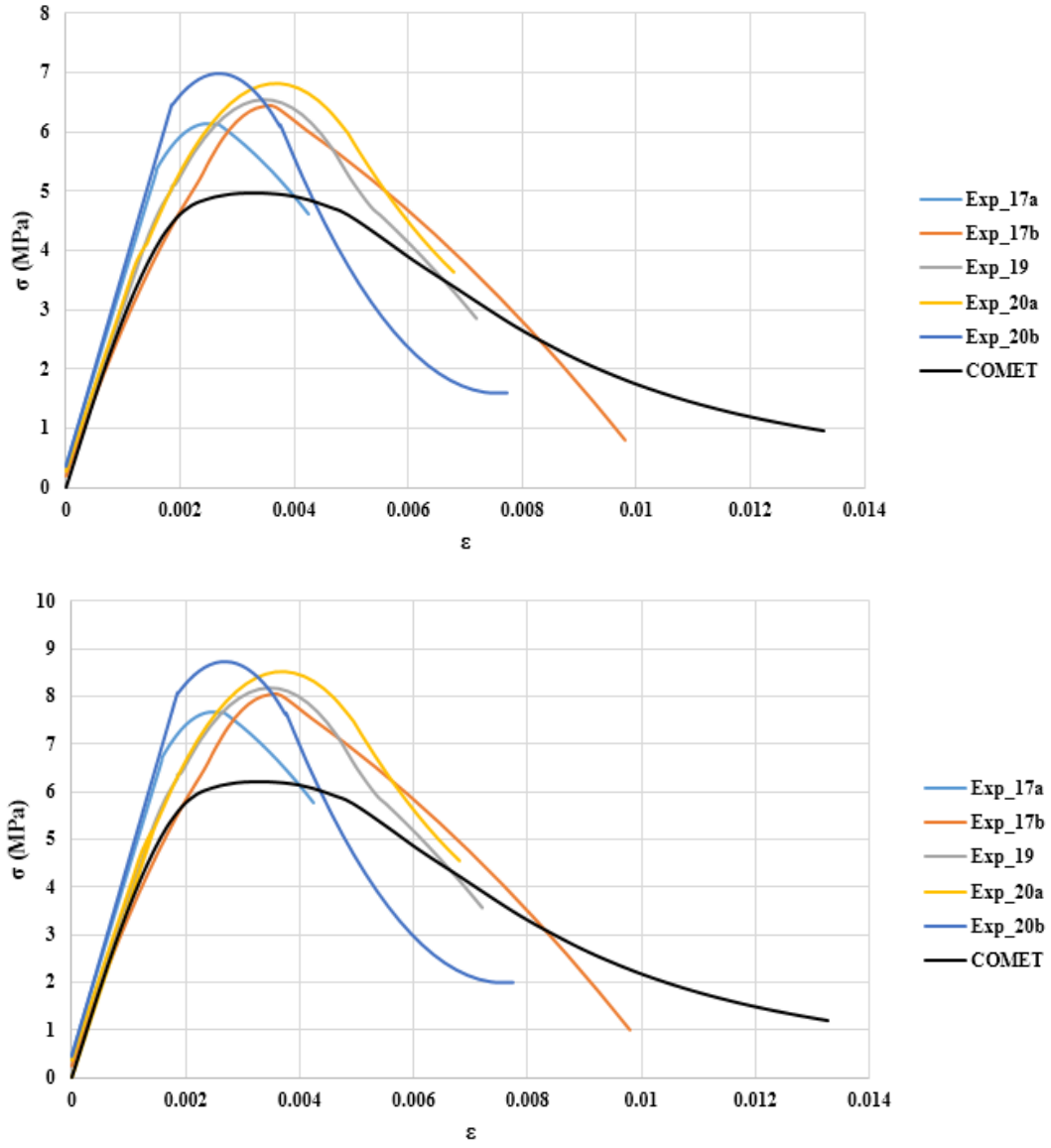

Graph 5.12 Stress strain diagram of experimental and numerical (three joint cylinders), considering (a) Diametric area of cross section & (b) Area below the loaded cap

The failure mode of experimental results are discussed in section 3.6, where the failure of the three joint specimen is due to the tensile failure of the brick and the splitting of external part of brick even before the maximum value is reached. The numerical results also draw the same conclusion (Figure 5.10, Figure 5.11 & Figure 5.12).

One of the objective of the thesis is to give proof regarding the area to be considered for the evaluation of compressive strength. If the diametric area of the section is considered then the compressive strength is 4.96 MPa and if area under the loaded cap is considered then the compressive strength increases to 6.20 MPa, an increment by 25%.

Comparing the figures from Figure 5.8 to Figure 5.12, it can be observed that, in all the damage and the stress distribution, area (sand glass shape) below the loaded cap contributes more to the compressive strength than the diametric area of the section.

5.5.3. NUMERICAL AND EXPERIMENTAL TWO JOINT CYLINDER

The force displacement diagram of the numerical and experimental result is shown in Graph 5.13. It is observed that the displacements of the experimental results are more. Hence the experimental results are reduced by 3.5 times, the explanation is given in the previous section. The corrected experimental and the comparison is shown in Graph 5.13 (b). The comparison of maximum force, modulus of elasticity and compressive strength is shown in Table 5.8.

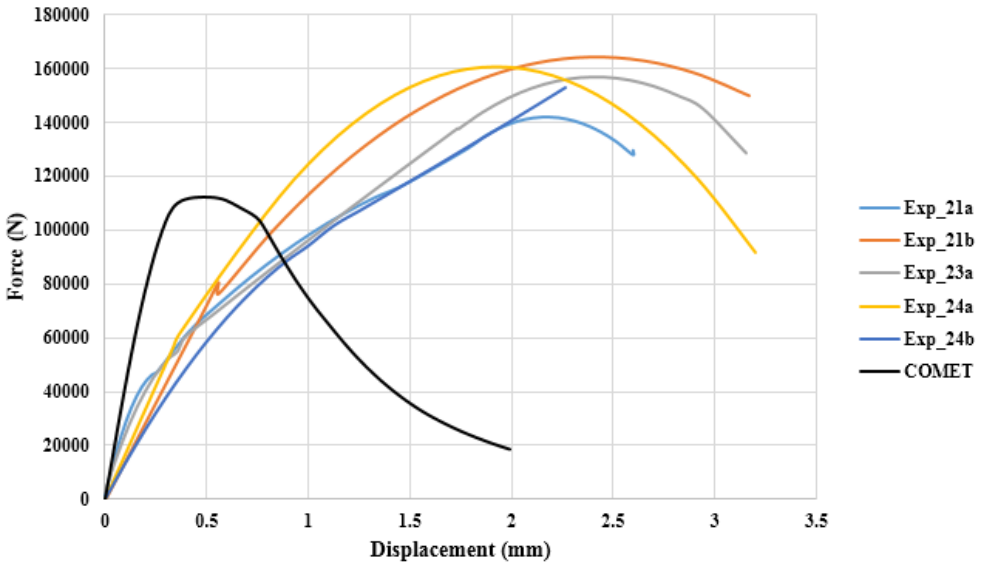

(a)

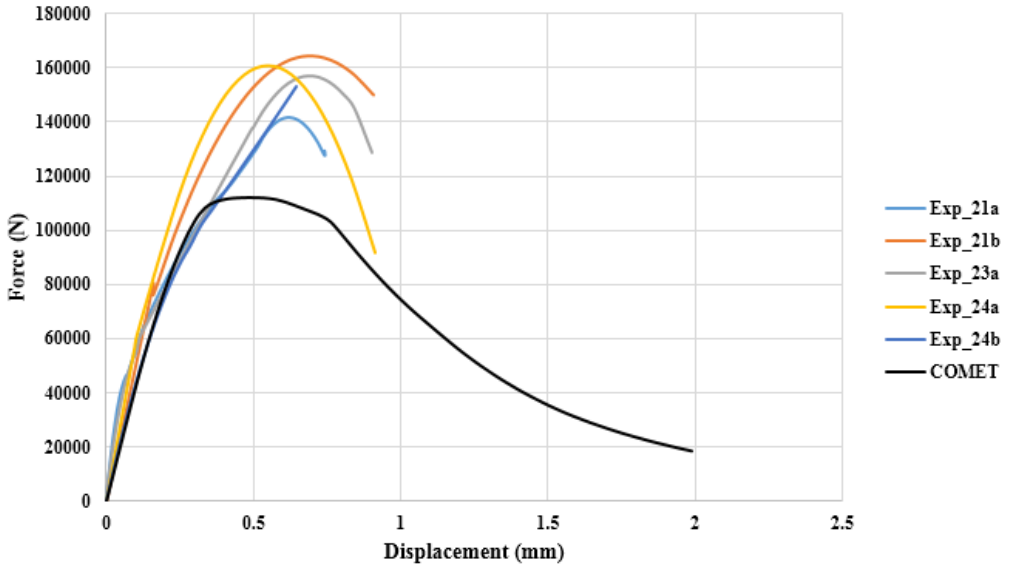

(b)

Graph 5.13 Force displacement diagram of experimental and numerical analysis (Two joint cylinder) (a) Original results & (b) Corrected results

Table 5.8 Comparison of experimental and numerical results of two joint cylinders

	Exp. (Diametric area)	**Exp. (Area below loaded cap)**	**Num. (Diametric area)**	**Num. (Area below the loaded cap)**
Max. Force (kN)	157.87	157.87	112.02	112.02
Displacement at max force (mm)	0.65	0..65	0.47	0.47
Modulus of Elasticity (MPa)	2888	3610	2956	3695
Compressive strength (MPa)	8.10	10.12	5.64	7.02
Variation of compressive strength	-	25%	-43.62%	-15.40%

5.6. FINAL REMARKS

According to the results obtained from the experimental and numerical analysis, all the results are comparable. The evolution of damage and failure mode is same in both the cases for masonry prism and cylindrical specimens. Only the numerical results for the cylindrical specimens are lower by 27%. Based on the results obtained the following relation has been established (Table 5.9 and Table 5.10)

Table 5.9 Relation between experimental and three joint numerical results

		Compressive strength	Modulus of elasticity
Experimental	Diametric area	$f_c^{prism} = 1.22 f_c^{cyl}$	$E_c^{prism} = 1.31 E_c^{cyl}$
	Area below loaded cap	$f_c^{prism} = 0.98 f_c^{cyl}$	$E_c^{prism} = 1.05 E_c^{cyl}$
Numerical	Diametric area	$f_c^{prism} = 1.63 f_c^{cyl}$	$E_c^{prism} = 1.40 E_c^{cyl}$
	Area below loaded cap	$f_c^{prism} = 1.3 f_c^{cyl}$	$E_c^{prism} = 1.12 E_c^{cyl}$

Table 5.10 Relation between experimental and two joint numerical results

		Compressive strength	Modulus of elasticity
Experimental	Diametric area	$f_c^{prism} = 1.07 f_c^{cyl}$	$E_c^{prism} = 1.63 E_c^{cyl}$
	Area below loaded cap	$f_c^{prism} = 0.85 f_c^{cyl}$	$E_c^{prism} = 1.29 E_c^{cyl}$
Numerical	Diametric area	$f_c^{prism} = 1.44 f_c^{cyl}$	$E_c^{prism} = 1.33 E_c^{cyl}$
	Area below loaded cap	$f_c^{prism} = 1.15 f_c^{cyl}$	$E_c^{prism} = 1.07 E_c^{cyl}$

The relations shown above are valid for this case, but a general conclusion cannot be given since further research needs to be carried out.

5.7. SENSITIVITY ANALYSIS RESULTS

5.7.1. MASONRY PRISM

The sensitivity analysis is carried out based on the results obtained from the numerical analysis, to understand the parameters which affect the compressive strength of masonry. The results of the sensitivity analysis for the masonry prism are shown in Graph 5.14 , where the tensile strength of brick, compressive strength of mortar and the modulus of elasticity of mortar are shown. Graph 5.14(a) shows the variation of tensile strength of brick, it is seen that increasing the tensile strength increases the compressive strength of masonry prism. Similarly Graph 5.14(b) shows the variation of compressive strength of mortar, which also increases or decreases linearly with the increment or decrement. Graph 5.14(c) shows the variation of mortar modulus of elasticity with the compressive strength of masonry.

The tensile strength of brick and the compressive strength of mortar are directly proportional to the compressive strength of masonry, the proof is given by both numerical and the experimental results. In case of mortar compressive strength a linear proportionality is observed. The modulus of elasticity of mortar is inversely proportional to the compressive strength of masonry, even if its effect is minor and not as important as the other two parameters.

The effect of compressive strength of mortar is shown in Table 5.11, since the variation, affects the strength of masonry more than the other parameters.

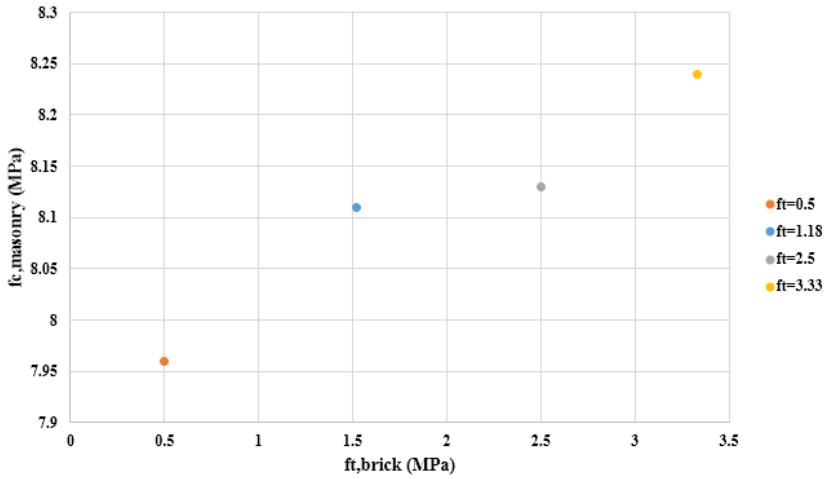

(a)

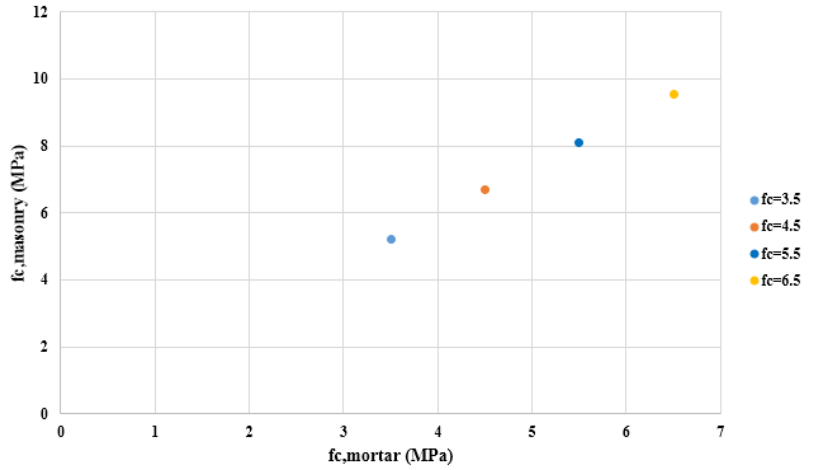

(b)

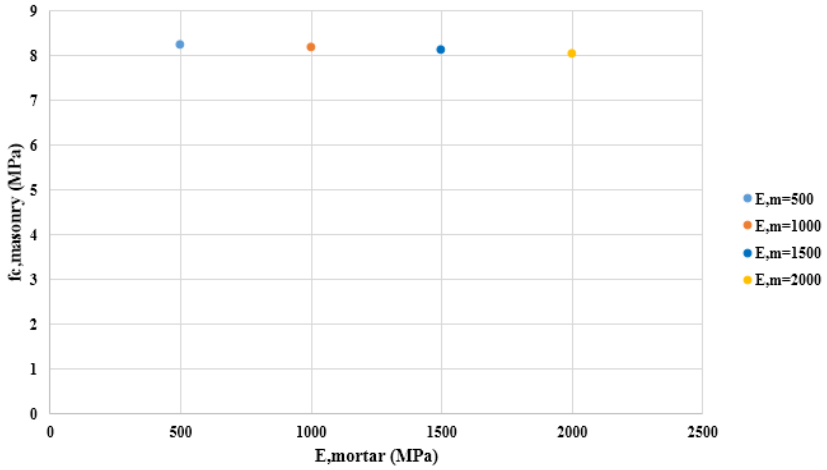

(c)

Graph 5.14 Results of sensitivity analysis (a) Variation of tensile strength of brick (b) Variation of compressive strength of mortar (c) Variation of modulus of elasticity of mortar

Table 5.11 Relation of compressive strength of mortar on masonry strength

Compressive strength of mortar (MPa)	Compressive strength of Masonry (MPa)
3.5	5.21
4.5	6.69
5.5	8.11
6.5	9.53

Graph 5.15 shows the variation of compressive fracture energy from 1500 N/m to 2000 N/m. it can be inferred that increasing the fracture energy, only prolongs the post peak behavior of the structure. But the failure is not affected by increasing the fracture energy. If the compressive fracture energy is reduced below the minimum value, then the analysis does not run, since there will not be any convergence, because the energy is not sufficient to calculate the succeeding step. If the value considered is too high, then it results in almost a horizontal line after failure.

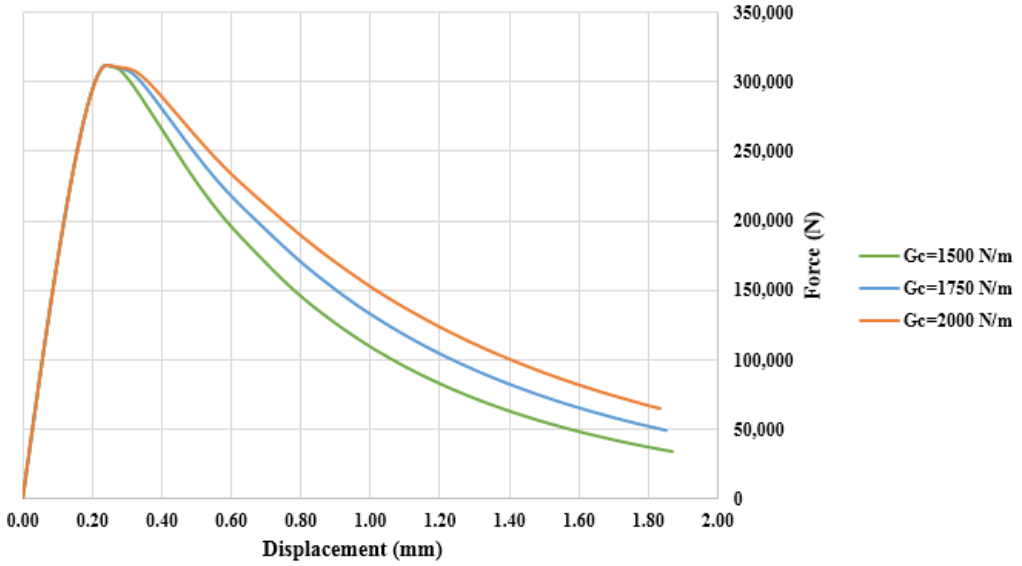

Graph 5.15 Variation of compressive fracture energy of mortar

5.7.2. CYLINDRICAL SPECIMEN

Sensitivity analysis also for the cylindrical three joint specimens is carried out. The comparison of different parameter affecting the compressive strength of masonry is shown from Table 5.12 to Table 5.15.

Figure 5.21 shows the variation of tensile strength of brick (a: strength variation and b: stress strain variation) and its effect on compressive strength of masonry. It can be observed from Table 5.12, decreasing the tensile strength of brick to 0.50 MPa (63%), the compressive strength of masonry decreases to 4.24 MPa. Variation of different values for tensile strength of brick is shown in Table 5.12. It can be concluded that the tensile strength does affect much the overall compressive strength of masonry, not as much as compressive strength of mortar which is explained next.

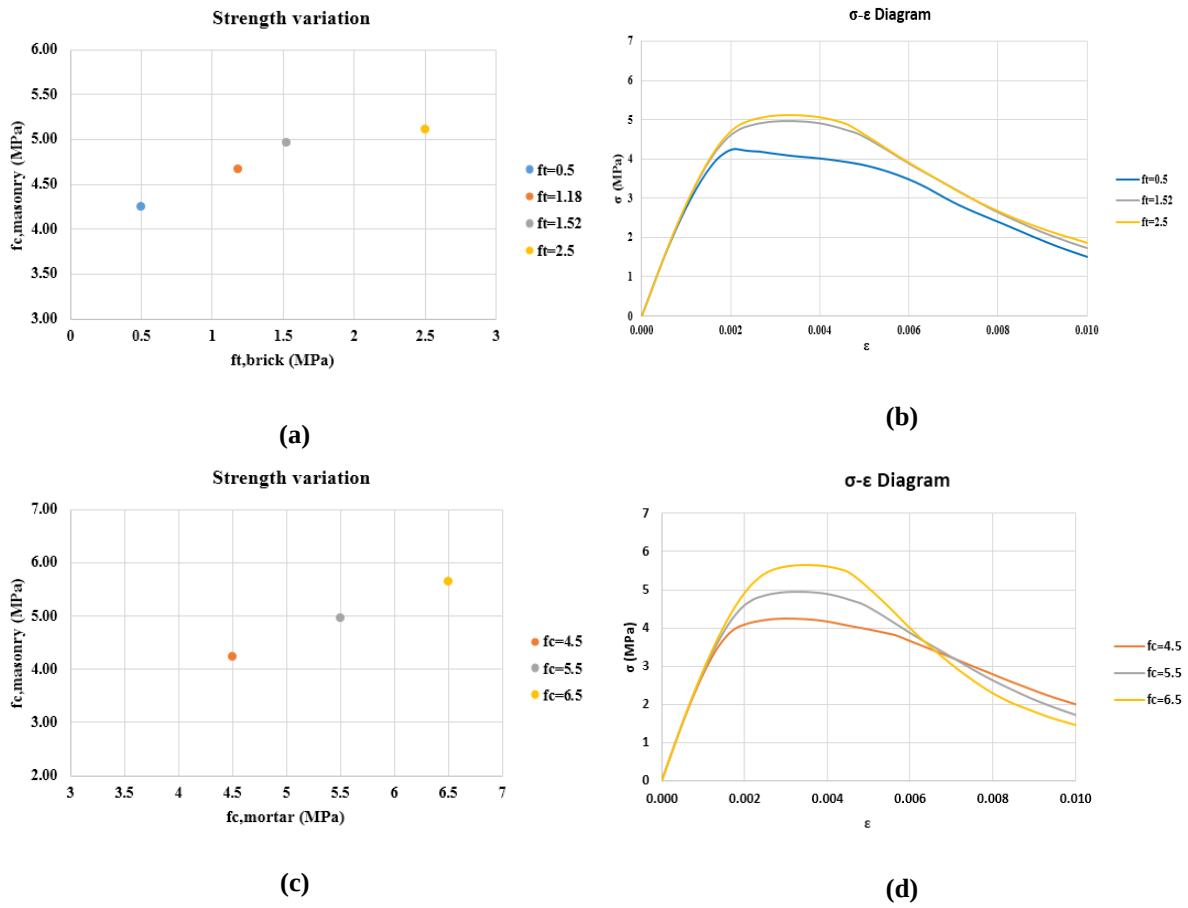

Figure 5.21 Sensitivity analysis results (a) & (b) Variation of tensile strength of brick (c) & (d) Variation of compressive strength of mortar

The effect of varying the compressive strength of mortar is shown in Figure 5.21 (c: strength variation) and (d: stress strain variation) and the values in Table 5.13. It can be seen from the graph that the variation is linearly dependent on compressive strength of mortar. For 18% decrease in strength of mortar, the strength of masonry has to be increased by 17%, which is more with respect to tensile strength of brick.

Table 5.12 Relation of $f_{t,b}$ on compressive strength of masonry

Tensile strength of brick ($f_{t,b}$) MPa	Compressive strength of masonry (f_c) MPa
0.5	4.24
1.18	4.67
1.52	**4.96**
2.5	5.11

Table 5.13 Relation of $f_{c,m}$ on compressive strength of masonry

Compressive strength of mortar ($f_{c,m}$) MPa	Compressive strength of masonry (f_c) MPa
4.5	4.24
5.5	**4.96**
6.5	5.64

The variation of modulus of elasticity and the compressive fracture energy of mortar is shown in Figure 5.22. As the modulus of elasticity of mortar increases the compressive strength of masonry slightly decreases. This decrement can be neglected since it is below 1% for a decrease of 66% in modulus of elasticity as shown in Table 5.14. It is the initial stiffness of the structure which changes due to the variation.

The compressive fracture energy also does not contribute much towards the strength of masonry. Since the variation is 3% for a 50% variation of fracture energy. Table 5.15 shows the relation for few values. As it can be seen from Figure 5.22(d), by changing the fracture energy, only the post peak behavior of the masonry is affected. It completely controls the softening curve of the masonry. If the fracture energy is less than the minimum limit then the analysis will not take place, since there will not be any convergence.

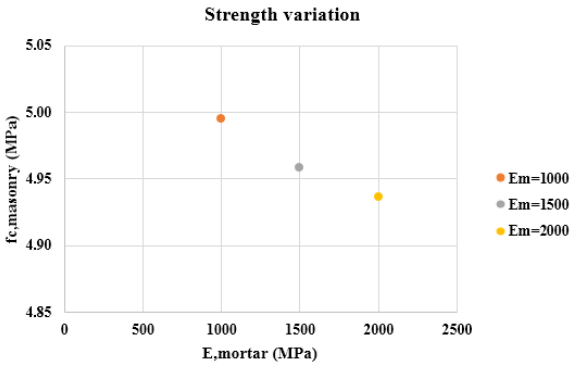

(a)

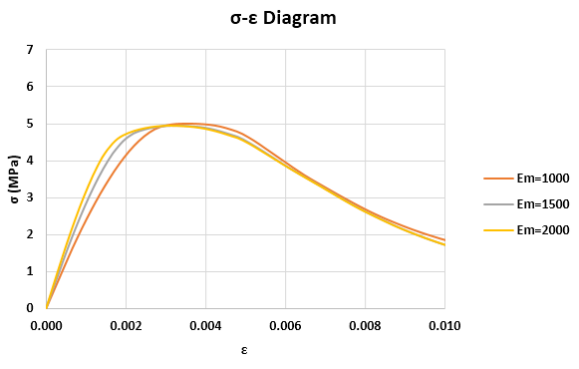

(b)

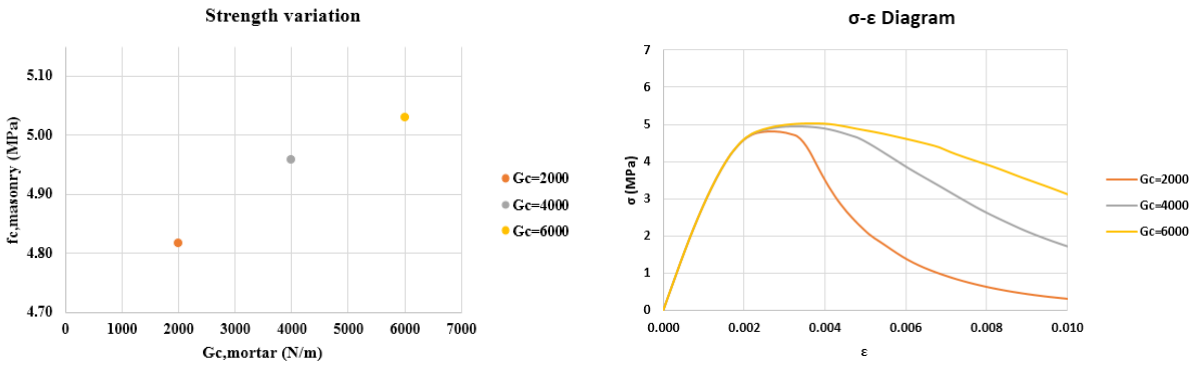

(c) **(d)**

Figure 5.22 Sensitivity analysis results (a) & (b) Variation of modulus of elasticity of mortar (c) & (d) Variation of compressive strength of mortar

Table 5.14 Relation of E_m on compressive strength of masonry

Modulus of elasticity of mortar (E_m) MPa	Compressive strength of masonry (f_c) MPa
1000	5.00
1500	**4.96**
2000	4.94

Table 5.15 Relation of $G_{c,m}$ on compressive strength of masonry

Compressive fracture energy of mortar ($G_{c,m}$) MPa	Compressive strength of masonry (f_c) MPa
2000	4.82
4000	**4.96**
6000	5.03

Not all the parameters discussed above affect remarkably the compressive strength of masonry. The maximum influence is governed by the compressive strength of mortar (Figure 5.21 (a & b)) and the tensile strength of brick (Figure 5.21 (c & d)). This is because, as the strength of mortar increases there is an overall shift in the compressive strength of masonry.

This shift is only up to a limit viz., until the difference between compressive strength of mortar and brick is high.

The failure of masonry is governed by the tensile failure of brick. As there is an increment in compressive strength of mortar the tensile stresses contributing to the failure also increases, mainly in the out of plane direction.

The variation of modulus elasticity controls the initial stiffness and the variation of fracture energy controls the post peak behavior majorly, but both parameters do not affect appreciably the compressive strength of masonry.

6. CONCLUSIONS

6.1. SUMMARY

The present work deals with performing numerical analysis on cylindrical masonry specimens to determine the compressive strength. The main idea is to extract cylindrical specimens from a masonry wall and performing laboratory tests to determine their strengths according to UIC 778-3R guidelines (UIC 1995). In order to check the experimental results obtained and to understand better the evolution of damage and stress distribution, numerical analysis is carried out by assuming the same properties obtained from the experimental results of previous research by Peverini (2014) and Usan Cano (2014).

Chapter 1 and 2 present the introduction and state of art of the thesis, with a general description on the behaviour of masonry, units and mortar. The uniaxial behaviour of masonry in tension and in compression is also mentioned. Few theories and formulae are presented which are used in general to calculate the compressive strength of masonry which involves the Euro code 6, equation proposed by Hilsdorf (1969), Khoo and Hendry (1975), Ohler (1986). Methods to determine the compressive strength of old and new masonries is also discussed, introducing the research on cylindrical specimens.

In chapter 3, the experimental campaign carried out and the results of the previous research are presented. The chapter explains the new way of extracting cylindrical specimens from masonry wall, which was carried out to overcome the drawbacks of previous campaign. Then the methodology, codes, experiments and the results on brick, mortar, masonry prism and cylindrical specimens carried out in the laboratory are discussed.

Chapter 4 deals with a brief introduction of constitutive model used in the present work. The numerical analysis is carried out in the Finite element software “COMET (Cervera et al. 2002). In order to validate and check the results obtained by the new software, a bench mark analysis in 2D and 3D is carried out referring to Berto et al (2005), from which the model was referred and analysed. This analysis was chosen since the author uses almost the same constitutive model, used in the present thesis. The results of both the analysis are in good agreement.

After the calibration of the constitutive model and the software, the masonry prism was analysed, taking the results from the experimental research. This was carried out to check and

compare the results with the experimental testing, for the same properties of prisms and cylindrical specimens. The tensile damage, compressive damage, tensile stress, compressive stress and the vector distribution are all explained in detail with figures referring to specific points in the force displacement diagram. After performing the sensitivity analysis, the results were matched. Then the comparison of the results with the experimental results is carried out.
Finally the three joint and two joint cylindrical specimens are modelled and analysed. First the linear analysis is carried out and then the non-linear analysis. Comparison of linear and non-linear analysis is performed to understand the initiation of damage and the failure modes. The experimental results are compared with non-linear analysis, to analyse if the strength, damage and failure are in the same pattern. It is observed that in both the experimental and numerical results, the damage and the failure appear to be the same. But only the strengths are lower in the numerical analysis than in the experiments.
In the conclusion, relation between the experimental and numerical results are carried out, which are closer to the relation given in Bilello et al., (2007). The results of the sensitivity analysis carried out by varying the tensile strength of brick, compressive strength of mortar, modulus of elasticity of mortar and compressive fracture energy of mortar and their effect on the compressive strength of masonry is presented. It shows that varying tensile strength of brick and compressive strength of mortar affects most the compressive strength of masonry.
All the research carried out is to widen the data available for the experimental and numerical analysis in compressive strength determination of cylindrical masonry specimens.

6.2. CONCLUSIONS

In the light of the results obtained and observations made during the present investigation, it is possible to draw the following conclusions:

- The compressive strength of masonry can be adequately simulated by extracting cylindrical masonry specimens from the existing structures and subjecting them to laboratory testing;
- The compressive strength of cylindrical specimens shows good relation with the compressive strength of masonry prisms. The results are closer if the area below the loaded cap is considered for strength estimation;

- The compressive strength of mortar and the tensile strength of brick are the main parameters influencing the compressive strength of masonry;
- The compressive fracture energy of mortar controls the post peak behaviour of masonry and the Young's modulus of mortar controls the stiffness of the masonry structures.
- The tensile damage initiates closer to the mortar propagating within the brick and the compressive damage initiates in the mortar joints.
- In brickwork, with strong brick and weak mortar combination, the failure is due to the tensile failure of the bricks. Considerable contribution of the out of plane stresses for the failure can be noticed.

6.3. SCOPE FOR FUTURE WORK

Based on the results obtained from numerical model and the experimental works, the following suggestions can be carried out to deepen the information regarding the research topic.

- Performing experimental and numerical analysis simultaneously. It helps in understanding the problem better. Because of the time constrain, the experimental works were not completed viz., the testing of extracted cylindrical specimens needs to be carried out in future.
- To understand the position of extraction, which involves three joint, two joint or one joint specimens for testing.
- Research on dimensions of the regularization mortar, as it effects the confinement of cylindrical specimens which in turn affects the results.
- Performing experimental testing with the data necessary to obtain the tensile and compressive fracture energies of brick and mortar, since they play an important role as a value of input in the numerical analysis, affecting the results.
- Improving the constitutive law, by changing the compression failure criterion of mortar with one more pressure sensitive to account for the confinement effects.
- Since this is a non-standard test carried out by following the UIC 778-3R guidelines, scope for standardising the method.

- Carrying out tests also on bigger wallets, according to the EN 1052-1 standard, in order to obtain a broader comparison between the behaviour of cores and that of larger specimens.

REFERENCES

Berto, L. (2005). Failure mechanism of masonry prism loaded in axial compression: computational aspects. *Materials and Structures*, *38*(276), 249–256. doi:10.1617/14096

Benedetti, Andrea & Pelà Luca (2012). Experimental characterization of mortar by testing on small specimens, 15th International Brick and Block Masonry conference, Florianó.

Bilello, C., Brencich, A., Corradi, C., Paola, M. Di, & Sterpi, E. (2007). Experimental tests and theoritical issues for the identification of existing brickwork, Tenth North Americal masonry Conference, St. Louis, Missouri, USA pp 964–974.

Brencich, a., Corradi, C., & Gambarotta, L. (2008). Eccentrically loaded brickwork: Theoretical and experimental results. *Engineering Structures*, *30*(12), 3629–3643. doi:10.1016/j.engstruct.2008.05.010

Brencich, A., Corradi, C., Gambarotta, L., Mantegazza, G., & Sterpi, E. (2006). Compressive Strength of Solid Clay Brick Masonry under Eccentric Loading.

Brencich, A., & Sterpi, E. (2006). Compressive Strength of Solid Clay Brick Masonry : Calibration of Experimental Tests and Theoretical Issues, Structural analysis of Historical Constructions, New Delhi.

Brencich, A., Corradi, C., & Sterpi, E. (2004). Experimental Approaches to the compressive response of solid clay brick masonry, 13th International Brick and Block Masonry Conference Amsterdam, pp 1–10.

CEB-FIP - 1993 - Model Code 1990 COmite Euro-International Du Beton.

CEN - 2007 - BS-EN 1015-11 - Methods of test for mortar for masonry - Part 11 Determination of flexural and compressive strength of hardened mortar.

Cervera M, Agelet de Saracibar C, Chiumenti M. COMET: Coupled mechanical and Thermal analysis – data input manual version 5.0. Technical report IT-308. CIMNE, Technical University of Catalonia; 2002.

EN 772-1 (2002). Methods of test for masonry units. Part 1: Determination of the compressive strength. European Committee for Standardization, Brussels, Belgium.

EN 1015-11 (1999). Methods of test for mortar masonry. Part 11: Determination of flexural and compressive strength of hardened mortar. European Committee for Standardization, Brussels, Belgium.

Eurocode 6 part 1-1 (1996). Design of masonry structures, part 1-1: General rules for reinforced and unreinforced masonry structures. UNE - ENV 1996-11.

Faria, R., Oliver, J., & Cervera, M. (1998). A strain-based plastic viscous-damage model for massive concrete structures. *International Journal of Solids and Structures*, *35*(14), 1533–1558. doi:10.1016/S0020-7683(97)00119-4

GiD: the personal pre and post-processor. CIMNE, Technical University of Catalonia; 2002. <http://gid.cimne.upc.es.

Hendry A.W. (1990). Structural masonry. Macmillan Education, London, UK.

Hilsdorf, H. K. (1969). Investigation into the failure mechanism of brick masonry loaded in axial compression. Designing, engineering and constructing with masonry products, Gulf Publishing Company, Houston, Texas, USA.

C.L. Khoo and A.W. Hendry, 'A failure criterion for brickwork in Axial Compression' *Proceeding of the Third International Brick Masonry Conference* (Essen) 1973, eds L.Foertig and K. Gobel, pp. 139-45

C.L. Khoo and A.W. Hendry, 'Strength Tests on brick and mortar under complex Stresses for the Development of a Failure Criterion for Brickwork in Compression', *Proc. Br. Ceram. Soc*, 21 (1973) 57-66

Lourenço, P. B., Fernandes, F. M., & Castro, F. (2010). Handmade Clay Bricks: Chemical, Physical and Mechanical Properties. *International Journal of Architectural Heritage*, *4*(1), 38–58. doi:10.1080/15583050902871092

Ohler A, 'Zur Berechnung der Druckfestigeit von Mauerwerk unter Berucksichting der mehrachsigen Spannungszustande in Stein und Mortel', *Bautechnk*, 5 (1986)

Page A W - 1978 - Finite element model for masonry. *Journal of the structural division.*

Page A W - 1981 - The biaxial compressive strength of masonry. *Proc. Inst. Civil Engrs,*; 71(2):893-906.

Pelà L, Benedetti A., Marastoni D. (2012). Interpretation of experimental tests on small specimens of historical mortars. *8th International Conference on Structural Analysis of Historical Constructions.* Wroclaw, Poland.

Pelà, L., Cervera, M., & Roca, P. (n.d.). Author ' s personal copy An orthotropic damage model for the analysis of masonry structures.

Peverini, A. (2014). Experimental evaluation of the compressive behaviour of existing masonry. Dissertation. Polytechnico Di Torino.

R. H. Atkinson, J. L Noland and D. P. Abrams, 'A Deformation Theory for Stack Bonded Masonry Prisms in Compression', *Proceedings of the Seventh International Brick Masonry Conference* (Melbourne) 1982, pp 565-76

Samarasinghe W., Hendry A.W. (1980). The strength of brickwork under biaxial tensile and compressive strength. Proc. of the 7th Symposium on load bearing brickwork, London

Samarasinghe W., Page A. W., Hendry A. W. (1982). A finite element model for the in plane behavior of brickwork. Proc. Inst. Civ. Eng., 71 (2): 171-178.

Sassoni, E., & Mazzotti, C. (2013). The use of small diameter cores for assessing the compressive strength of clay brick masonries. *Journal of Cultural Heritage*, *14*(3), e95–e101. doi:10.1016/j.culher.2012.11.027

UIC 1995: UIC – International Union of Railways: UIC code 778-3R. Recommendations for the assessment of the load carrying capacity of the existing mas. and mass-concrete arch bridges. UIC, Paris.

Usan Caño C. (2014). Caracterización mecánica experimental de ladrillos macizos. Dissertation. Polytechnic University of Catalonia. Barcelona